CENOZOIC THERMAL AND TECTONIC HISTORY OF THE COAST MOUNTAINS OF BRITISH COLUMBIA AS REVEALED BY FISSION TRACK AND GEOLOGICAL DATA AND QUANTITATIVE THERMAL MODELS

by

Randall Richardson Parrish

B.A., Middlebury College, 1974

M.Sc., University of British Columbia, 1977

A THESIS SUBMITTED IN PARTIAL FULFILLMENT OF

THE REQUIREMENTS FOR THE DEGREE OF

DOCTOR OF PHILOSOPHY

in

THE FACULTY OF GRADUATE STUDIES

DEPARTMENT OF GEOLOGICAL SCIENCES

UNIVERSITY OF BRITISH COLUMBIA

We accept this thesis as conforming

to the required standard

THE UNIVERSITY OF BRITISH COLUMBIA

January, 1982

In presenting this thesis in partial fulfilment of the requirements for an advanced degree at the University of British Columbia, I agree that the Library shall make it freely available for reference and study. I further agree that permission for extensive copying of this thesis for scholarly purposes may be granted by the head of my department or by his or her representatives. It is understood that copying or publication of this thesis for financial gain shall not be allowed without my written permission.

Department of Geological Sciences

The University of British Columbia
2075 Wesbrook Place
Vancouver, Canada
V6T 1W5

Date December 18, 1981

DE-6 (2/79)

Abstract

Fission track dating of zircon and apatite has been used to determine the Cenozoic uplift history of the British Columbia Coast Mountains from 50°-55°N. 115 dates were obtained from rocks of variable geographic location and altitude, and the resulting date pattern constrains the movement and deformation of the fission track retention isotherms (175°C for zircon, 105°C for apatite) within the crust.

Because date-altitude correlations (apparent uplift rates) cannot always be used confidently to estimate actual rates of uplift, a finite difference numerical scheme was formulated to construct models of heat flow, uplift, denudation, and cooling that satisfy not only fission track dates, but also present heat flow, other isotopic dates, geologic considerations, and fission track-derived estimates of paleo-geothermal gradient. In most cases, apparent uplift rates derived from apatite date-altitude correlations are very close to modeled rates of uplift. Zircon-derived apparent rates, however, often exceed modeled rates and reflect post-orogenic cooling and relaxation of isotherms. The relationship of the movement of isotherms to rates of uplift and fission track-derived apparent uplift rates is quantified and discussed.

Orogenic rapid cooling and uplift occurred from Cretaceous to Eocene time in most of the Coast Mountains. Rates during orogenic uplift were near 1.0 km/Ma, causing

setting of K-Ar clocks in biotite and hornblende. Uplift rates during the middle Cenozoic ranged from 0.2 km/Ma in the axial region of the mountains between 52° and 55°N to less than 0.1 km/Ma south of 52°N. The moderate rates north of 52°N were likely the result of gradual erosion of crust thickened during Eocene orogeny. A thermal origin for this northern uplift is not likely. Rates of uplift south of 52°N were low despite arc-related volcanic activity during the Oligocene and Miocene.

Accelerated uplift in the Late Miocene near Bella Coola-Ocean Falls was probably the result of passage of the transverse Anahim Volcanic Belt or hotspot beneath the area about 10 Ma ago, after which uplift slowed.

Rapid Pliocene-Recent uplift south of 52°N at rates of up to 0.75 km/Ma elevated a broad region creating the present southern Coast Mountains and deforming 7-10 Ma lavas erupted on the mountains' east flank. It is suggested that this uplift resulted from thermal expansion in the mantle related to a westward jump in the locus of late Neogene arc volcanism. The extent of this rapid Pliocene-Recent uplift correlates with the area above the Juan de Fuca-Explorer subducted slab and confirms a relation between continental uplift and plate tectonic setting.

TABLE OF CONTENTS

LIST OF TABLES

LIST OF FIGURES

INTRODUCTORY REMARKS

This thesis is a study of the Cenozoic tectonics of the Coast Mountains of British Columbia from 50°-55°N. The late Neogene uplift has received special attention because its fundamental cause is poorly understood.

The first paper documents the timing and patterns of uplift throughout the area. This was done by means of fission track dating of apatite and zircon separated from plutonic rocks of the Coast Mountains. In addition, by utilizing fission track data, it was possible to measure paleo-geothermal gradients at two localities. Reasonable estimates of these gradients can in turn help to refine the track retention temperature for zircon, which is not precisely known. The first paper concludes with a discussion of the geological implications and correlations of the fission track-derived uplift data, and it places these observations in a broad regional framework.

The second paper of the thesis integrates thermal modeling and the fission track data. A finite difference computer program was written to simulate the flow of heat in the earth's crust while experiencing variable uplift, variable sub-crustal geothermal flux, variable surface temperature, and non-equality of uplift and erosion. The program accepts as input the uplift history derived from fission track dating. It produces, by trial and error, a set of values of uplift rate, sub-crustal heat flux, and other

parameters, that fit all observed fission track dates, paleo-geothermal gradients, and present heat flow measurements. These models are used to analyse mantle processes. It is shown that thermal expansion of the mantle beneath the Coast Mountains has been responsible for the late Neogene uplift. This situation differs from most of the world's great mountain systems (Himalaya, European Alps, South Island New Zealand) in that crustal thickening is not involved. In this respect, the uplift in the British Columbia Coast Mountains is more similar to areas like the Colorado Plateau of the western United States.

The possible causes of uplift are discussed in a framework of plate tectonics, and an explanation for the Cenozoic tectonic patterns is suggested.

The third paper discusses the caution that must be exercised when interpreting fission track data. In previous studies, the apparent uplift rates derived from zircon and apatite fission track dates (the slope of the date vs. altitude curve) has been assumed equal to the true rate of uplift. In the common situation where the isotherms are either moving upwards (by uplift) or downwards (by isotherm relaxation with or without uplift), the slope of this curve (the <u>apparent uplift rate</u>) will not be the true rate. The departure of apparent from true rate is quantified using thermal models, and geological situations where the apparent and true rates are grossly different are identified. Corrections can be applied to real situations if knowledge

of the geological history and probable geothermal gradient is available. This correction has been overlooked in previous studies, and it emphasizes the importance of uplift and denudation on the upward flow of heat.

CHAPTER 1.

CENOZOIC THERMAL EVOLUTION AND TECTONICS OF THE COAST MOUNTAINS OF BRITISH COLUMBIA I: FISSION TRACK DATING, APPARENT UPLIFT RATES, AND PATTERNS OF UPLIFT

Abstract

The dramatic scenery of the Coast Mountains of British Columbia has been produced by rapid late Neogene uplift; this uplift, however, is not obviously related to the present plate tectonic regime off the west coast of British Columbia. To study this problem, the areal patterns, rates, and total amounts of Cenozoic uplift from 50° to 55°N have been determined using fission track dating of zircon and apatite separated from rocks collected at high and low altitudes along several traverses through the mountains.

Assuming blocking temperatures of 105°C and 175°C for apatite and zircon, respectively, paleo-geothermal gradients have been measured at Kemano (26°+4-6°C/km 35 Ma ago) and near Ocean Falls-King Island (17°±2°C/km 20 Ma ago). Sub-crustal heat flow can be shown to have significantly changed through time near King Island.

During the middle Cenozoic, uplift rates in the axial part of the northern (52°-55°N) Coast Mountains were 0.1-0.2 km/Ma from 25 to 15 Ma ago; this uplift was temporally and tectonically related to subsidence in the adjacent Queen Charlotte basin. Uplift rates increased slightly in the Late Miocene to 0.4 km/Ma, probably because of passage of the Anahim 'hot spot' beneath the area. Late Miocene-Recent erosion in the north has reduced summit altitudes and been more extensive than farther south. Despite this, relicts of Miocene river valleys and

topography are still occasionally preserved.

The area of the present southern (50° to 52°N) Coast Mountains was near sea level and experienced very low uplift rates (<0.1 km/Ma) throughout the middle Cenozoic, despite its more active volcanism. Late Miocene basaltic lavas that were erupted onto a mature erosion surface near Taseko Lakes were elevated and warped by rapid Pliocene-Pleistocene uplift (>0.5 km/Ma) of the southern Coast Mountains. The profile of this uplift was broadly plateau-like, and this uplift led to the inversion of the Miocene topography.

Middle Cenozoic uplift from 52° to 55°N was probably the result of denudation and diminishing uplift after the terminal Eocene orogenic episode which grossly thickened the crust. This middle Cenozoic erosion resulted in the restoration of a normal crustal thickness. Late Neogene uplift in the Coast Mountains was the result of thermal expansion in the mantle caused by a mantle hot spot near 53°N and changes in the geometry of the subducted slab farther south.

Introduction

The Coast Mountains of British Columbia, which rise from sea level to altitudes of up to 4 km, are a climatic and physiographic barrier over 150 km wide and about 1000 km in length (Figure 1). They merge with the St. Elias Mountains of the Yukon Territory and the Cascade Mountains of the northwestern United States in nearly unbroken continuity. The topography is considerably younger than both the rocks themselves and the terminal orogeny in late Cretaceous to early Tertiary time. Geological evidence indicates rapid Late Miocene-Pliocene uplift (Douglas et al 1970). For the most part, the uplifted region is continuous despite its juxtaposition with both subduction and transform fault plate boundaries off the west coast of British Columbia. The relation of uplift to plate motions is therefore unclear. Lack of clear correlation with volcanic episodes adds to this ambiguity.

To explain the late Cenozoic uplift, it is necessary to quantify its areal and temporal variability. Geological mapping of uplifted Late Miocene lavas in southern British Columbia (Tipper 1963, 1978), paleontological work on Cenozoic deposits (Rouse and Mathews 1979) and study of possible Miocene erosion surfaces (Baer 1973, Culbert 1971, Mathews 1968) has provided some data relevant to this problem, but the magnitude and timing of uplift is unknown in areas that lack deposits of late Cenozoic age.

The technique of fission track dating of apatite has

recently been applied to chronology of uplift in several areas of the world (Schaer et al 1975, Wagner and Reimer 1972, Gleadow and Lovering 1978a,b, Naeser 1979). The technique promises quantitative data on uplift in areas where geological data are sparse. Determination of both the timing of uplift (Gleadow and Lovering 1978a) and, where sufficient relief is present, uplift rates (Schaer et al 1975, Wagner et al 1977) are possible. Studies on batholiths and eroded material from such rocks has also yielded chronologies of plutonic emplacement, uplift and unroofing, and deposition of detritus in adjacent basins (Wagner et al 1979).

This paper uses fission track dating of apatite and zircon to quantify the middle and late Cenozoic uplift history of the Coast Mountains of British Columbia. Detailed uplift histories are useful for examining the causes of uplift and building paleo-geological reconstructions. Chapter 2 describes the application of the uplift data to models of heat transfer in order to evaluate various geophysical parameters important in explanations of uplift.

Geological Setting of the Coast Mountains

The Coast Mountains, as physiographically defined (Holland 1964), are largely coincident with the Coast Plutonic Complex. The Complex (Roddick and Hutchison 1974) is dominated by Jurassic to Eocene plutonic granitic rocks

intruded into a varied assemblage of metamorphosed supracrustal rocks. In recent years the interpretation of eugeoclinal stratified rocks in terms of accreted terranes or tectonostratigraphic assemblages has become popular (Monger 1977, Coney 1980). For instance the greater part of the southern Coast Plutonic Complex in addition to Vancouver Island and part of Queen Charlotte Islands is thought to consist of a terrane termed Wrangellia in which thick Triassic pillow lavas are found (Monger and Price 1979, Woodsworth and Tipper 1980).

Near Kemano, however, the eastern margin of the Complex is underlain by rocks common to the Intermontane zone, part of the Stikine terrane or Stikinia (Woodsworth and Tipper 1980). West of these rocks and occupying the axial, high-grade core of the complex are granitic gneisses and metasediments, best known and exposed between Terrace and Prince Rupert (Figure 1). These rocks are called the Central Gneiss Complex and have been extensively studied by Hollister (1979) and Hutchison (1970). The protolith age is largely unknown, although probably Paleozoic or early Mesozoic (Armstrong and Runkle 1979, Woodsworth 1979). These gneisses pinch out southwards in the Bella Coola region. West of the core gneisses in the Prince Rupert area and farther south along strike are metamorphic rocks that are correlative with the early to middle Paleozoic rocks of the Alexander terrane of southeast Alaska (Armstrong and Runkle 1979). Recently discovered Devonian fossils on Melville

Island northwest of Prince Rupert confirm this correlation (G.Woodsworth, personal communication 1981). This Paleozoic terrane is faulted against a portion of Wrangellia near the east edge of Hecate Strait (Woodsworth and Tipper 1980) and perhaps elsewhere on Queen Charlotte Islands (Yorath and Chase 1981).

These terranes were accreted to the North American continent and welded together by plutonism and metamorphism during Mesozoic time (Monger and Price 1979). Some of the plutonic, metamorphic, and structural features were likely related to this accretionary, collisional process, but a large part of the plutonic and volcanic activity is due to a magmatic arc above an east-dipping late Mesozoic to early Cenozoic subduction zone (Monger et al 1972).

The plutonic chronology of the Coast Mountains is poorly established; only near Skeena River, Squamish, and in the Bella Coola region are there reliable Rb-Sr or U-Pb dates which clearly define the age of intrusives (Harrison et al 1979, R.L.Armstrong and R.Parrish unpublished data). K-Ar determinations, which range between 40 and 140 Ma (Figure 2), indicate approximate plutonic ages in a few cases but in most, they give merely the time since final uplift-related cooling (Roddick and Hutchison 1974, Harrison et al 1979). There is a general decrease in both K-Ar dates and the probable ages of plutonic rock from west to east. Plutonism culminated, especially in the northern segment (latitude 53°-60° N), with an intense Eocene plutonic and

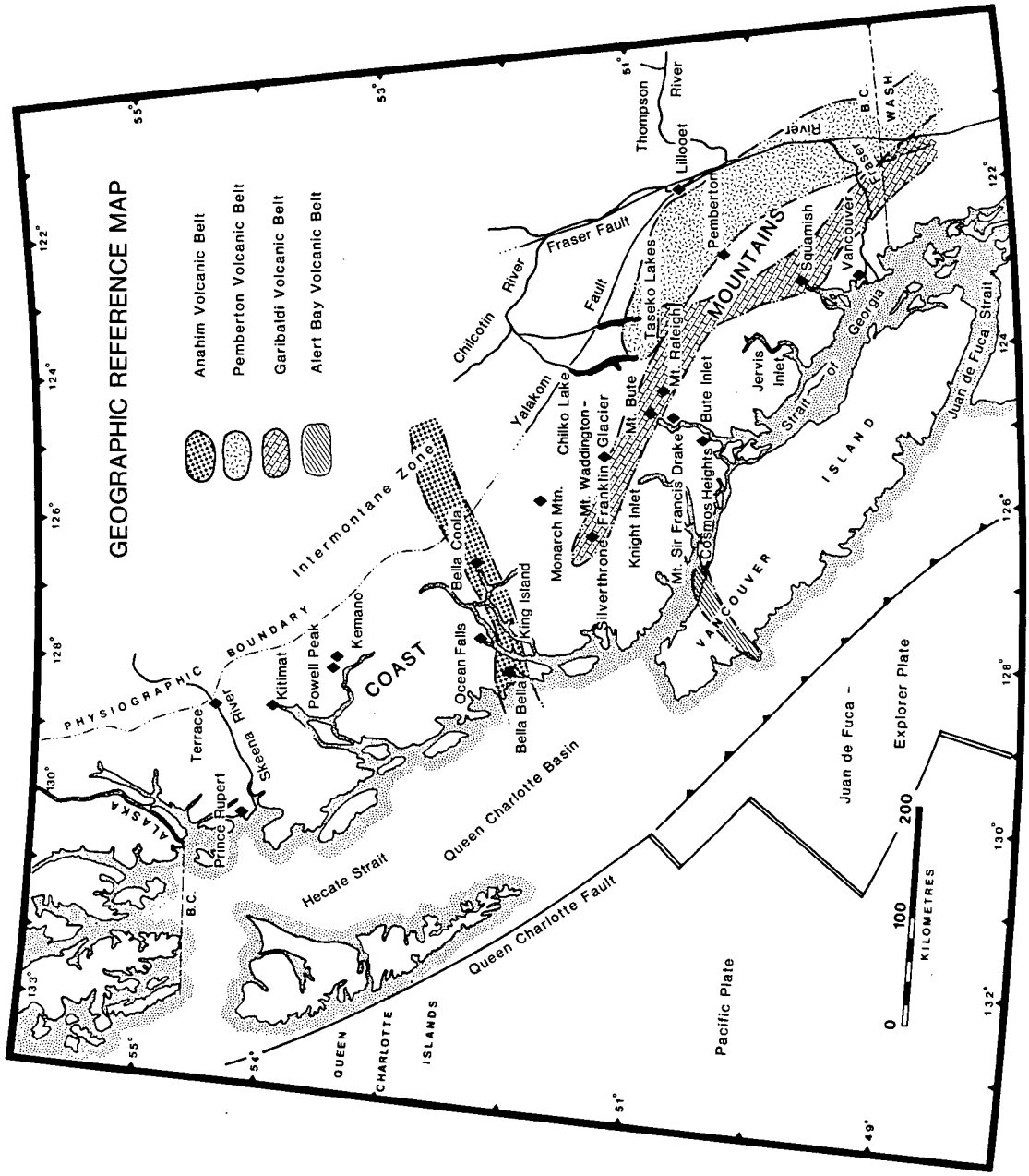

Figure 1. Geographic and geologic reference map. Plate boundaries offshore are modified from Riddihough (1977), and the location of volcanic belts is from Bevier et al (1979) and Berman and Armstrong (1980). The dashed and dotted line refers to the physiographic boundary of the Coast Mountains (Holland 1964), and it merges along trend farther south with the Yalakom and Fraser faults.

orogenic event, after which activity virtually ceased. Only in the south, approximately above the subducting Juan de Fuca plate, did Oligocene to Recent arc-related volcanism and plutonism continue, albeit on a reduced scale (Berman and Armstrong 1980).

A major change in plate motion at about 40-50 Ma likely caused a cessation of rapid subduction along the entire coast and a change to transform motion north of about 52°N and slowed subduction to the south (Coney 1978). This resulted in a middle Cenozoic period of relative quiescence over much of the Coast Mountains (Monger et al 1972), interrupted only by scattered igneous events in the south (Berman and Armstrong 1980) and by the Miocene Anahim Volcanic Belt (Bevier et al 1979) in the Bella Coola region (Figure 1).

Volcanic activity east of the Coast Mountains revived in the Late Miocene with the eruption of voluminous plateau basalts, which flowed over the present eastern flank of the mountains. Climatic evidence suggests no middle Cenozoic mountainous barrier (Mathews and Rouse 1963, Rouse and Mathews 1979) prior to the Late Miocene or Pliocene initiation of uplift. Plateau lavas were deformed during this uplift (Tipper 1963, Douglas et al 1970).

The present plate tectonic regime of subduction south of 51°N and transform motion to the north (Figure 1) has not significantly changed since at least 10 Ma ago (Riddihough 1977). It is possible that the same basic plate

configuration has been present for much of the middle Cenozoic as well (Atwater 1970, Byrne 1979, Coney 1978). This relatively stable middle to late Cenozoic plate tectonic setting contrasts sharply with the rapid Late Miocene to Pliocene uplift that gave rise to the present topography.

Fission Track Dating and its Interpretation

Both the theory and the interpretive aspects of fission track dating have been treated by Fleischer et al (1975), Naeser (1979), and Wagner and Reimer (1972). For rocks in most geologic conditions, fission tracks in apatite and zircon will anneal at temperatures of about 100°C (Naeser and Faul 1969, Haack 1977, Wagner and Reimer 1972, Zimmermann and Gaines 1978) and 175°C (Harrison et al 1979), respectively. In this paper a value of 105°C for apatite has been used. These estimates are based on experimental annealing studies (Naeser and Faul 1969, Wagner and Reimer 1972), theoretical analysis of such data (Haack 1977, Zimmermann and Gaines 1978) and perhaps more importantly, studies of natural annealing in boreholes (Naeser and Forbes 1976). Data on zircon is much less abundant, but its effective annealing temperature appears well constrained between that of apatite fission track and K-Ar biotite/sphene fission track, as deduced from cooling histories of well-dated plutons (Harrison et al 1979, Harrison and McDougall 1980).

The track retention temperature is a simplification representing the effective closure temperature (Haack 1977) in a process of increasingly efficient track retention over a narrow temperature interval. The effective closure temperature is a function of cooling rate, but for example, varies only from 98°C to 111°C for apatite when cooling rate changes from 1°C/Ma to 10°C/Ma, respectively (Zimmermann 1977). Dating zircon and apatite from a single rock will reveal average cooling rate between 175°C and 105°C, which can be used to further define the closure temperature. Cooling rates for the vast majority of rocks in this study over the 175° to 105°C temperature interval varied only from 3° to 10°C/Ma, resulting in date differences between apatite and zircon of 7 to 25 Ma. For the purposes of this work, the track retention temperature will be considered to be constant. This simplification facilitates data treatment and modelling and introduces little additional uncertainty. The error in apatite and zircon closure temperatures is estimated at ±5-10°C and ±20°C, respectively.

Given normal (25°C/km) geothermal gradients, these temperatures (105°, 175°C) correspond to depths of about 4 and 7 km in the crust. Rocks experiencing uplift and erosion pass upwards and will retain fission tracks first in zircon and later in apatite. Deeper samples will consequently have younger dates than shallower ones at any one locality.

If rocks are sampled at different altitudes in areas of large relief, an increase in fission track date at higher

altitudes is usually present. The difference in altitude divided by the difference in date will be termed, in this study, the apparent uplift rate. This apparent uplift rate, in fact, however, is the rate at which the critical isotherms (105°, 175°C) moved downward with respect to the rock column. The apparent rate does not necessarily represent the uplift rate of the rocks with respect to sea level, nor does it necessarily equal the denudation rate with respect to the average surface of the land. The uplift connotation in the term, apparent uplift rate, is retained both for convenience and because the mechanism by which the date-altitude trends are developed is primarily uplift of crustal rocks. Cooling, denudation, and isotherm movement are consequences of the primary uplift. The reader should continually bear in mind the true meaning of this term; a consistent usage has been maintained throughout this study.

The apparent uplift rate will strictly equal the true uplift-erosion rate only when several conditions are met. These conditions are that 1) isotherms must have been horizontal and uninfluenced by either surface topography or variable thermal conductivity, 2) isotherms must remain at a constant depth with respect to the surface regardless of uplift rate and 3) uplift must be equal to erosion. A complex interrelationship exists between isotherm migration, uplift, denudation, and cooling, and since these conditions are rarely met, caution in interpreting apparent uplift rates must be exercised. Corrections for these effects are

discussed in Chapter 3, but for most conditions, fission track-derived apparent uplift rates are approximately correct.

By dating apatites collected at various altitudes and locations in the Alps, Schaer et al (1975) and Wagner et al (1977) were able to document uplift rates, spatial variation of rates, and deformation of paleoisotherms. No such detailed data are available for a mountain system in North America.

Sampling Techniques

Fresh granitic rock samples were collected for this study along four traverses across the British Columbia Coast Mountains (Figure 3). Because the coastline of the province is indented by numerous deep fjords immediately adjacent to mountains of 2-4 km topographic relief, the area is ideal for sampling both low and high altitude rocks across the width of the mountains. In addition to the four traverses, two other areas were sampled in detail, Powell Peak near Kemano, and Mount Waddington near the head of Knight Inlet (Figures 2,3). The samples in the Bella Coola traverse and the southern traverse were collected by a combination of foot, boat, and helicoptor transportation. The rocks at Powell Peak, Bute Inlet, Mount Raleigh, and Mount Waddington were collected by the Geological Survey of Canada and were made available by Glen Woodsworth. In total, over 70 rocks were processed resulting in 115 fission track dates.

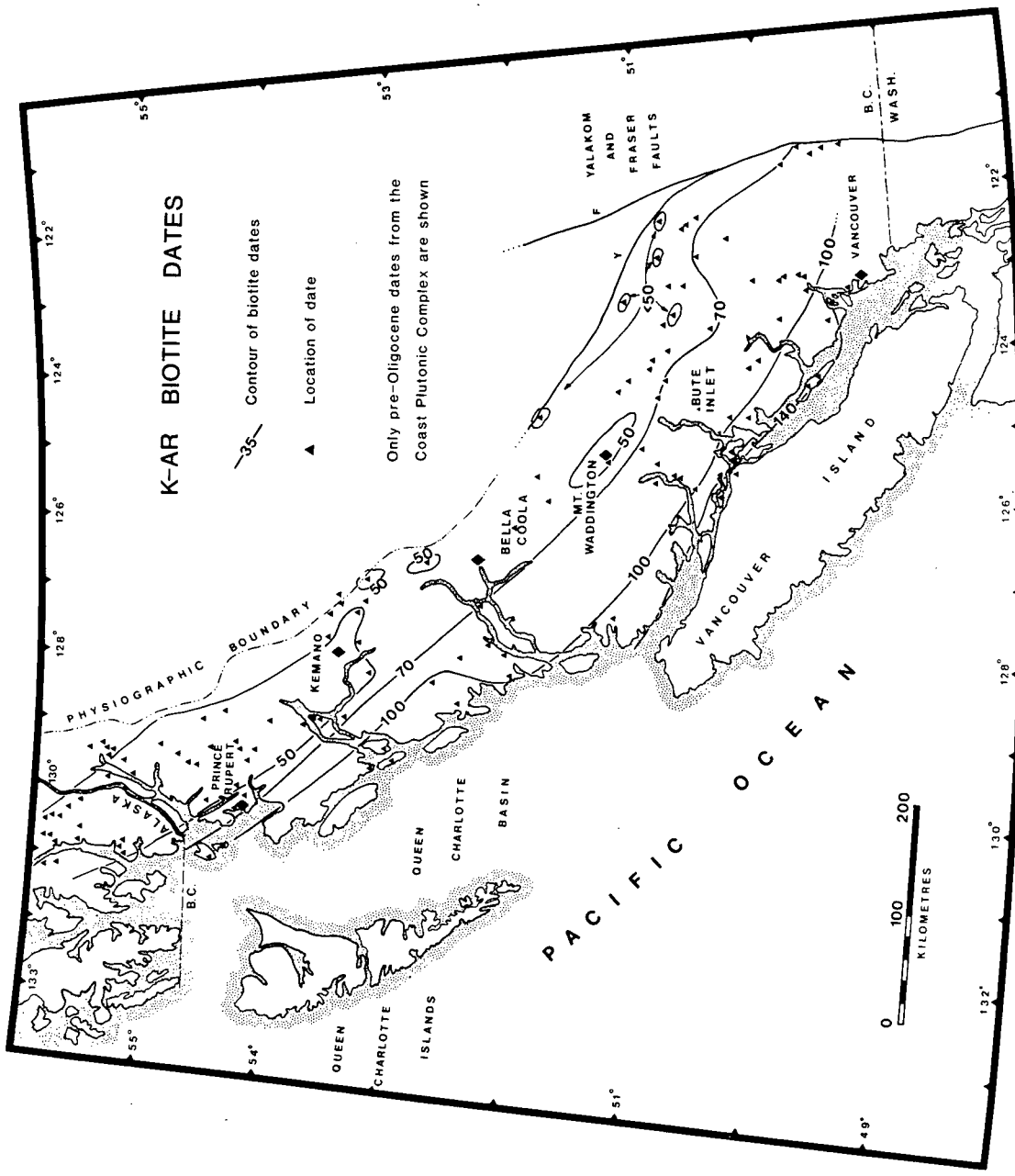

Figure 2. K-Ar biotite dates in the Coast Mountains. Only data from the Coast Mountains are shown, and only from pre-Oligocene rocks. Contoured from a compilation of R. L. Armstrong which includes data from Wanless et al (1964-1979), Richards and White (1970), Richards and McTaggart (1976), Nelson (1979), Bartholomew (1979), Carter (1974), Harrison et al (1979), and unpublished data of R. L. Armstrong.

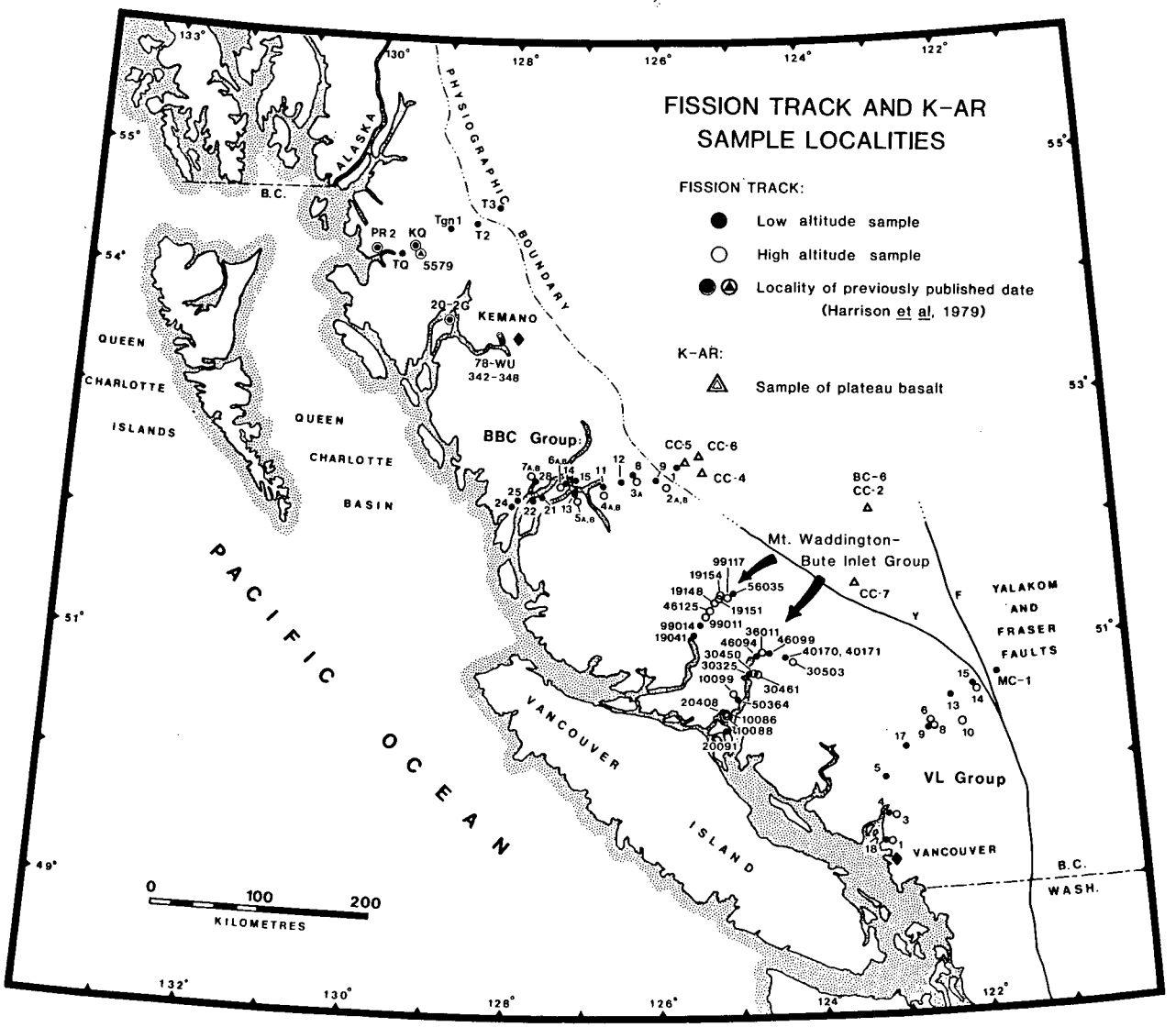

Figure 3. Location of samples dated by fission track (plutonic rock) or K-Ar (basalt).

Analytical Techniques

Techniques adapted from Naeser (1976) and Gleadow and Lovering (1975) were used to date apatite and zircon in this study using the population and external detector methods, respectively. Accessory minerals were abundant and easily separated from nearly all rocks collected. Initial mineral separation involved crushing and sieving 1 kg samples of rock to retain the -80+170 fraction, rapid high volume magnetic separation using a CARPCO separator, washing in water and acetone, and heavy mineral separation using bromoform. Further separation involved a Frantz magnetic separator and methylene iodide.

In dating apatite by the population method, two splits were made, one being annealed at 480°-520°C for at least two hours to remove spontaneous, naturally occuring tracks. This annealed split was irradiated and subsequently mounted, polished, and etched together with the other split which retained the natural tracks. Apatite etching conditions were 7% nitric acid at 22°-24°C for about 30 seconds. Tracks were counted at 800x.

Zircons were mounted and etched according to the procedure of Gleadow et al (1976) using FEP teflon and a eutectic KOH-NaOH etch at 200°-210°C for about 48 hours (depending on track density). Zircons were etched until natural tracks were fully exposed. Muscovite detectors were used to record the induced track density and were etched in 48% HF for 12 minutes at 22°-24°C. Tracks in zircon were

counted at 1250x or 1600x in oil. A geometry factor of 0.5 was assumed for the external detector method.

Dates were calculated according to the fission track age equation,

$$\text{date}=\ln(1+(\rho s/\rho i)\Phi(\lambda^{238}\text{alpha}/\lambda^{238}\text{fission})(U^{235}/U^{238})\underline{X}^{235}) \times (1/\lambda^{238}\text{alpha})$$

where λ^{238}alpha and λ^{238}fission are U^{238} decay constants for alpha and fission, respectively, Φ is the thermal neutron dose, U^{235}/U^{238} is the atomic ratio of uranium isotopes, and $\underline{X}^{235}$ is the cross-section for neutron fission reaction of U^{235}. With appropriate substitution of numerical constants listed in Table II, the equation becomes,

$$\text{date(Ma)}=6.446\text{x}10^{3}\ \ln(1+9.322\text{x}10^{-18}(\rho s/\rho i)\Phi).$$

Thermal neutron irradiation was performed in Denver, Colorado at the USGS TRIGA research reactor (United States Geological Survey 1974) under the supervision of C.W.Naeser and D.Rusling. Neutron dose measurements and internal gradients were calibrated by the use of mica detectors on NBS 962 glass (Carpenter and Reimer 1974) and by repeated dating of apatite and zircon standards from the tuff of Fish Canyon provided by C.W.Naeser. Seven different irradiations over a period of one year were done to arrive at a consistent calibration constant, β, relating thermal neutron dose (Φ) to induced track density (ρi) in muscovite set against the NBS 962 glass according to the relation,

$$\Phi=\beta/\rho i.$$

For the calculation, the neutron dose (Φ) was determined by

back-calculation using the counted track density ratio, $\rho s/\rho i$, for the tuff mineral standards assuming their age as 27.9 Ma (Steven et al 1967, based on constants listed in Table II). Substituting 27.9 Ma as the date of the tuff of Fish Canyon and rearranging the above equation, the neutron dose for irradiations and calibration was estimated by

$$\Phi(\text{neutron/cm}^2)=4.653\text{x}10^{14}/(\rho s/\rho i)$$

where ρs and ρi refer to track densities in minerals of the tuff of Fish Canyon. This method was preferred since the NBS irradiated glasses RT-1 and RT-2 (Carpenter and Reimer 1974) were found to be somewhat unreliable as Φ calibrators. The NBS 962 glass did, however, continue to be used for the source of induced tracks in adjacent detectors. These Fish Canyon tuff-derived Φ estimates were consistently close, but slightly less than, the independent estimates provided by reactor personnel for each irradiation. For eight different irradiations using minerals from the tuff of Fish Canyon for dose calibration, the value and standard error of β were found to be $5.41\pm0.22 \times 10^9$ neutrons/track (8 irradiations, Table I).

This value was then used in turn to determine Φ using the induced track density, ρi, of the NBS 962 muscovite detectors bracketing samples in each irradiation. Φ estimates for samples were made by interpolation. Apatite and zircon ages from the tuff of Fish Canyon calculated using this dose, and corrected for gradient (determined as 4%/cm of material for the USGS TRIGA reactor), average

27.3±1.0 Ma (standard error) for zircon and 27.3±0.8 Ma for apatite (Table II). The calculated mean and standard deviation of uranium content for the minerals is 352±42 ppm for zircon and 10.8±1.4 ppm for apatite, in close agreement with values reported by Naeser et al (1979). If estimates provided by the USGS reactor facility are used and no correction for gradient is made, the mean and standard error of the tuff ages are 29.4±1.0 and 29.6±1.1 for zircon and apatite, respectively. Necessary flux gradient corrections will lower these values by about 5%, in close agreement with the known age of the minerals determined by Steven et al (1967, new constants).

Dating results for zircon and apatite are reported in the format suggested by Naeser et al (1979), and errors for dates are calculated according to formulae given by Johnson et al (1979). Instead of assuming Poisson statistics in the calculation of the standard deviation of track density (where (standard deviation)^2=mean), standard deviation of the counts was calculated from individual counting statistics. A standard deviation of 3% on neutron dose estimates was assumed in the calculation of errors for all dates. The uranium decay constants of Steiger and Jager (1977) and Hurford and Gleadow (1977) were used in this study. Analytical results are presented in Table III.

Another important element in fission track dating involves the necessity of eliminating, as far as possible, all counting bias on the part of the researcher. In this

Table I. Values of 'β' Determined from Dating the Tuff of Fish Canyon (27.9 Ma)[1]

Irradiation	Mineral	$\rho s/\rho i$	ρ^{std} detector, t/cm^2	Φ[2], 10^{14}n/cm^2	β[3], 10^{9}n/track
9-79	apatite	1.47	7.21 x10^4	3.17	4.40
2.1-80	zircon	1.38	6.55 x10^4	3.37	5.15
2.1-80	zircon	1.48	6.55 x10^4	3.14	4.79
2.1-80	apatite	1.34	6.55 x10^4	3.47	5.30
3.1-80	zircon	1.03	7.70 x10^4	4.52	5.87
3.1-80	apatite	1.25	7.70 x10^4	3.72	4.83
4.1-80	apatite	1.45	5.56 x10^4	3.21	5.77
4.1-80	apatite	1.60	5.56 x10^4	2.91	5.23
4.1-80	zircon	1.30	5.56 x10^4	3.58	6.44
4.2-80	zircon	1.48	6.50 x10^4	3.14	4.83
4.2-80	apatite	1.31	6.50 x10^4	3.55	5.46
4.2-80	apatite	1.36	6.50 x10^4	3.42	5.26
6.1-80	apatite	0.80	8.57 x10^4	5.82	6.79
6.1-80	apatite	0.85	8.57 x10^4	5.47	6.38
8.1-80	apatite	1.85	5.02 x10^4	2.52	5.02
8.1-80	zircon	1.67	5.02 x10^4	2.79	5.56
8.2-80	apatite	1.49	5.83 x10^4	3.12	5.35
8.2-80	zircon	1.39	5.83 x10^4	3.35	5.75

Mean and standard error of β Using 1 average value from each irradiation:

$\beta = 5.41 \pm 0.22 \times 10^9$ neutrons/track

Assumed age of Fish Canyon Tuff = 27.9 Ma[4]

---

[1] See Table II for explanation of symbols

[2] For the tuff of Fish Canyon, $\Phi = 4.653 \times 10^{14}/(\rho s/\rho i)$; U constants listed in Table II.

[3] $\beta = \Phi/\rho^{std}$; ρ^{std} is the density of the detector on NBS962 glass.

[4] based on K-Ar dating of Steven et al (1967) and recalculated with:
$\lambda e = 0.581 \times 10^{-10}$/yr; $\lambda b = 4.962 \times 10^{-10}$/yr; $^{40}K = 0.01167$ atom%

Table II. Fission Track Analytical Data for the Tuff of Fish Canyon

Irr.	Mineral	ρs[1] (10^5 t/cm^2)	Tracks,s	ρi[1] (10^5 t/cm^2)	Tracks,i	Φ[1] (10^{15} n/cm^2)	Tracks,Φ	Date±S[2]	n,(s/i)[3]	r,S'[4]	U,(ppm)	USGS Φ est.[5] (10^{15} n/cm^2)
9-79	apatite	0.134	1699	0.091	1157	3.16	8673	27.9±1.0	300/300	4.4%	10	3.15
2.1-80	zircon	5.84	841	4.24	610	3.32	2171	27.4±1.5	9	0.90	414	3.44
2.1-80	zircon	4.45	712	3.00	480	3.32	2171	29.5±1.2	10	0.96	293	3.44
2.1-80	apatite	0.137	283	0.102	648	3.31	2171	26.7±1.7	49/150	3.5%	10	3.44
3.1-80	zircon	3.95	1392	3.85	1356	4.15	2802	25.5±0.8	22	0.97	322	4.30
3.1-80	apatite	0.14	356	0.112	212	4.13	2802	30.9±2.7	60/45	11.1%	9	4.30
4.1-80	apatite	0.137	526	0.095	364	2.98	5673	25.8±1.8	60/60	4.9%	10	3.44
4.1-80	apatite	0.160	511	0.100	321	2.98	5673	28.6±2.1	50/50	5.6%	11	3.44
4.1-80	zircon	4.20	806	3.24	622	3.00	5673	23.3±1.2	12	0.78	347	3.44
4.2-80	apatite	0.121	464	0.093	356	3.48	5673	27.1±1.9	60/60	5.2%	10	3.44
4.2-80	apatite	0.160	511	0.118	378	3.48	5673	28.3±2.1	50/50	4.6%	12	3.44
4.2-80	zircon	5.24	838	3.53	564	3.49	5673	31.1±1.7	10	0.97	364	3.44
6.1-80	apatite	0.120	692	0.150	433	4.64	2055	22.3±1.7	90/45	5.2%	12	5.16
6.1-80	apatite	0.150	630	0.176	372	4.64	2055	23.7±1.8	100/50	5.2%	14	5.16
8.1-80	apatite	0.150	630	0.081	171	2.72	2055	30.2±3.1	100/50	8.9%	10	3.44
8.1-80	zircon	4.43	528	2.66	317	2.73	2055	27.3±1.1	12	0.99	327	3.44
8.2-80	apatite	0.150	630	0.101	214	3.20	2055	28.5±2.2	100/50	5.7%	11	3.44
8.2-80	zircon	5.02	698	3.61	502	3.21	2055	26.8±1.0	14	0.94	394	3.44

Zircon mean ± standard deviation, (standard error) = 27.3±2.5,(1.0)Ma
Apatite mean ± standard deviation, (standard error) = 27.3±2.6,(0.8)Ma
Zircon mean U (ppm) ± standard deviation = 352±42
Apatite mean U (ppm) ± standard deviation = 10.8±1.4
Zircon mean date using USGS Φ estimate = 29.4±2.7,(1.0)Ma
Apatite mean date using USGS Φ estimate = 29.6±3.8,(1.1)Ma

---

[1] ρs, spontaneous track density; ρi, induced track density; Φ, thermal neutron dose
[2] S, standard error
[3] number of grains or fields counted: s, spontaneous; i, induced
[4] r, correlation coefficient; S', relative standard error of induced tracks
[5] not adjusted for flux gradient
decay constants: λ^{238}(fission)=7.00 x 10^{-17}/yr; λ^{238}(alpha)=1.55125 x 10^{-10}/yr; λ^{235}(alpha)=9.8485 x 10^{-10}/yr
other constants: U^{238}/U^{235}=137.88; $\underline{X}^{235}$=580 x 10^{-24}cm^2

Table III. Fission Track Analytical Data

Sample	Latitude	Longitude	Alt. (m)	Mineral	ρs (10^6t/cm²)	Tracks,s	ρi (10^6t/cm²)	Tracks,i	Φ (10^{15}n/cm²)	Date±S	n,(s/i)	r.S'
Terrace area												
TQ	54°12'30"	129°35'30"	<100	apatite	1.36	655	3.27	784	8.76	21.9±1.5	30/15	4.8%
Tgn1	54°25'40"	128°52'00"	<100	apatite	0.107	204	0.303	577	8.77	18.6±1.8	45/45	5.0%
T2	54°30'20"	128°32'30"	<100	apatite	0.037	70	0.088	168	8.41	21.2±3.0	45/45	9.3%
T3	54°41'15"	128°20'00"	<100	apatite	0.062	131	0.099	209	8.42	31.6±4.6	50/50	9.2%
Kemano-Powell Peak area												
78-WU-342	53°51'25"	128°01'10"	1951	apatite	0.372	707	0.213	405	3.22	33.7±2.9	45/45	6.2%
78-WU-342	53°51'25"	128°01'10"	1951	zircon	2.70	1208	1.18	528	3.24	44.4±1.6	28	0.91
78-WU-343	53°50'55"	127°59'15"	1570	apatite	0.455	865	0.257	488	3.20	34.0±2.7	45/45	5.8%
78-WU-343	53°50'55"	127°59'15"	1570	zircon	3.69	1182	1.70	546	3.21	41.7±2.4	20	0.79
78-WU-344	53°50'05"	127°58'40"	1189	apatite	0.179	447	0.111	280	3.18	30.7±2.9	59/60	6.2%
78-WU-344	53°50'05"	127°58'40"	1189	zircon	3.50	671	1.51	289	3.19	44.3±3.1	12	0.89
78-WU-345	53°49'50"	127°58'35"	945	apatite	0.336	639	0.190	362	3.16	33.5±3.2	45/45	7.6%
78-WU-345	53°49'50"	127°58'35"	945	zircon	2.94	1082	1.27	468	3.17	43.9±1.8	23	0.91
78-WU-347	53°49'25"	127°57'40"	305	apatite	0.276	524	0.213	405	3.14	24.4±2.2	45/45	6.6%
78-WU-347	53°49'25"	127°57'40"	305	zircon	2.95	1744	1.36	806	3.15	40.9±1.5	37	0.87
78-WU-348	53°49'25"	127°57'30"	91	apatite	0.169	321	0.126	240	3.12	25.1±2.7	45/45	7.6%
78-WU-348	53°49'25"	127°57'30"	91	zircon	4.80	614	2.51	321	3.13	35.9±1.8	8	0.65
Bella Bella-Bella Coola area												
BBC-1	52°26'40"	125°52'00"	1052	zircon	5.51	882	2.04	326	3.82	61.7±4.3	10	0.97
BBC-1	52°26'40"	125°52'00"	1052	apatite	0.270	571	0.166	351	3.84	37.4±3.6	50/50	7.4%
BBC-2A	52°18'25"	125°57'10"	2085	zircon	3.24	829	1.39	356	3.92	54.7±4.0	16	0.98
BBC-2A	52°18'25"	125°57'10"	2085	apatite	0.809	1537	0.352	670	3.90	53.6±3.9	45/45	5.4%
BBC-2B	52°18'25"	125°57'10"	2085	apatite	1.31	1382	0.659	668	3.86	45.9±3.9	25/24	5.1%
BBC-2B	52°18'25"	125°57'10"	2085	zircon	3.79	1092	1.74	500	3.88	50.6±3.0	18	0.81
BBC-3A	52°24'00"	126°24'25"	1920	apatite	0.440	372	0.188	191	3.94	55.2±6.3	20/24	9.7%
BBC-3A	52°24'00"	126°24'25"	1920	zircon	3.51	786	1.66	372	3.96	50.1±3.0	14	0.51
BBC-4A	52°18'40"	126°48'00"	1868	apatite	0.106	340	0.082	268	2.87	22.3±2.5	50/51	8.4%
BBC-4A	52°18'40"	126°48'00"	1868	zircon	1.73	360	1.08	225	2.89	27.8±1.0	13	0.97
BBC-4B	52°18'40"	126°48'00"	1868	apatite	0.263	824	0.207	661	2.90	22.1±2.8	49/50	8.3%
BBC-4B	52°18'40"	126°48'00"	1868	zircon	1.85	504	0.903	246	2.91	35.7±1.2	18	0.97
BBC-5A	52°15'35"	127°05'20"	2023	apatite	0.027	130	0.020	95	2.93	23.7±3.5	75/75	10.7%
BBC-5A	52°15'35"	127°05'20"	2023	zircon	3.05	684	1.53	343	2.94	35.1±1.5	14	0.85
BBC-5B	52°15'35"	127°05'20"	2023	apatite	0.024	92	0.020	77	2.96	21.3±3.4	60/60	11.3%
BBC-5B	52°15'35"	127°05'20"	2023	zircon	4.83	1159	2.20	528	2.97	39.1±1.6	15	0.95
BBC-6A	52°20'45"	127°18'45"	1579	apatite	0.284	599	0.351	742	3.26	15.8±1.9	50/50	8.1%
BBC-6B	52°20'45"	127°18'45"	1579	apatite	0.151	482	0.145	465	3.25	20.3±2.4	50/50	7.9%
BBC-6B	52°20'45"	127°18'45"	1579	zircon	10.4	1163	5.18	580	3.23	38.9±2.4	7	0.95
BBC-7A	52°22'30"	127°42'05"	1237	apatite	0.267	565	0.309	653	3.30	17.1±1.3	50/50	4.0%
BBC-7A	52°22'30"	127°42'05"	1237	zircon	6.76	1407	3.49	726	3.31	38.4±2.2	13	0.70
BBC-7B	52°22'30"	127°42'05"	1237	apatite	0.255	815	0.307	982	3.28	16.4±1.1	50/50	4.0%
BBC-8E	52°26'20"	126°23'15"	146	apatite	0.072	151	0.049	103	4.00	35.2±4.0	50/50	7.9%
BBC-8E	52°26'20"	126°23'15"	146	zircon	2.24	574	1.46	374	4.01	36.9±2.2	16	0.77
BBC-9	52°21'30"	126°00'45"	274	apatite	0.601	1524	0.334	860	4.05	43.6±3.3	60/61	4.9%
BBC-9	52°21'30"	126°00'45"	274	zircon	8.34	1467	3.56	626	4.07	57.0±4.2	11	0.77

Table III, continued. Fission Track Analytical Data

Sample	Latitude	Longitude	Alt. (m)	Mineral	ρs (10^6t/cm²)	Tracks,s	ρi (10^6t/cm²)	Tracks,i	Φ (10^{14}n/cm²)	Date±S	n,(s/i)	r,S'
BBC-11S	52°22'30"	126°48'00"	30	apatite	0.246	944	0.264	1014	3.04	17.0±1.3	60/60	5.0%
BBC-11S	52°22'30"	126°48'00"	30	zircon	3.89	810	1.87	388	3.07	38.3±2.2	13	0.78
BBC-12G	52°23'00"	126°33'30"	94	apatite	0.021	29	0.015	15	4.09	34.3±12.2	33/23	31.0%
BBC-12G	52°23'00"	126°33'30"	94	zircon	2.66	510	1.57	301	4.11	41.7±2.7	12	0.94
BBC-13	52°18'45"	127°06'30"	0	apatite	0.080	261	0.146	472	3.08	10.1±1.2	50/50	8.3%
BBC-13	52°18'45"	127°06'30"	0	zircon	4.21	1012	2.28	547	3.09	34.2±2.2	15	0.91
BBC-14	52°22'15"	127°14'05"	0	apatite	0.019	91	0.046	146	3.32	8.2±1.1	75/50	7.5%
BBC-14	52°22'15"	127°14'05"	0	zircon	5.22	752	2.89	416	3.33	36.0±2.5	9	0.96
BBC-15	52°23'20"	127°13'00"	0	apatite	0.019	60	0.038	122	3.34	10.0±1.7	50/50	10.3%
BBC-21	52°15'30"	127°06'45"	0	apatite	0.635	805	1.23	1301	3.36	10.4±0.8	30/25	4.8%
BBC-21	52°15'30"	127°06'45"	0	zircon	3.32	797	1.53	367	3.35	43.5±3.3	15	0.62
BBC-22	52°14'45"	127°45'00"	0	apatite	0.221	467	0.329	709	3.38	13.6±1.4	50/51	7.8%
BBC-22	52°14'45"	127°45'00"	0	zircon	18.7	2094	5.91	662	3.39	64.1±2.9	7	0.92
BBC-24	52°10'30"	127°58'35"	0	apatite	0.201	709	0.205	721	3.41	20.1±1.7	55/55	6.1%
BBC-24	52°10'30"	127°58'35"	0	zircon	8.58	1785	3.23	671	3.40	54.0±4.4	13	0.78
BBC-25	52°12'25"	127°51'10"	0	apatite	0.141	297	0.213	450	3.43	13.6±1.1	50/50	5.2%
BBC-28	52°21'25"	127°42'10"	10	apatite	0.111	356	0.206	660	3.46	11.2±0.9	50/50	5.2%
BBC-28	52°21'25"	127°42'10"	10	zircon	8.00	1408	3.48	613	3.47	47.8±2.1	11	0.93
Mount Waddington												
19041	51°04'40"	125°35'00"	0	apatite	0.039	82	0.048	102	2.67	13.0±2.3	50/50	11.0%
19041	51°04'40"	125°35'00"	0	zircon	1.95	866	0.622	262	2.67	50.1±3.4	14	0.51
19148	51°22'30"	125°16'10"	3960	apatite	1.27	1119	0.606	536	2.75	34.5±3.0	21/21	5.8%
19148	51°22'30"	125°16'10"	3960	zircon	2.42	1433	0.991	586	2.73	39.9±2.4	14	0.86
19151	51°23'30"	125°14'00"	3800	apatite	0.141	295	0.082	172	2.76	28.5±3.7	50/50	8.9%
19154	51°24'20"	125°14'10"	2900	apatite	0.117	296	0.065	164	2.77	29.9±4.0	60/60	10.2%
19154	51°24'20"	125°14'10"	2900	zircon	3.48	724	1.40	292	2.77	41.2±1.8	13	0.98
46125	51°19'35"	125°20'00"	2210	apatite	0.019	47	0.030	77	2.70	10.3±1.7	50/50	10.0%
46125	51°19'35"	125°20'00"	2210	zircon	4.78	2628	1.40	769	2.70	55.2±2.6	13	0.94
56035	51°27'30"	125°02'45"	910	apatite	0.075	190	0.063	161	2.80	20.0±2.8	60/60	9.8%
56035	51°27'30"	125°02'45"	910	zircon	7.55	1449	2.49	478	2.80	50.8±3.1	12	0.96
99011	51°16'00"	125°26'50"	1295	apatite	0.016	34	0.022	47	2.69	11.7±2.9	50/50	16.2%
99011	51°16'00"	125°26'50"	1295	zircon	1.88	703	1.64	637	2.70	18.6±1.8	13	0.87
99014	51°13'40"	125°30'00"	760	apatite	0.058	122	0.179	375	2.68	5.2±0.6	50/50	6.7%
99117	51°25'30"	125°05'00"	2290	apatite	0.125	272	0.094	198	2.79	22.3±2.2	50/50	6.2%
Bute Inlet area												
10086	50°27'34"	125°11'10"	1600	apatite	0.088	112	0.031	39	2.90	49.3±10.0	30/30	15.3%
10088	50°26'42"	125°10'10"	762	apatite	0.320	406	0.088	111	2.91	63.3±11.7	30/30	14.3%
10099	50°38'44"	125°04'50"	1600	apatite	0.651	1101	0.174	368	2.98	66.7±7.0	40/50	7.9%
10099	50°38'44"	125°04'50"	1600	zircon	3.88	497	0.922	118	2.99	75.2±5.4	8	0.62
20091	50°17'50"	125°12'35"	0	apatite	0.404	682	0.080	169	2.87	86.5±7.6	40/50	7.4%
20408	50°27'28"	125°16'10"	0	apatite	1.05	498	0.203	211	2.92	90.1±8.5	32/35	8.4%
30325	50°48'54"	124°53'00"	0	apatite	0.779	988	0.343	435	3.08	41.9±3.7	30/30	6.0%
30325	50°48'54"	124°53'00"	0	zircon	3.95	506	0.993	127	3.09	73.4±4.9	8	0.92
30450	50°48'22"	124°50'20"	1753	apatite	0.483	408	0.114	96	3.07	77.7±10.0	20/20	9.3%
30461	50°47'18"	124°47'10"	2515	apatite	2.39	1517	0.573	726	3.06	76.2±6.2	15/30	4.5%
30461	50°47'18"	124°47'10"	2515	zircon	4.58	586	0.836	107	3.06	99.9±3.8	8	0.96

Table III, continued. Fission Track Analytical Data

Sample	Latitude	Longitude	Alt. (m)	Mineral	ρs (10^6 t/cm^2)	Tracks,s	ρi (10^6 t/cm^2)	Tracks,i	Φ (10^{14} n/cm^2)	Date±S	n,(s/i)	r,S'
30503	50°54'28"	124°17'25"	2789	apatite	1.67	1130	0.888	600	3.18	35.8±2.6	16/16	5.4%
30503	50°54'28"	124°17'25"	2789	zircon	3.99	511	1.56	200	3.19	48.8±2.7	8	0.89
36011	50°55'22"	124°42'25"	2286	apatite	0.925	1172	0.313	662	3.15	55.7±3.7	30/50	4.7%
36011	50°55'22"	124°42'25"	2286	zircon	2.83	407	0.944	136	3.16	56.7±3.3	9	0.74
40170,171	50°56'58"	124°22'35"	152	apatite	0.056	61	0.137	151	3.17	7.8±1.3	11	0.53
46094	50°54'10"	124°44'40"	1295	apatite	0.167	352	0.093	235	3.12	33.6±3.3	50/60	7.1%
46099	50°54'50"	124°38'05"	610	apatite	0.561	711	0.255	431	3.11	41.0±2.9	30/40	4.3%
46099	50°54'50"	124°38'05"	610	zircon	4.50	648	1.44	207	3.10	58.0±4.1	9	0.91
50364	50°35'00"	124°57'40"	0	apatite	0.436	737	0.175	369	2.97	44.3±3.5	40/50	5.5%
50364	50°35'00"	124°57'40"	0	zircon	8.69	556	1.53	98	2.94	99.6±4.3	4	0.99
Vancouver-Lillooet area												
VL-1	49°26'50"	123°12'05"	1417	apatite	0.047	60	0.015	19	4.05	75.8±21.2	30/30	23.4%
VL-3	49°40'05"	123°06'25"	1417	apatite	2.30	438	1.13	262	4.11	50.1±7.7	9/11	8.6%
VL-4	49°40'30"	123°09'35"	0	apatite	0.019	25	0.030	39	4.15	15.8±4.7	30/30	18.9%
VL-4	49°40'30"	123°09'35"	0	zircon	11.2	895	2.99	239	4.17	93.2±4.9	5	0.15
VL-5	49°55'30"	123°09'45"	305	apatite	0.014	35	0.008	21	4.19	43.9±13.1	60/60	26.2%
VL-6	50°20'25"	122°36'00"	1722	apatite	0.229	387	0.144	243	4.24	40.4±5.5	40/40	10.5%
VL-8	50°19'10"	122°34'35"	823	apatite	0.349	590	0.196	332	4.28	45.6±5.2	40/40	8.6%
VL-9	50°18'40"	122°36'00"	198	apatite	0.560	710	0.349	442	4.32	41.5±5.5	30/30	8.8%
VL-9	50°18'40"	122°36'00"	198	zircon	4.34	833	1.67	320	4.34	67.4±4.0	12	0.96
VL-10	50°23'55"	122°26'40"	2134	apatite	0.704	595	0.543	459	4.36	33.9±3.6	40/40	7.3%
VL-13	50°39'15"	122°24'40"	518	apatite	0.125	271	0.077	162	4.40	42.8±4.6	50/50	7.7%
VL-14	50°45'45"	122°10'05"	2179	apatite	0.124	263	0.090	190	4.45	36.7±4.4	50/50	8.9%
VL-15	50°47'05"	122°13'20"	655	apatite	0.066	84	0.065	124	4.49	27.3±4.8	30/45	9.9%
VL-15	50°47'05"	122°13'20"	655	zircon	6.13	392	5.58	357	4.47	29.4±1.2	4	0.94
VL-17	50°10'30"	122°53'00"	625	apatite	0.054	114	0.041	86	4.53	35.8±5.2	50/50	10.6%
VL-17	50°10'30"	122°53'00"	625	zircon	5.73	916	2.38	381	4.51	64.9±3.5	10	0.97
VL-18	49°25'35"	123°13'50"	76	apatite	3.71	1019	1.35	715	4.07	66.9±5.1	13/25	5.1%
VL-18	49°25'35"	123°13'50"	76	zircon	8.43	944	2.70	302	4.09	76.3±4.9	7	0.99
MC-1	50°53'51"	121°47'11"	820	apatite	0.343	725	0.106	224	4.57	88.3±8.1	50/50	6.9%

Note: see Table II for explanation of symbols and decay constants.
Sample 40170,40171 was dated by the external detector method.

study, all sample numbers were masked, and thus, samples were objectively counted without knowledge of sample identity. The sample identities were revealed only when all dates from a batch (10-20) were complete. This "blind" counting method should greatly reduce the possibility of counting bias.

Areal Variation of Apatite and Zircon Dates

Sea level apatite dates

Figure 4 shows the distribution and contours of all sea level-low altitude apatite dates. The dates range from a low of about 5 Ma near Mount Waddington to more than 80 Ma near the western margin of the southern Coast Mountains. Dates have been contoured at values of 10, 20, 35, and 50 Ma, and there are virtually no exceptions outside of experimental error in the pattern, which is remarkably consistent and regular. All dates, with the possible exception of VL-14,-15 (Figure 3) are from pre-Oligocene rocks and clearly reflect uplift and final cooling, and reveal a clear pattern of the deformation of the 105°C isotherm. The two apatite and zircon dates from VL-14,-15 average 31.1±4.9 Ma (apatite and zircon are concordant) and probably reflect uplift of an Oligocene granitic intrusive near Lillooet, British Columbia.

In general, the axial region of the mountains or the area to its immediate west gives the youngest dates at a

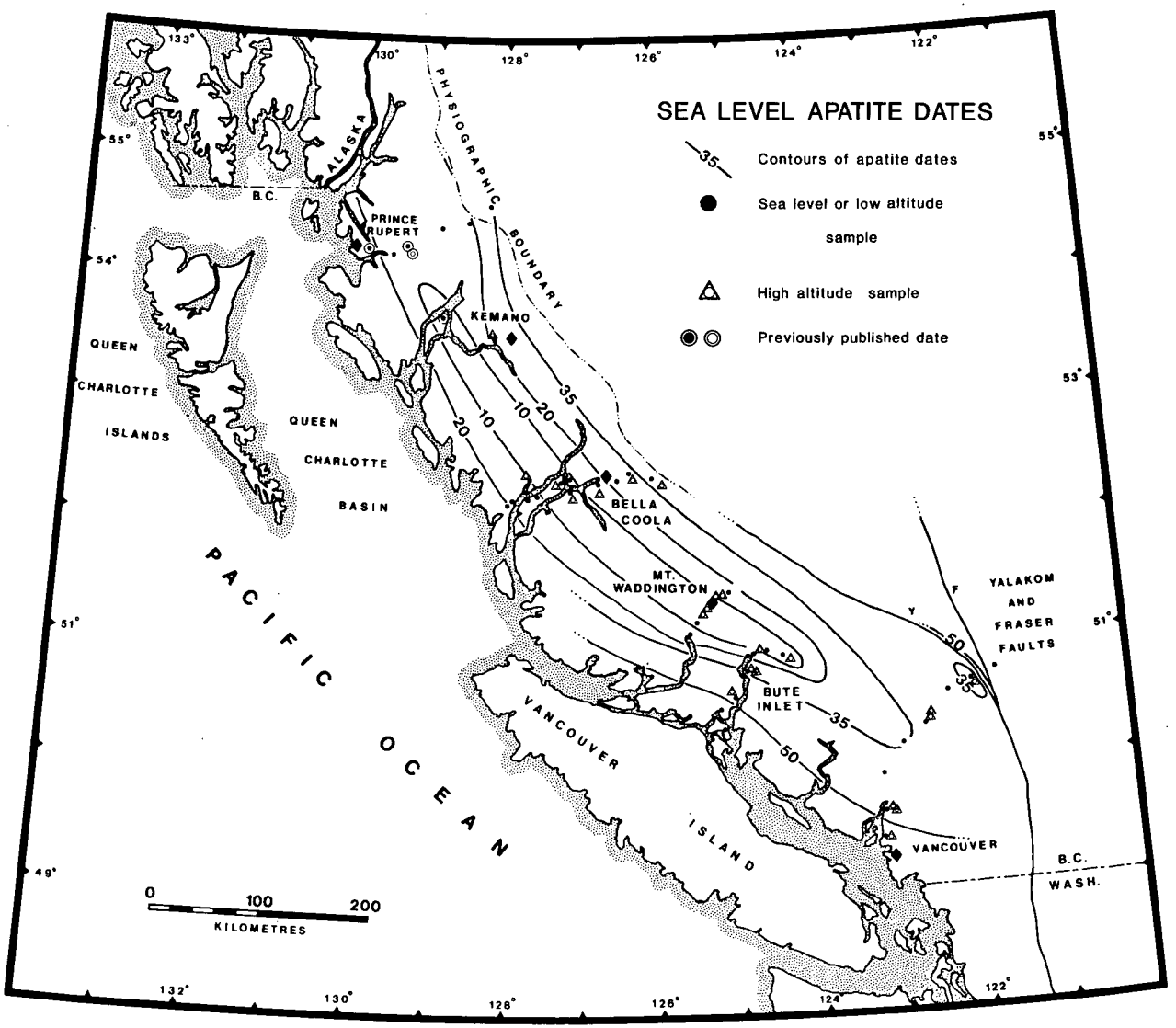

Figure 4. Sea level or low altitude fission track apatite dates.

given latitude, and dates increase east and west from this region. The date gradient is steeper in the east than the west, which partly relates to the younger age of relatively high level, rapidly cooled plutons on the east side of the mountains.

North-south variations are present as well; except for VL-14 and VL-15, none of the dates in the southern traverse is less than about 40 Ma. In the Bute Inlet traverse, one sample beneath Mount Raleigh (40170,40171) is very young, 7.8 Ma, and indicates its recent passage upwards above the 105°C crustal isotherm. Farther north near Mount Waddington, and extensively in the Bella Coola-Ocean Falls area and farther north, dates over a width of nearly 40 km are 10 Ma or less. Younger dates are clearly more characteristic of the northern Coast Mountains area, which in this paper refers to that part between latitudes 52° and 55°N, northwest of Mount Waddington. The southern part, from 49° to 52°N, however, has higher summits and average altitude. In the northern part (Bella Coola and Skeena River traverses), the youngest dates are clearly displaced west from the axial area of highest topography and local relief. This may reflect more rapid erosion on the windward side of the mountains, and is not a feature produced by a thermal high.

Sea level zircon dates

Figure 5 shows the distribution of sea level or low

altitude zircon dates and contours. In general the pattern is a hybrid having similarities to both the apatite pattern and the pattern of K-Ar biotite dates (Figure 2), which have a blocking temperature of about 250°C (Harrison et al 1979, Harrison and McDougall 1980). Some zircon dates reflect rapid cooling of relatively high level plutons, especially along the east and west margins of the Coast Mountains, but large areas in the northern axial region clearly reflect uplift and cooling, many being younger than 40 Ma. In the northern Coast Mountains between Prince Rupert and Terrace, a large area was subject to Eocene metamorphic resetting and rapid uplift giving uniformly young K-Ar biotite dates (Hutchison 1970, Harrison et al 1979).

The young zircon dates mimic this pattern in the north but remain more erratic and older in the southern traverses, correlating more with local intrusive ages, as deduced by K-Ar dates. Zircon dates, as in the apatite pattern, are significantly older in the west than the east, reflecting both eastward decreasing age of plutonism and broadly sequential unroofing from west to east.

Variation of Dates with Altitude and Apparent Uplift Rates

Figures 4 and 5 do not in themselves allow a calculation of uplift rate unless an assumption of paleogeothermal gradient is made. To arrive at an estimate of uplift rate, low and high altitude samples and samples at closely spaced altitude intervals were dated. The location

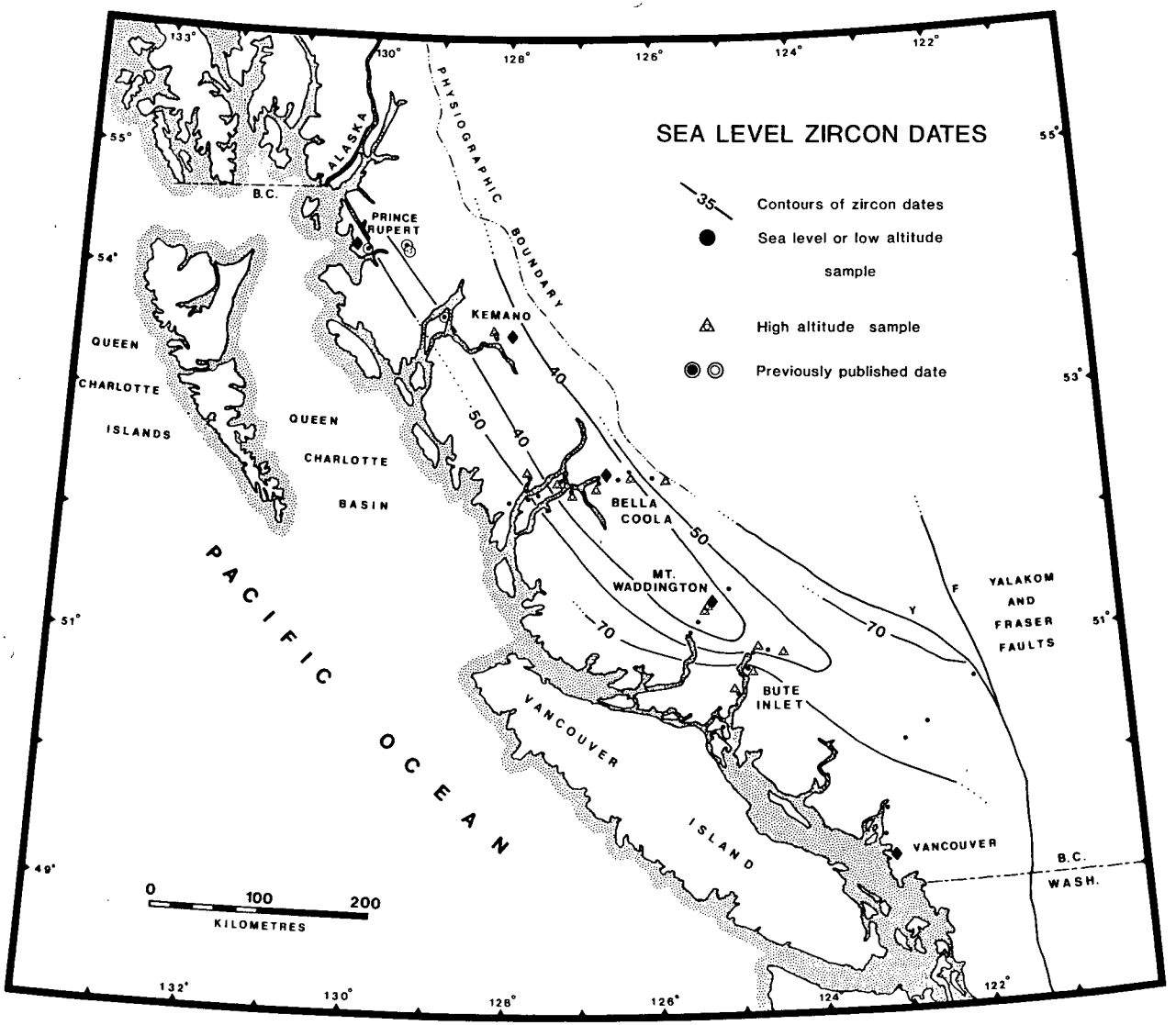

Figure 5. Sea level or low altitude fission track zircon dates.

of medium or high altitude samples is shown in Figure 3, 4, and 5.

Kemano

Six samples of foliated quartz diorite were collected at various altitudes on Powell Peak (Figure 1) by Glen Woodsworth of the Geological Survey of Canada. A total of twelve apatite and zircon dates were obtained and are shown in Figure 6a. Zircon and apatite dates vary from 44 to 36 Ma and 34 to 24 Ma, respectively, correlating well with altitude. Regressing the zircon data leads to a slope of about 0.25-0.30 km/Ma for the period 35-45 Ma. The 30-35 Ma slope on apatite data was assumed to be the same, but must flatten somewhat to accomodate the low altitude apatite data. The probable minimum slope is 0.1 km/Ma for the period 15-25 Ma, after which the rate increases to 0.15-0.20 km/Ma.

The present depth at which the apatites have a date of zero (i.e. at 105°C) was estimated according to the formula,

$$T(Z)=(Q^*Z/\kappa) + (D^2Ao/\kappa)(1-\exp(-Z/D)) + a$$

where T(Z) is the temperature at depth Z, below the average surface altitude, Q* is the reduced heat flow, κ is the conductivity, D is the scale height, Ao is the surface heat production, and a is the approximate mean atmospheric temperature at the average altitude. An exponentially downward decreasing heat production is assumed in this model

calculation. Values of Q*, κ, Ao, and D of 50 kW/km^2, 2.5 kW/km°C (5.98x10^{-3} cal/sec-cm-°C), 1.0 kW/km^3 (T.Lewis, personal communication 1980), and 10 km, respectively, were used. The average altitude, in the vicinity of Powell Peak, is 1.0 km and the probable mean annual temperature at that altitude is approximately 5°C, yielding a depth of -3.3 km for the 105°C apatite annealing isotherm. The effect of recent uplift will be to decrease this figure somewhat so that it should represent a maximum estimate of the zero-age depth.

At Kemano, the high altitude apatite curve and the low altitude zircon curve nearly overlap at 35 Ma. Using the relation of Parrish (1980), the difference in blocking temperature (175°-105°=70°) divided by the actual or projected altitude difference (2.9±0.6 km; error indicates the likely range) yields a paleogeothermal gradient of 26°+4°-6°/km at 35 Ma ago. The gradient of 26°/km is similar to the present value of 27°/km for the Stewart area to the northwest (Mathews 1972b). The Kemano data thus indicate rather low apparent uplift rates with a small increase in the last 10 or 15 Ma.

Northern King Island-Ocean Falls

Fission track dates are remarkably uniform in the northern King Island-Ocean Falls region (Figure 4). Included in this analysis are all dates from samples east of BBC-22 (Figure 3) and west of samples BBC-4 and BBC-11, a width of

about 25 km. All apatite and zircon dates from this area are shown on Figure 6b. Ten apatite and six zircon dates representing a vertical altitude difference of 2.1 km vary from 8 to 24 Ma and 34 to 39 Ma, respectively, and correlate very well with altitude. The K-Ar biotite dates for this area, recalculated with constants listed in Table IV, range from 58 to 89 Ma (Figure 2), except for the distinctly younger King Island syenite, which is 12-13 Ma old (Baer 1973).

It could be argued that this syenite was partly responsible for the young apatite dates; however, the fission track dates are very regular, do not vary with distance to the syenite, and at sea level are 3-4 Ma younger than the age of the syenite. A two-dimensional conductive heat flow model of an infinitely long dyke 6 km wide introduced at 750°C into rock at 0°C with its top and bottom at 2 and 10 km below the surface, respectively, was formulated according to Carslaw and Jaeger (1959). The conductivity for the model was assumed to be 2.5 kW/km°C (5.98×10^{-3} cal/sec-cm-°C). The nearest fission track sample is 9 km from the nearly straight margin of the syenite (Baer 1973), and the maximum rise in temperature for such a sample 3-4 km below the surface is about 8°C after 1 Ma and 15°C after 3 Ma. The farthest fission track samples are 20 km away, and their temperature increase related to intrusion is only about 5°C. If the syenite cooled predominantly by convection, the effect on the fission track samples would be

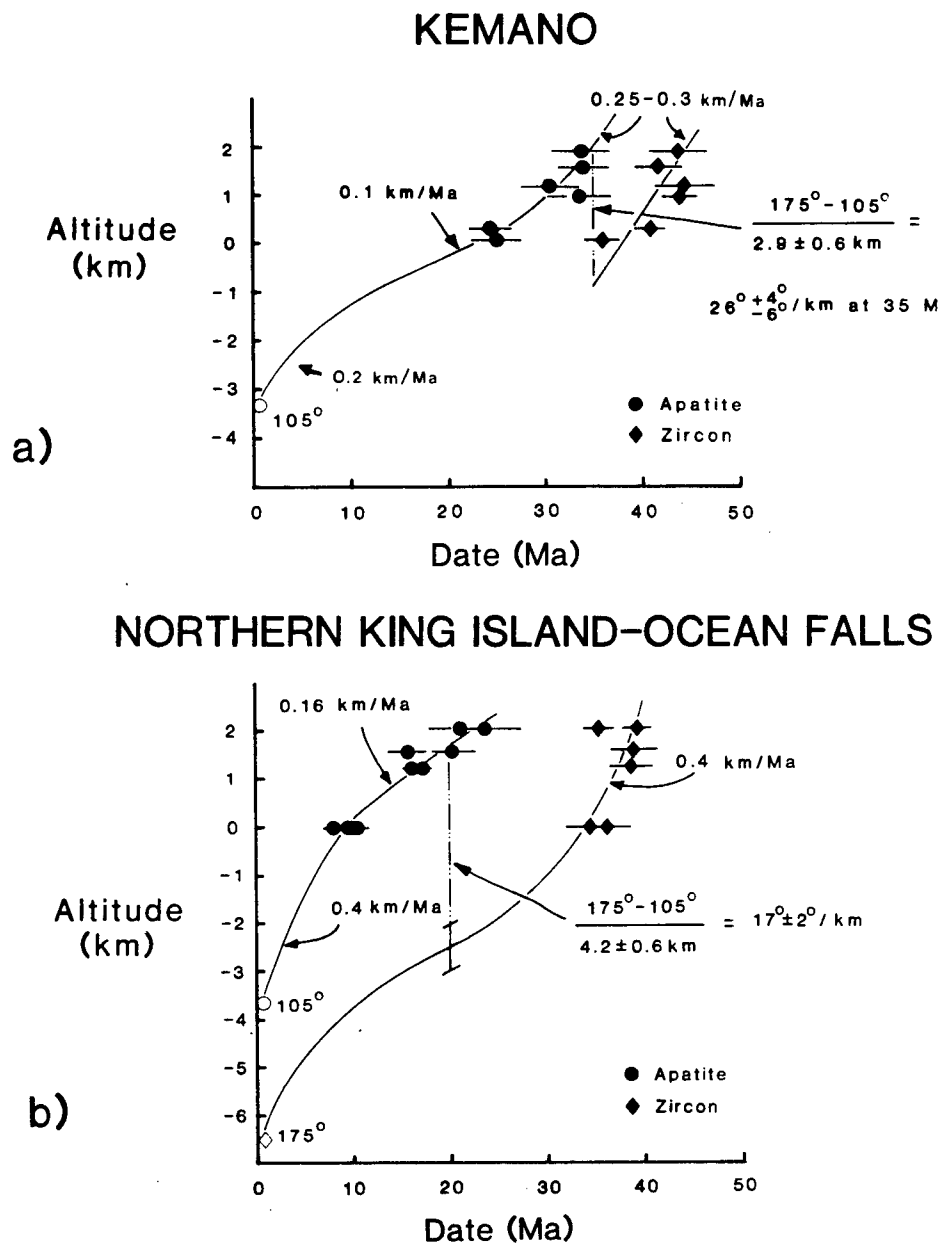

Figure 6. Fission track date vs. altitude for samples from Kemano (a) and northern King Island-Ocean Falls (b) areas. Sample numbers and analytical data are listed in Table III. The zero-date point below sea level was calculated according to a procedure discussed in the text.

even less. Since they preserve the same fission track dates, the effect of the intrusion is considered very minor, although it cannot be ignored completely.

The present depths of the 105° and 175° isotherms have been calculated using the same parameters as at Kemano, except that the average surface altitude is 0.6 km. The depths are -3.7 km for apatite and -6.6 km for zircon. Using both fission track data and these estimated depths of zero date, the apparent uplift rates are about 0.4 km/Ma for 30-40 Ma ago (zircon dates), 0.16 km/Ma for 12-24 Ma ago (apatite dates), and about 0.4 km/Ma in the last 10 Ma (Figure 6b). Extrapolation of the zircon curve yields an altitude difference and approximate error of 4.2±0.6 km for the zircon-apatite overlap at 20 Ma ago. This yields a rather low paleo-geothermal gradient of 17°±2°C/km. The present heat flow can be roughly estimated from preliminary ocean probe heat flow data obtained by the Earth Physics Branch (T.Lewis, R.Hyndman personal communication 1980). Uncorrected values of 34-75 kW/km^2 were obtained in Dean, Burke, and Bentinck Channels, and probably indicate somewhat higher gradients than obtained for 20 Ma ago by using fission track data. An average surface value of heat flow of 60 kW/km^2 was used in calculating the depths of zero-age temperatures, along with known surface heat production of about 1.0 kW/km^3 (T.Lewis unpublished data, 1980).

The apparent uplift rate values near northern King Island indicate that rates changed from 0.16 to 0.4 km/Ma at

about 10 Ma ago. The latter rate is nearly double the projected rate of Kemano for the same time interval.

Bella Coola Valley

Nearly all dates east of BBC-15 (Figure 3) are plotted in Figure 7a. The data fall into two groups: those from North Bentinck Arm (samples BBC-4 and BBC-11) and the rest. The North Bentinck Arm apatite dates are clearly transitional between the samples to the west and east and vary from 17-22 Ma over an altitude range of 1.9 km, giving an apparent uplift rate of 0.2-0.25 km/Ma from 20 Ma to the present. The data from Bella Coola Valley are more scattered, and the zircon and apatite dates are very similiar, probably indicating relatively high level rapid cooling, with considerable experimental scatter. Apparent uplift rates vary from 0.07 to 0.18 km/Ma for apatite. The zircon dates lack a clearcut younging with decreasing altitude. The apatite zero age depth varies from -2.8 km to -3.5 km, assuming the same geothermal parameters as in the Kemano model. An increase in the uplift rate in the Late Miocene cannot be documented, but could be accomodated if, for instance, the curves actually flatten between 30 and 10 Ma, and subsequently steepen again. Only samples from below present sea level could establish this alternate interpretation.

Mount Waddington

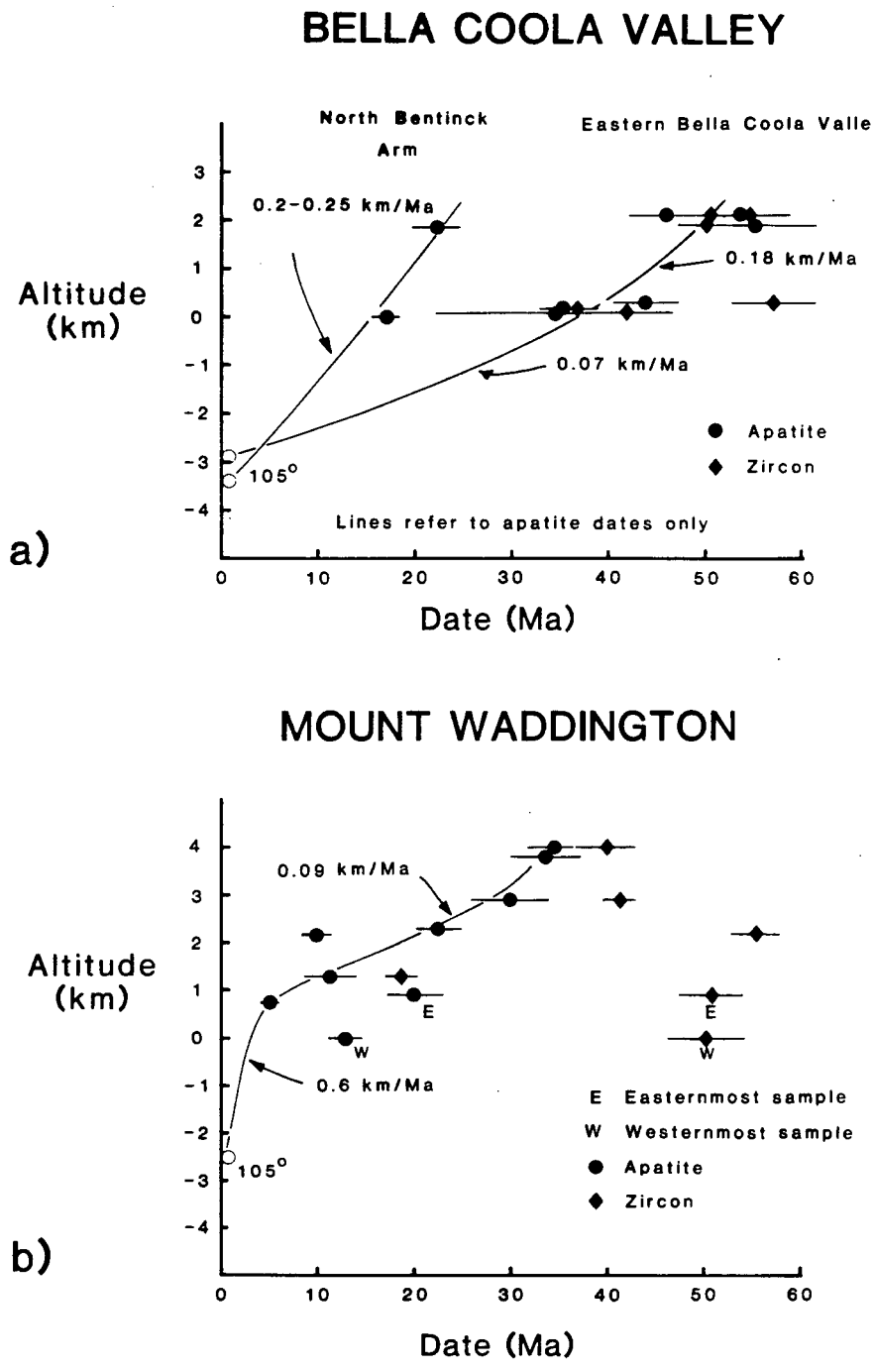

Figure 7. Fission track date vs. altitude for samples from Bella Coola Valley (a) and Mount Waddington (b). The E and W symbols in (b) refer to easternmost and westernmost samples, respectively. They are not considered when drawing the best fit curve through apatite data.

Samples from Mount Waddington, collected by Geological Survey of Canada personel from 1970-1979, range in altitude from sea level to the summit at nearly 4 km. Figure 7b shows 9 apatite and 6 zircon dates for the area. Because the samples were collected at distances of up to 40 km from the summit, there is clearly some geographic variation to account for. Dates marked E or W in Figure 7b are the easternmost and westernmost samples, respectively, and clearly fall off the main pattern. The remainder of apatite dates form a clear pattern of younging with decreasing altitude, ranging from 35 to 5 Ma over a 3.3 km altitude range. The zircon data, however, are much more scattered and difficult to interpret. The apparent uplift rate calculated from apatite data for the period 30-10 Ma is about 0.09 km/Ma. This slope appears to persist to 5 Ma. The average altitude of the area is 1.7 km, and assuming a reduced heat flow, Q*, of 40 kW/km^2 as well as the remainder of the Kemano geothermal parameters, the zero-age depth is about -2.5 km. Assuming this depth to be approximately correct, the apparent uplift rate from 5 Ma to present is about 0.6 km/Ma. These data clearly document the effect of latest Miocene-Recent uplift which produced the present relief. This uplift history is consistent with the unroofing of young (6.8 Ma) sub-volcanic plutons of the Franklin Glacier complex, 10 km southwest of Mount Waddington, (R.L. Armstrong and J.G. Souther, unpublished data) during the Pliocene and Pleistocene.

Central Bute Inlet

Data from Bute Inlet include rocks from Mount Sir Francis Drake and Cosmos Heights (Figure 1) and are summarized in Figure 8. Apatite dates vary from 76 to 42 Ma and yield an apparent uplift rate of 0.063 km/Ma for 75 to 40 Ma, and probably younger. The zero-age 105°C isotherm is about -4.8 km. It was derived using the Kemano parameters except that the assumed Q* and the average altitude are 30 kW/km^2 and 1.1 km, respectively. This results in a present low surface heat flow consistent with the data of Hyndman (1976) for the Bute Inlet area. The apparent uplift rate between 40 Ma and present is not constrained by fission track data and is drawn assuming an unchanged rate of 0.063 km/Ma until about 7-8 Ma. Although clearly not required by the data, this cooling history is consistent with the Late Miocene to Recent accelerated uplift indicated by the Mount Waddington, Ocean Falls, and Mount Raleigh data and the present physiography.

Mount Bute-Mount Raleigh area

East from the head of Bute Inlet, samples were analyzed from Mount Bute and Mount Raleigh (Figure 1). These dates are shown on Figure 9a, differentiated between the two areas. The apatite dates, which form a more consistent pattern than zircon, vary from 56 Ma to 8 Ma over an altitude range of nearly 3 km. Separate apatite lines are

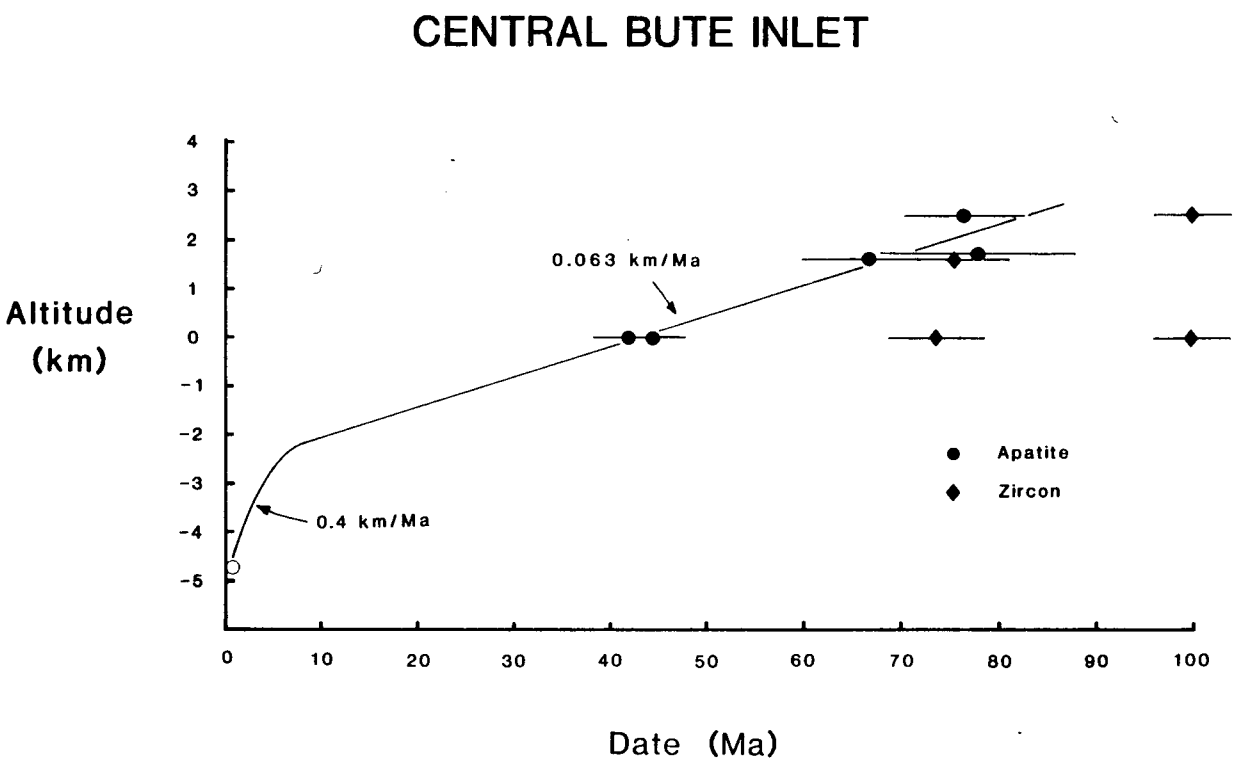

Figure 8. Fission track date vs. altitude for samples from central Bute Inlet. Only apatite data were used to define the curve.

shown on Figure 9a for Mount Raleigh and for Mount Bute. The Mount Raleigh apparent uplift rate varies from 0.1 km/Ma for the period 40-10 Ma, and increases to 0.4 km/Ma since 8 Ma. The Mount Bute data indicate a rate of 0.04 km/Ma from 40-10 Ma, although it is not particularly well-constrained. Since these two areas are nearly along strike and about 30 km distant from each other, their uplift histories are probably similiar, suggesting that the best apparent uplift rate value probably is an average of the two curves shown. The very young, 7.8 Ma, date below Mount Raleigh in the Southgate River valley probably dates the approximate time since inception of recent rapid uplift, and is consistent with very young, low altitude dates on Mount Waddington. Zero-age depths were calculated assuming Q* of 50 kW/km^2, an average altitude of 1.7 km, and other parameters as in the Kemano example. The >3 km relief in the area suggests very recent uplift and erosion, consistent with the fission track data.

Pemberton area

In the southern traverse, fission track dates are the oldest, none being less than about 40 Ma (Figure 4). Consequently, it is more difficult to document small differences in dates between samples at different altitudes. Samples from the Spetch Creek Pluton (Woodsworth 1977) in the Pemberton area (VL-6,-8,-9,) range from about 40-46 Ma over an altitude difference of 1.6 km, and show no

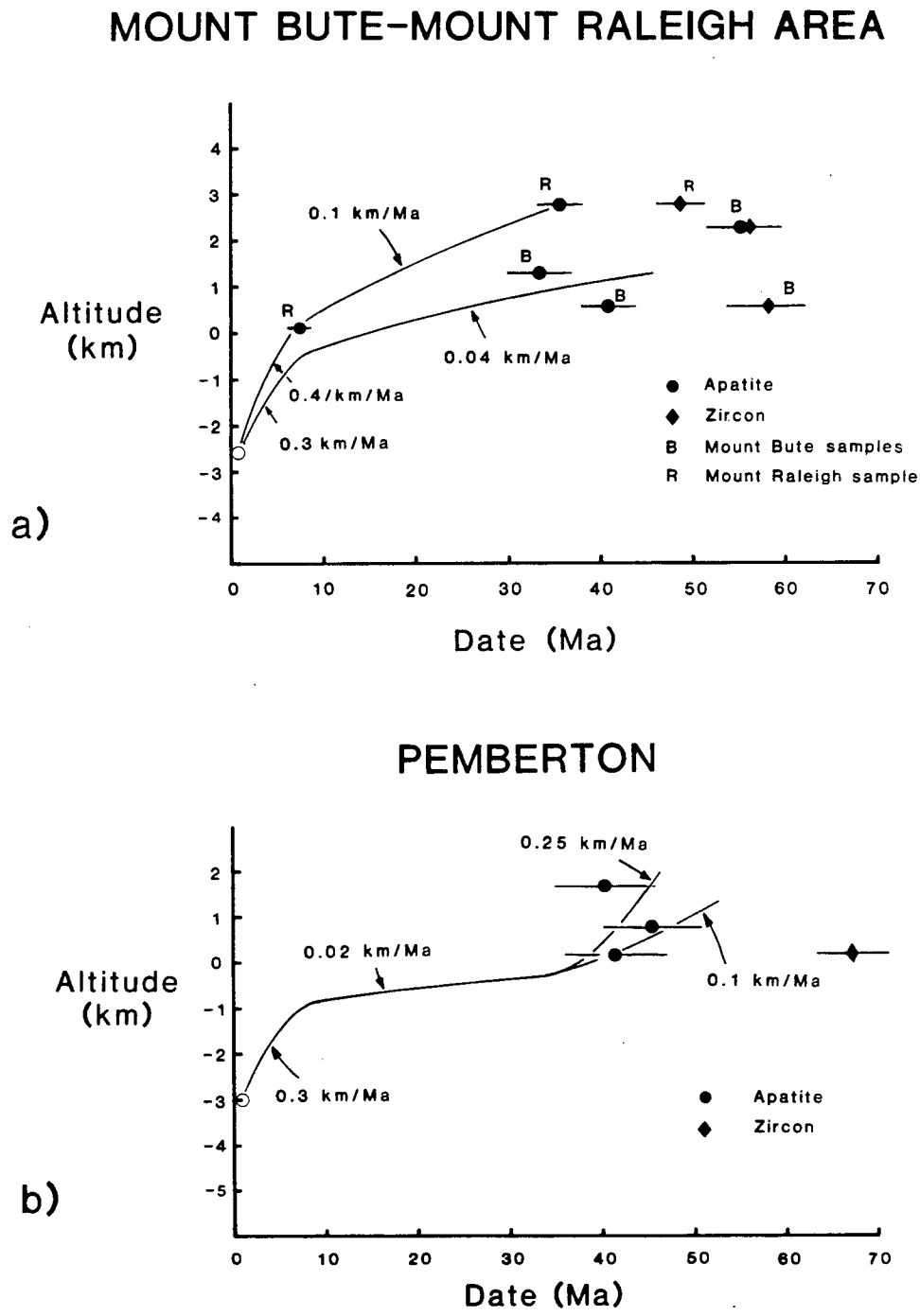

Figure 9. Fission track date vs. altitude for samples from Mount Bute (B) and Mount Raleigh (R), shown in (a), and Pemberton (b) areas. Only apatite data were used to define the curves.

demonstrable correlation with altitude (Figure 9b). The present zero-age depth for apatite is about -3 km assuming Q* of 50 kW/km^2 and an average altitude of about 1-1.2 km. Since Late Miocene-Recent uplift must be greater than 2 km on geologic and physiographic grounds, the apparent uplift curve has been drawn to take this into account. A consequence is a very low (0.02 km/Ma) apparent uplift rate from 35-10 Ma. The low altitude zircon date, 67.4 Ma, is close to the biotite and hornblende K-Ar dates of 86±3 and 77±4 respectively, and indicates fairly rapid cooling of the Spetch Creek Pluton. The cluster of 40-45 Ma dates could indicate a period of moderately rapid uplift during the Eocene. This Eocene uplift is also suggested by the 35-45 Ma low altitude dates that span nearly the entire width of the southern Coast Mountains (Figure 4).

The presence of thick Eocene nonmarine clastic deposits in the Fraser Lowland (Rouse et al 1975) and in northwest Washington (Frizzell 1979, Johnson 1981), adds additional support to this possibility.

Spatial and Temporal Variations of Apparent Uplift Rates

The assumptions involved in equating the apparent uplift rates derived from fission track studies with actual uplift rates have been briefly discussed earlier in this paper. The assumption most likely to cause large deviations is the stability, with respect to the surface, of isotherms during uplift. It is shown in Chapter 3 that this assumption

can rarely be met. In addition, making specific corrections to apparent uplift rates depends not only on the rates of uplift and erosion but also the heat production, reduced heat flow, and on the geologic history of the sample. For example, fictitous positive apparent uplift rates can be produced by a downward relaxation of isotherms following a period of high heat flow, rapid uplift and erosion. This may explain the higher apparent rates in the Mount Waddington, Kemano, and Ocean Falls areas (Figures 6a, 6b, 7b) during the Eocene, immediately following orogenic activity.

Despite these cautions in interpreting the fission track data, there are spatial and temporal patterns in the apparent rates which contain valuable geologic information.

Nearly all areas indicate a rather slow uplift in the middle Cenozoic from 30 to 15 Ma ago. Maximum rates during this time were in the northern axial region near Ocean Falls-Bella Coola and were up to 0.2 km/Ma. It appears that these smaller middle Cenozoic rates were maintained for at least 15 Ma in most areas. The rates in the southern part (Vancouver and Bute Inlet traverses) were definitely lower (maximum 0.1 km/Ma) and may have been virtually zero (Pemberton area).

The more rapid middle Cenozoic uplift in the north is synchronous with the sinking and consequent infilling of the adjacent Queen Charlotte basin, which developed mainly in Miocene time (Shouldice 1971). This basin terminates near the north tip of Vancouver Island, adjacent to the southern

Coast Mountains where middle Cenozoic uplift was low or nil. The middle Cenozoic Coast Mountains uplift and adjacent basin subsidence north of 51°N therefore appear to be related.

The Late Miocene-Recent apparent uplift rates are more rapid in the south (>0.6 km/Ma) than farther north (<0.4 km/Ma). In general, the northern samples show only modest evidence of late Cenozoic acceleration of uplift. These differences appear to correlate well with the physiography, in that the higher summits and more rugged topography are concentrated in the southern Coast Mountains.

Other supporting evidence for contrasting uplift histories comes from the relation of the Late Miocene plateau basalts to physiography along the eastern flank of the Coast Mountains. In the Taseko Lakes area (Tipper 1963,1978) the basalts were extruded on an erosion surface of low to moderate relief and subsequently tilted up in the west. Their basal altitude varies from about 3,500' (1.1 km) on the plateau to greater than 8,000' (2.4 km) southeast of Taseko Lakes. Farther north near Bella Coola, the basalts are essentially flat lying at 4,500'-5,000' (1.4-1.5 km) and flowed into valleys already developed beneath peaks which presently rise above 7,500' (2.3 km)(Baer 1973). The basalts in the north postdate the development of the mountainous physiography, whereas in the south they predate it.

Several samples of the basalt were collected from basal, columnar-jointed flows and were dated by the K-Ar

whole rock method. Most of these samples are from the west side of the basalt cover near the eastern margin of the Coast Mountains and are shown in Figure 3 and labelled as CC-2, -4, -5, -6, and -7 and BC-6. Analytical data are listed in Table IV. The ages of the flows sampled range from 6.0-9.9 Ma. Basal flows along the eastern flank of the Coast Mountains (CC-4,-5, -6) range from 7.6-9.9 Ma and demonstrate the essentially contemporaneous eruption of the plateau basalts along the eastern margin of the Coast Mountains. A basalt date of 14 Ma from the Taseko Lakes area (Farquharson and Stipp 1969) is of uncertain significance as it is in conflict with numerous dates on plateau basalts (Bevier and Armstrong unpublished data; Rouse and Mathews 1979). The broadly synchronous eruption of plateau lavas emphasizes the difference in existing Late Miocene physiography between north and south.

Estimates of Total Uplift

Values of total uplift since 40 Ma (Figure 10) and 10 Ma (Figure 11) have been estimated by a composite of three different methods: 1) by geologic control consisting of stratigraphic thicknesses and altitudes of projected unconformities and erosion surfaces, 2) by calculating the depth of the 40 Ma and 10 Ma 105°C apatite annealing isotherms based on an assumed 25°C/km gradient, and 3) estimating the depth of the 175°C 40 Ma zircon annealing isotherm using thermal models (Chapter 2) and subsequently

Table IV. K-Ar Analytical Data

Sample[1]	Latitude	Longitude	%K[8]	Ar^{40}*(x10-^{6}cc/gm)[9]	%rad.Ar^{40}	Date±s(Ma)[10]
BC-6[2]	52°05'30"	123°23'18"	0.337	0.0787	24.8	6.0±0.2
CC-2[3]	52°05'30"	123°23'18"	0.333	0.0815	17.2	6.3±0.3
CC-4[4]	52°25'30"	123°38'05"	0.995	0.3067	59.0	7.9±0.3
CC-5[5]	52°31'10"	125°49'35"	0.901	0.3478	61.3	9.9±0.3
CC-6[6]	52°32'50"	125°42'30"	0.784	0.2541	65.5	8.3±0.3
CC-7[7]	51°26'15"	123°39'10"	0.355	0.1051	30.3	7.6±0.3

---

[1] whole rock basalt, -30+50 mesh
[2] collected by M.L. Bevier from top of section at Bull Canyon on the Chilcotin River
[3] bottom of section, same locality as BC-6
[4] collected from the Precipice on the Hotnarko River, basal flow
[5] collected near mouth of north branch of Young Creek; contains plagioclase megacrysts (5 cm)
[6] erratic boulder from nearby bedrock at Heckman Pass; contains smaller plagioclase megacrysts (1.5 cm)
[7] collected near bottom of section of Taseko River basalts
[8] %K determined by atomic absorption by K. Scott, University of British Columbia
[9] Ar isotopic composition and concentration determined by J. Harakal, University of British Columbia
[10] constants: $\lambda b = 4.962 \times 10^{-10}$/yr; $\lambda e = 0.581 \times 10^{-10}$/yr; $^{40}K = 0.01167$atom %

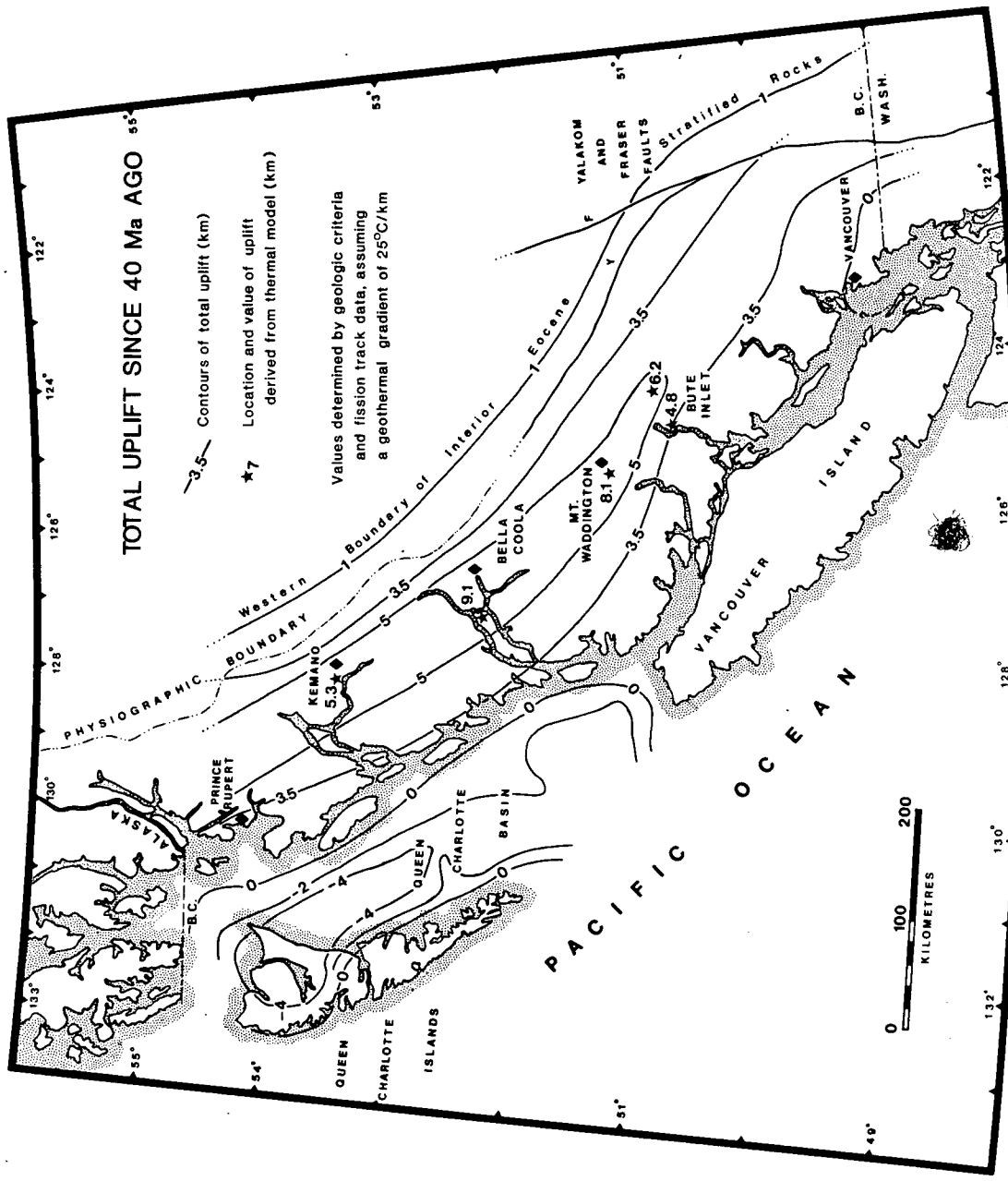

Figure 10. Total uplift, with respect to sea level, since 40 Ma ago (Late Eocene). The interpretation is made assuming a sea level land surface 40 Ma ago.

generalizing over the area.

Geological control comprises sediment thickness and subsidence data from the Queen Charlotte basin (Shouldice 1971) and Whatcom basin (Hopkins 1968), the basal altitude of Late Miocene plateau basalts or other volcanic rocks of Eocene (40 Ma) or Late Miocene (10 Ma) age on the eastern side of the Coast Mountains, and in places the altitudes of accordant summits.

Using surface temperatures (Rouse and Mathews 1979) of 20°C and 10°C, respectively, the depth to the 105°C isotherm for 40 Ma and 10 Ma sea level apatite dates gives a fairly accurate indication of total uplift even when a uniform gradient of about 25°C/km is assumed. Following Eocene orogeny in the north, gradients were much steeper, and no uniform gradient should be assumed when calculating depths to the 175°C zircon annealing isotherm. Heat flow models can correct for thermal relaxation and provide uplift estimates where geologic control is absent (see Chapter 2).

Uplift since 40 Ma

The presence of Eocene-Early Oligocene terrestrial stratified rocks at sea level, whether volcanic or sedimentary, indicates net subsidence since 40 Ma. Such areas include the northern Queen Charlotte Islands and part of Hecate Strait underlain by the Masset Formation, part of which may be as old as Late Eocene (Sutherland Brown 1968, Young 1981), the Whatcom basin near Vancouver which contains

Late Cretaceous, Eocene, and younger Cenozoic strata (Hopkins 1966, Rouse et al 1975, Johnson 1981), and the western Interior Plateau where Eocene volcanic and sedimentary rocks are preserved (Ewing 1980, Souther 1977) at 0-1 km altitude. No such strata are preserved within the Coast Mountains.

The values of uplift derived from 40 Ma zircon and apatite contours are approximately 5-6 km and 3.5 km, respectively (Figure 10). Subsidence estimates in the northern Queen Charlotte Islands and Hecate Strait, shown in Figure 10, are based on the cumulative thickness of late Cenozoic sediments (Shouldice 1971) and the underlying Oligocene-Miocene Masset Formation (Sutherland Brown 1968, Young 1981). Because the basal age of the Masset volcanics may be both time-transgressive and younger than 40 Ma, the estimate of uplift since 40 Ma may be somewhat in error. New information on structure and subsidence in southern Queen Charlotte basin (Yorath and Chase 1981) may require modifications to the pattern shown in Figure 10.

There is clear evidence that the northern portion (latitude 52° to 55°N) has been elevated more than the southern Coast Mountains since Late Eocene time. The difference would be even more dramatic if Paleocene uplift was taken into account (see Hollister 1979).

Uplift since 10 Ma

The total uplift since 10 Ma is shown in Figure 11. The

3.5 km contour follows the 10 Ma apatite contour and represents the approximate depth of the 105°C isotherm 10 Ma ago. Values of uplift determined using thermal models (Chapter 2) are also shown.

Subsidence in the Queen Charlotte basin is the depth below sea level of the Miocene-Pliocene boundary (Shouldice 1971). This may be an underestimate because this time span involved (6 Ma) is somewhat less than 10 Ma. Estimates for the westernmost Queen Charlotte Islands and Vancouver Island are based upon the altitudes of summits which may represent a former erosion surface of Miocene age (Mathews 1968). The presence of Late Miocene to Pliocene volcanic rocks (Muller et al 1974) and sediments (Cox 1962) around the perimeter of Vancouver Island broadly supports this conclusion. Whatcom basin was probably a continuous site of deposition and subsidence during the Neogene (Hopkins 1968). Finally, volcanic rocks of Middle and Late Miocene age in the eastern fringe of the Coast Mountains and in the Pemberton Volcanic Belt provide estimates of the altitude of the pre-eruptive land surface. These include plateau basalts less than 10 Ma old (see Table IV), unroofed 8 Ma plutonic rocks (Wanless et al 1979) and erosional unfaulted remnants of lavas (Woodsworth 1977, Baer 1973, Berman and Armstrong 1980, Mathews et al 1981) within the Pemberton and Anahim Volcanic Belts.

The area of maximum late Neogene uplift occupies the central part of the Coast Mountains from the head of Bute

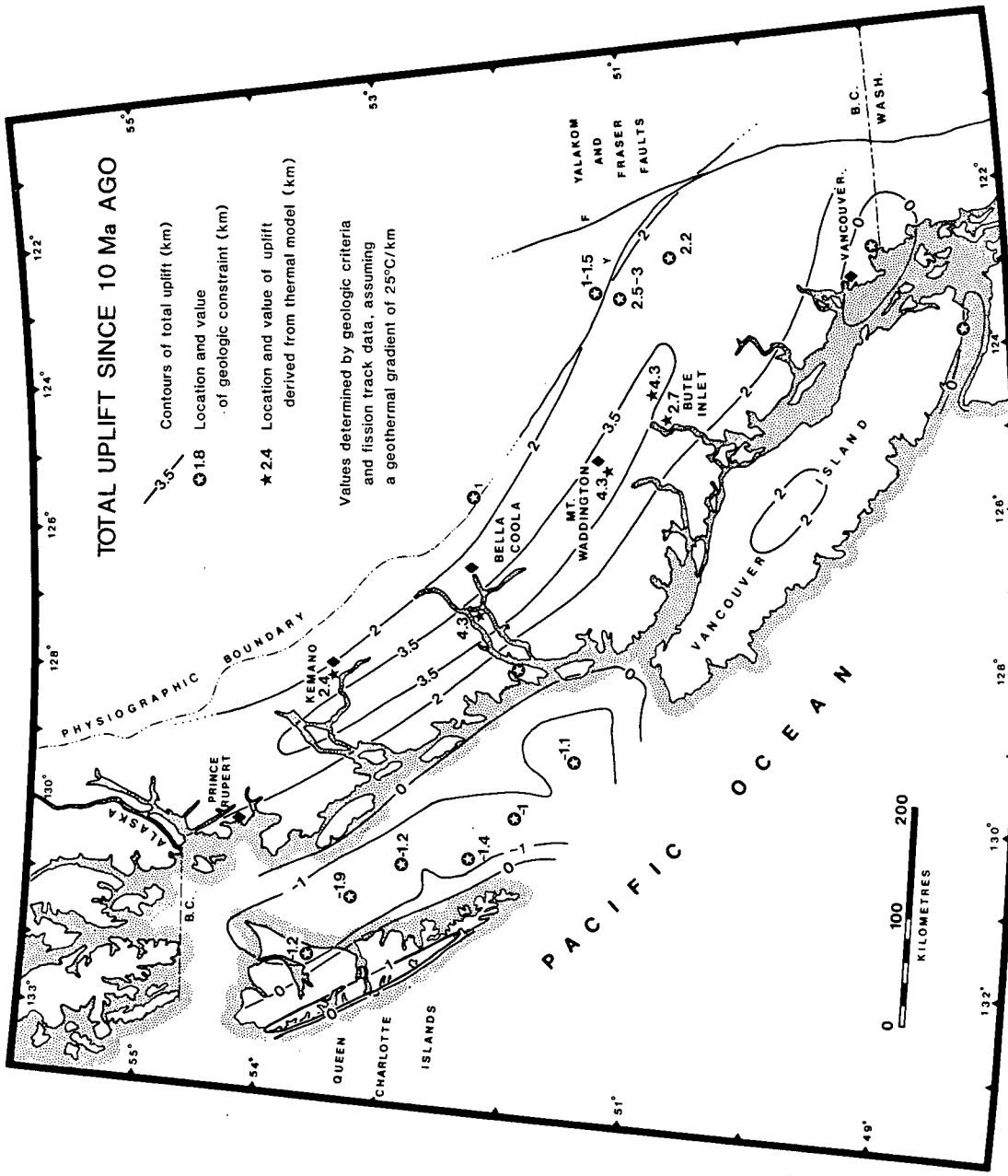

Figure 11. Total uplift, with respect to sea level, since 10 Ma ago (Late Miocene). The interpretation is made assuming a sea level land surface 10 Ma ago. This assumption is probably reasonable in the southern Coast Mountains, but must be considered with caution in the north where Late Miocene paleo-relief and altitude were considerable. The uplift figures in the north, therefore, are maximum values.

Inlet to Hawkesbury Island (Figure 1). Though the total amounts of uplift between the Mount Waddington-Bute Inlet area and the King Island-Kemano area are comparable (about 3.0-3.5 km), the present relief is considerably higher in the south (Holland 1964). This indicates that the age of most of the uplift in the north is predominately Late Miocene whereas in the south it is mostly Pliocene-Pleistocene. The area of maximum uplift in the Bella Coola-Kemano portion of the Coast Mountains is offset westwards at least 20 km from the highest altitudes and relief. This may be a result of more rapid erosion on the windward side of the mountains, as well as proximity to base level. Since both average and summit altitudes in the King Island area are considerably less (<2 km) than the uplift since 10 Ma (3.5 km), it is clear that erosion is keeping pace with uplift. This situation is not yet met in the south where the summit altitudes (>3 km) are approximately the altitude of the 10 Ma surface. There, the effects of more recent uplift are still very apparent, and this suggests that topographic relief of >3 km may be preserved only in mountain systems that are but a few million years old.

Miocene Paleogeography

Evidence from sedimentary and volcanic deposits when combined with data for uplift rate and amount allow the Miocene paleogeography to be accurately reconstructed. This reconstruction is shown in Figure 12.

The reconstruction depicts events about 15-20 Ma ago, but also shows the distribution of all post-Eocene, pre-Pliocene igneous rocks.

Many of the features of Middle Miocene paleogeography have been briefly discussed already. One of the main features is the contrast between the northern (52° to 55°N) and southern (49° to 52°N) Coast Mountains. Higher uplift rates (up to 0.2 km/Ma) in the north resulted in the maintenance of a mountain system of perhaps 1.5 km relief through the Cenozoic (Miocene Coast Mountains). The data of Rouse and Mathews (1979) require little climatic influence of the ancestral Coast Mountains until Late Miocene or Pliocene time; therefore, summit altitudes must have been considerably less than today. Adjacent to and probably linked with this uplift was the Queen Charlotte basin that received sediment derived from both the adjacent mountains and the Queen Charlotte Islands. Both the Sandspit and Queen Charlotte faults may have been active, as the Queen Charlotte Islands moved northwesterly with some rotation (Yorath and Chase 1981). Volcanism and rifting associated with the Anahim Volcanic Belt probably contributed to the unstable tectonics of the region. It seems likely that the coastal region northwards from northern Vancouver Island was

bounded on the west, as it is today, by a complex hot-spot and transform fault system not present adjacent to the southern Coast Mountains (Riddihough 1977).

The southern Coast Mountains, adjacent to the Juan de Fuca plate, were the site of low topography and scattered volcanic activity of the Pemberton Volcanic Belt. The Whatcom basin was subsiding (Hopkins 1968), but it is not clear where the northwest and southwest margins of this basin were, as Miocene sediments are only locally present in the Strait of Georgia. Miocene sediments on the southern coast of Vancouver Island indicate that at least in the south, Vancouver Island was low and partially submerged (Cox 1962).

The bulk of the Interior Plateau flood basalts was extruded between 6 and 10 Ma ago (Table IV; Rouse and Mathews 1979, M.L. Bevier and R.L. Armstrong unpublished data). These basalts filled in valleys which were the sites of the ancestral Fraser River and its tributaries (Rouse and Mathews 1979) and covered large areas of low relief both within the Interior Plateau and along the eastern flank of the Coast Mountains in the Taseko Lakes area. Farther north in the Bella Coola area, these basalts flowed into broad valleys adjacent to the Miocene Coast Mountains (Baer 1973). The contemporaneous peralkaline volcanics of the east-west Anahim Volcanic Belt were superimposed upon this setting, building several large shield volcanoes (Bevier et al 1979). Little evidence of paleo-relief is preserved in the present

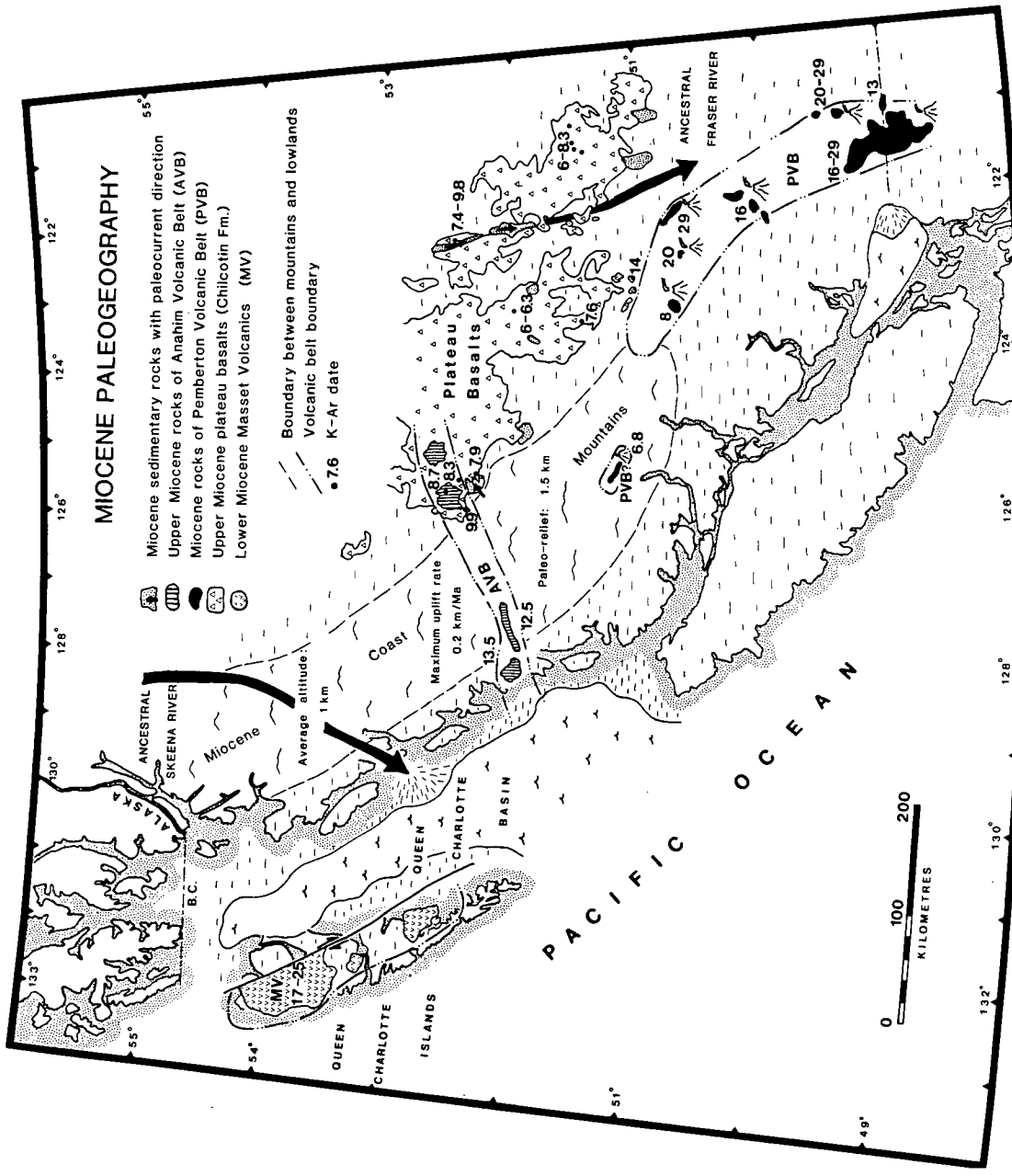

Figure 12. Miocene paleogeography. Included are all Miocene igneous rocks, areas of Miocene sedimentation, and estimates of average altitude and paleo-relief in the northern part.

southern Coast Mountains because only a few unfaulted remnants of Miocene lava remain. Where preserved, they are generally at high altitudes (> 2 km). East of the Fraser fault, several more silicic Miocene eruptive complexes were active (Berman and Armstrong 1980, Mathews et al 1981), and because of less subsequent uplift, volcanic rocks of these complexes are relatively well-preserved.

Perhaps the most surprising aspect of this Miocene tectonic setting is the negative correlation between uplift (confined to the north) and calc-alkaline volcanism related to subduction (the Pemberton Volcanic Belt). They appear to be mutually exclusive. The uplift in the south almost entirely post-dated these Middle and Late Miocene igneous rocks.

Neogene Erosion Surfaces and Deformation

During the middle Cenozoic considerable erosion occurred, especially in the northern Coast Mountains, where up to 4 km of rock was stripped. In the Interior Plateau, this period of erosion resulted in a very subdued land surface occasionally interrupted by resistant hills and broad river valleys. Plateau basalts flowed over this landscape to preserve its characteristics.

Various authors have suggested that extensions of this Interior erosion surface existed across the area of the present Coast Mountains. Arguments in favor of such a surface consist of rock shoulders in the mountains at the

approximate level of the Interior surface (Baer 1973), accordance of summits throughout large areas of the mountains (Culbert 1971, Holland 1964), the low relief Milbanke strandflat which contains Miocene volcanic and plutonic rocks (Baer 1973, Holland 1964), and the relatively flat gently east-dipping basal contact of the plateau lavas in the Taseko Lakes area (Tipper 1978).

The fission track data and the physiographic and geologic evidence indicate that this concept is too simple. For instance, if as Baer (1973) suggests in the Bella Coola area, the erosion surface crosses the mountains at maximum altitudes of 5,000'-6,000' (1.5-1.8 km), then regional thermal gradients would have to have exceeded 60°C/km to explain 8-10 Ma sea level apatite dates 1.5 km beneath a surface upon which 8-10 Ma basalts were extruded.

The suggestion that there are remnants of an erosion surface or surfaces within the Coast Mountains does indeed have merit. To explore this further, aerial photographs of the eastern flank of the Coast Mountains from latitude 51° to 53°N were examined. In this transition between mountains and plateau there are many examples of low relief, gently inland-sloping upland surfaces ranging in altitude from 5000' to 8000' (1.5 to 2.4 km). These surfaces cut across lithology indiscriminantly, and are variably dissected by cirques and other recent erosional features. The distribution of these surfaces is shown in Figure 13b, along with approximate altitudes.

In the southern area near Taseko Lakes, these surfaces are largely constructed on plateau basalts and in places are clearly controlled by their layering. The altitude of the surface gradually declines northeastwards and smoothly merges with the modern Interior Plateau. For the most part, these surfaces postdate the basalts.

As these surfaces are traced northwards near the headwaters of the Klinaklini River, their characteristics change. They are no longer built on Late Miocene basalt; in fact, the basalt is present only on the plateau to the east, several thousand feet lower in altitude. Elegant examples of "biscuit-board" topography developed on granitic rocks are present west of Tatla Lake and lie well above the present Interior Plateau. These upland surfaces do not smoothly merge with the Interior Plateau as in the Taseko Lakes area, and as they are higher in altitude and would project above the basalts, some of these surfaces must be remnants of an older erosion surface, one that predates the plateau basalts. Their age, however, remains unclear as apparently no geologic deposits overlie them.

Farther north, near the eastern Bella Coola Valley, there is an erosion surface of Late Miocene age that both underlies the basalt and extends westwards where the lavas have been eroded (Baer 1973). Mountains which rise up to 1.5 km above this surface represent monadnocks and extensions of the Miocene Coast Mountains into the Interior Plateau. These easternmost mountains are rounded and in

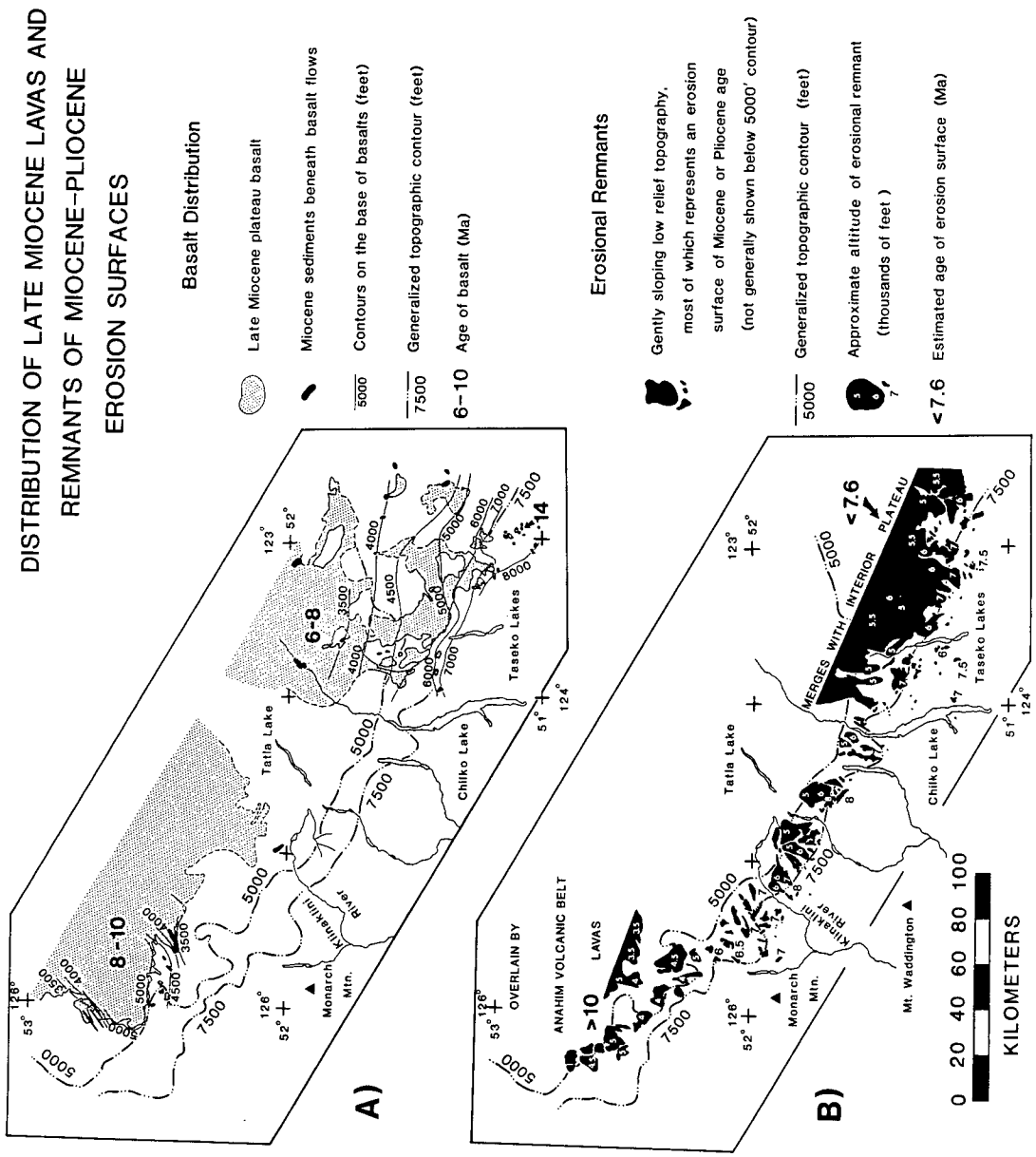

Figure 13. Distribution of Late Miocene lavas (a) and remnants of Miocene-Pliocene erosion surfaces (b). Figure (a) is compiled from Tipper (1969, 1978) and 1:250,000 topographic maps. Figure (b) has been constructed from aerial photographs and topographic maps. Gently sloping smooth topography, shown in solid black, is only shown on the mountain fringe and not on the Interior Plateau area.

places have pediment-like lower slopes that merge with the relatively flat sub-basalt surface. In this area the sub-basalt erosion surface which lies about 5,000' (1.5 km) in altitude penetrates deeply (20 km) into the Coast Mountains and has been little modified by Late Miocene-Pliocene uplift. The westward extension of the Late Miocene erosion surface must pass well over the summits of the peaks in the northern King Island-Ocean Falls area, probably at an altitude of 3-3.5 km. Clearly, the accordance of summits in this area must have a different explanation than simply representing relicts of a single Late Miocene erosion surface.

The distribution of Late Miocene basalts and low relief upland surfaces can be compared in Figures 13a and 13b. Except for minor faulting probably associated with the Anahim Volcanic Belt (Baer 1973) the plateau basalts in the north are essentially flat lying at 4,500'±500' (1.4±0.2 km) and partly surrounded by higher topography that contains older remnant surfaces. In contrast, the lavas in the south are largely coextensive with the low relief surface, and they are distinctly bent up towards the southwest at the edge of the Coast Mountains. The 6 to 10 Ma lavas predate the topography in the south whereas they postdate much of it in the north. In this respect they demonstrate the contrast in post-Late Miocene tectonic history from north to south.

By contouring the altitude of the base of the basalts (Figure 13a), it is possible to evaluate the gross structure

of the late Neogene deformation in the southern Coast Mountains. Assuming the basal lavas were extruded on a more or less horizontal surface, the structural relief is estimated to be about 1.3 km. The lavas rise to more than 8000' (2.4 km) in a fairly smooth, apparently unbroken gradient with minor low amplitude undulations. Farther southwest within the Pemberton Volcanic Belt near Bralorne and Lillooet Lake are Miocene volcanic rocks (Woodsworth 1977) at about 7,500' (2.3 km). This suggests that the pre-Late Miocene (>10 Ma) land surface on which the rocks were extruded flattens over the southern Coast Mountains in a high plateau-like manner before dropping into the Strait of Georgia-Whatcom basin area. Thus the form of the deformation may be a gentle monocline on the east and perhaps also the west side. As yet there is little evidence to suggest that faulting has played an important role in this Pliocene-Pleistocene uplift.

That the Neogene uplift in the southern Coast Mountains is both Pliocene-Pleistocene in age and similiar to a broad plateau-like uplift is supported by the general physiography of the area. The summit altitudes in the Coast Mountains have been contoured and are shown in Figure 14 to illustrate this point. A broad >100 km wide area in the south has summits over 2-3 km in altitude with smooth gradients, especially on the southwest side. Because the uplift is relatively recent, it is more likely that the surface of summit altitudes in the south (49° to 52°N) reflects a

pre-uplift erosion surface than in the northern (52° to 55°N) area. Significantly, the unfaulted volcanic rocks of the Pemberton Volcanic Belt, though few, lie roughly at the same altitude as this surface.

In contrast the summit surface is considerably lower and more irregular north of 51°N (Figure 14). Only a small portion of the northern region lies above 2 km, and several of the main fjords and channels coincide with broad embayments which may in part be related to Miocene to Pliocene erosion, modified by later glaciation. The main embayment along Douglas Channel may represent the location of the ancestral Skeena River. A suggested paleo-drainage pattern of the Skeena River is shown diagramatically in Figure 12. There is, however, no direct evidence in support of this suggestion. The more irregular, embayed, and generally lower summit surface pattern suggests greater ancestry of relief and drainage patterns in the north.

Both the Queen Charlotte Islands and Vancouver Island have relatively smooth summit surfaces and probably reflect Pliocene-Pleistocene uplift of a relatively low relief land surface. Essentially flat lying Pliocene volcanic rocks of the Alert Bay Volcanic Belt, described by Muller et al (1974) and dated by the Geological Survey of Canada and University of British Columbia, lie on a fairly smooth surface and are consistent with this conclusion. Seismic and gravity data on Vancouver Island (Keen and Hyndman 1979) suggest a tectonic, subduction related, mechanism for the

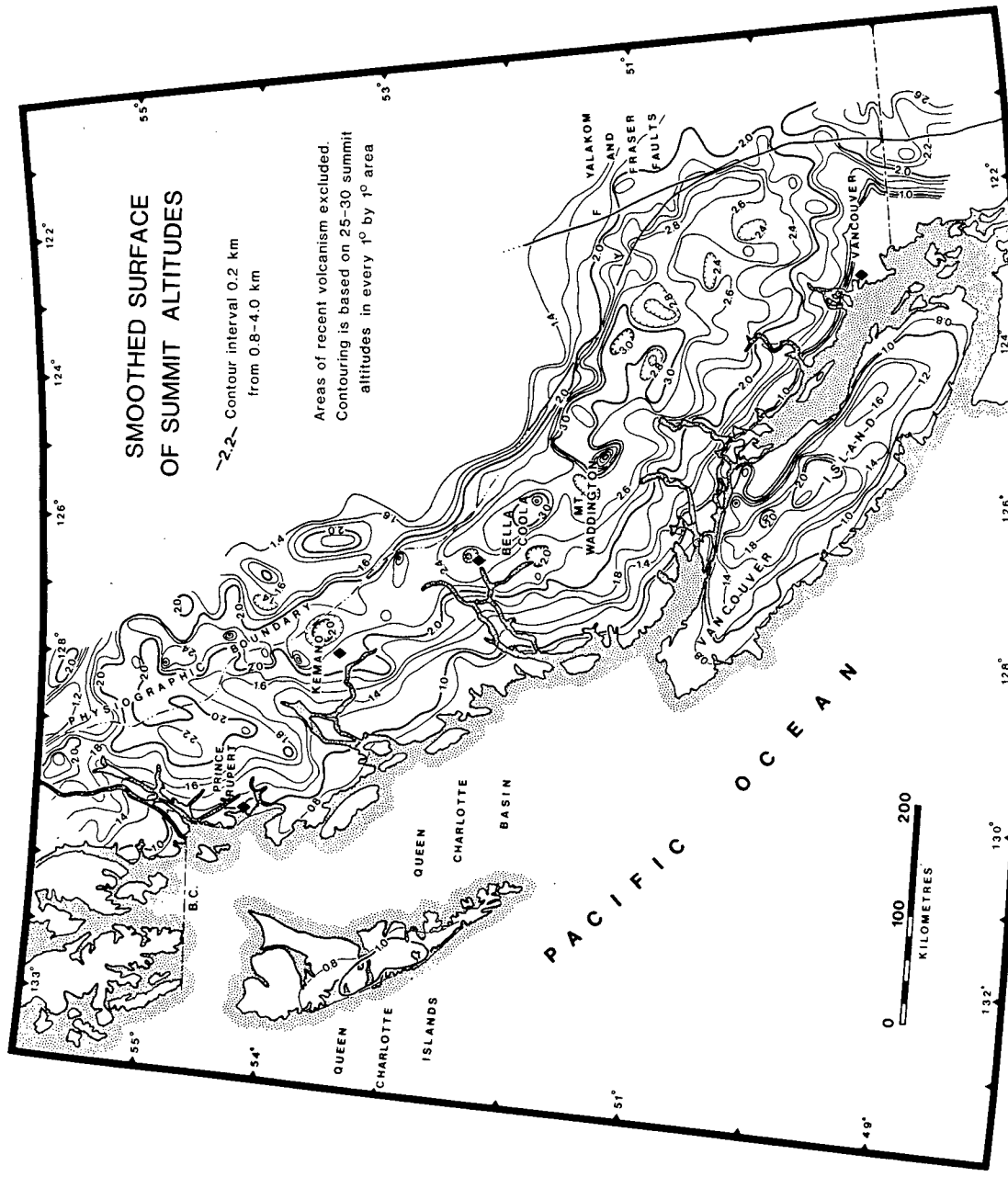

Figure 14. Smoothed surface of summit altitudes in the Coast Mountains. Recent volcanic summits are excluded. The map was constructed using 1:500,000 topographic maps by measuring about 25-30 summits per 1^{o}x1^{o} area.

recent and continuing uplift there.

Culbert (1971) presented an interpretation of physiography in the Coast Mountains based on a computer-assisted contouring of summit altitudes and concluded that a boundary, termed the axial fracture, separated areas of block uplift to the east from subsided areas to the west. This axial fracture was postulated to join the heads of Howe Sound, Jervis Inlet and Bute Inlet (Figure 1), and it coincides with the location of several hot springs. He also suggested that the transverse Bella Coola Valley bounded an uplifted block to the south. None of these features can be easily recognized on Figure 14. Unfortunately no direct comparison of summit contour maps is possible because no corresponding map was presented by Culbert (1971). The coincidence of thermal springs with this linear "axial fracture" may be related to it being an area of steepest thermal gradients resulting from maximum topographic relief, large uplift, and northwest structural trends, in a manner similiar to the development of hotsprings in New Zealand's Southern Alps (Allis et al 1979), although higher regional heat flow may also contribute (Hyndman 1976). Block faulting could aid convective hydrothermal transport of heat to explain the steep heat flow gradient of Lewis and Hyndman (1980), but no such fault(s) has yet been recognized, either physiographically or geologically.

In summary, the contrasts between the northern (52° to

55°N) and southern (49° to 52°N) Coast Mountains, apparent in the fission track data, are borne out by physiographic evidence. A presently higher altitude, plateau-like summit surface with remnants of Late Miocene lavas is characteristic of the southern region. In contrast, the northern region was never plateau-like; it has undergone continuous uplift during the middle and late Cenozoic, and probably contains erosion surfaces that are of several ages. Embayments in the northern summit surface may indicate the Miocene position of large valleys.

Discussion and Possible Causes of Uplift

There are three Cenozoic uplift stages in the Coast Mountains of British Columbia which can be distinguished. The first was an intense orogenic to post-orogenic uplift in the central and eastern Coast Plutonic Complex extending from Alaska southeastward. Discussion of this major event is beyond the scope of this paper; it is reviewed by Hollister (1979). The second stage was the less rapid middle Cenozoic uplift in the axial part of the Coast Mountains extending from southeast Alaska to the Mount Waddington area. This stage was responsible for the erosion of several kilometers of material from the northern Coast Mountains and the complementary subsidence of the Queen Charlotte basin. The third stage, of late Neogene age, involved rapid Pliocene to Recent uplift (>3 km) of the southern Coast Mountains over a broad region giving rise to the present topography. This

late Neogene uplift was manifest to a lesser degree in the northern area where it probably began in the Late Miocene.

Explanations for the Eocene orogenic event involve the interaction of the America and Farallon plates along a destructive margin. The intense Eocene event in the north-central Coast Mountains of British Columbia (latitude 52^{o}-56^{o}N) involved voluminous production of magma and rapid crustal thickening related to regional shortening during the final period of rapid convergence. Since Eocene erosion amounted to > 10 km, and perhaps significantly more (Hollister 1979), the crust must have been exceptionally thickened.

The ensuing middle Cenozoic uplift is coextensive with the Eocene event in the Coast Plutonic Complex and may be related. Assuming the formation of a large crustal root supporting high mountains during the Eocene, the present lack of such a thick crust (Berry and Forsyth 1975) indicates that it has been eroded. The linked process of erosion, diminishing uplift, and resultant crustal thinning would likely take several tens of million years to eliminate such a root. This process is thought to be responsible for the middle Cenozoic uplift stage in the northern and central Coast Mountains. The lack of a thermal high manifest in either volcanic activity or steep paleogeothermal gradients suggests that the uplift does not have a deep-seated thermal explanation. The linear arch-like form of the uplift is approximately what would be expected from an isostatic

recovery mechanism.

Other explanations are possible and could involve continued less intense oblique subduction throughout the middle Cenozoic. However, there is no middle Cenozoic volcanic expression except for the Anahim Volcanic Belt, and this possibility seems unlikely.

An explanation for the late Neogene acceleration of uplift, especially in the south, is much more elusive. Features that must be explained are: 1) >3 km of probably Pliocene-Pleistocene uplift over nearly the entire width of the southern Coast Mountains from about latitude 52°N southwards to the Fraser Valley, and 2) the moderate late Neogene uplift in the northern Coast Mountains axial zone, western Queen Charlotte Islands, and Vancouver Island.

Observations which should be considered are 1) the hiatus in calc-alkaline volcanic activity between >7 Ma activity of the Pemberton Volcanic Belt and the <2 Ma events in the Garibaldi Volcanic Belt (Bevier et al 1979, Berman and Armstrong 1980), 2) the subsequent development of the transverse, 'plate edge', Pliocene Alert Bay Volcanic Belt, 3) the changes at about 5 Ma in the relative velocity and orientation of convergence between Explorer and America plates (Riddihough 1977), and 4) the coincidence of the broadest and highest late Neogene uplift with the area on the mainland opposite the convergent boundary.

The production of 2-3 km of crustal uplift while maintaining isostatic equilibrium can be produced by several

mechanisms: crustal thickening by compression, as in South Island New Zealand (Walcott 1978) or the Himalaya (Molnar and Tapponier 1977); by underplating a large amount of low density arc-related magmatic material; or by thinning of the lithosphere as in the Basin and Range province of the western United States.

The most significant correlations with the uplift of the southern Coast Mountains are the reorientation of Juan de Fuca-Explorer-America plate motions about 5 Ma ago and the volcanic arc hiatus between 7 and 2 Ma. During this hiatus, the position of the volcanic front migrated westward to the Garibaldi Volcanic Belt (Figure 1), probably in response to steepening of the subducted slab. This westward jump would lead to warming of the formerly cool lithosphere causing thermal expansion and uplift beneath the Coast Mountains. The subduction of very hot (0-15 Ma) oceanic crust (Riddihough 1977) would certainly contribute to the high altitude of the overriding plate especially relative to the nonconvergent area to the north (Stacey 1974).

The less rapid predominately Late Miocene uplift in the northern part of the Coast Mountains is enigmatic since it is adjacent to a transform boundary and has no association with volcanic activity. Fission-track paleogeothermal gradient data and present heat flow estimates (T. Lewis unpublished data) indicate higher regional heat flow presently than 20 Ma ago, although this may be more related to the Anahim Volcanic Belt than a regional pattern. Whether

the thermal expansion caused by this hot spot could induce a longitudinal uplift in the north (52° to 55°N) is unclear and deserves further study.

Summary

Geological and physiographic data indicate that the Coast Mountains of British Columbia are predominately the result of vigorous late Neogene uplift. Quantitative examination of this uplift has been made possible by fission-track dating of apatite and zircon from rocks collected at various locations and altitudes in the Coast Mountains.

Uplift rates have varied in space and time, and estimates of total uplift have been calculated for the entire region. These results document significant middle Cenozoic uplift in the northern (52° to 55°N) Coast Mountains which was closely related to subsidence of the adjacent Queen Charlotte basin. Reconstruction of Miocene paleogeography using fission track data shows that the distribution of relief in the Miocene was opposite to the present situation of higher relief in the south; average altitudes in both areas, however, were lower. Estimates of paleo-geothermal gradients using detailed fission track date vs. altitude profiles indicate that the regional pattern of reduced heat flow may have varied considerably with time.

Explanations for the uplift are clearer for the two older (Eocene and middle Cenozoic) stages than for the

youngest (Late Miocene to Recent). Eocene orogenesis and crustal thickening in the northern Coast Mountains from latitude 52°-56°N was followed by a transition from a convergent to a strike-slip plate tectonic regime. Moderate but steady erosion and isostatic uplift in the Miocene and into the late Neogene gradually thinned the crust so that its present thickness is similar to stable continental crust.

During the middle Cenozoic the southern Coast Mountains were low in altitude and relief and subject to minimal uplift, despite subduction and intermittent volcanic activity above the subducting Juan de Fuca plate. In late Miocene or early Pliocene time, during a reorganization of Juan de Fuca - Explorer plate geometry and a volcanic arc hiatus in the Coast Mountains, uplift accelerated across the width of the southern Coast Mountains, leading to the present dramatic topography. This southern uplift is thought to be related to the westward migration of the volcanic arc front and the ensuing thermal expansion in the formerly cool lithosphere beneath most of the southern Coast Mountains.

Acknowledgements

The author is indebted to R.L.Armstrong for continuous support, advice, and ideas during the course of this study. The financial help provided by a Pre-doctoral Fellowship at the University of British Columbia, the Natural Sciences and Engineering Research Council as a grant to R.L.Armstrong, and a grant-in-aid from the Geological Society of America is gratefully acknowledged. The Geological Survey of Canada helped defray the costs of K-Ar dating. For stimulating discussion, the author thanks W.H.Mathews, J.K.Mortensen, G.K.C.Clarke, G.Woodsworth, and T.Lewis; for help with irradiations, I thank C.W.Naeser and D.Rusling of the United States Geological Survey. L. Gilmore and K. Parrish contributed greatly through cheerful field assistance, drafting and manuscript preparation. The staff of the University of British Columbia Department of Geology, especially E. Montgomery and B. Cranston, aided in technical aspects of this study, and I thank them sincerely.

References

Allis, R.G., Henly, R.W., and Carman, A.F. 1979. The thermal regime beneath the Southern Alps. Royal Society of New Zealand, Bulletin 18, pp.79-86.

Armstrong, R.L., and Runkle, D. 1979. Rb-Sr geochronometry of the Ecstall, Kitkiata, and Quottoon plutons and their country rocks, Prince Rupert region, Coast Plutonic Complex, British Columbia. Canadian Journal of Earth Sciences, 16, pp.387-399.

Atwater, T. 1970. Implications of plate tectonics for the Cenozoic tectonic evolution of western North America. Geological Society of America Bulletin, 81, pp.3515-3536.

Baer, A.J. 1973. Bella Coola-Laredo Sound map-areas, British Columbia. Geological Survey of Canada, Memoir 372, 122 p.

Bartholomew, P.R. 1979. Geology and metamorphism of the Yale Creek area, British Columbia. M.Sc.thesis, University of British Columbia, 105p.

Berman, R.G., and Armstrong, R.L. 1980. The geology of the Coquihalla volcanic complex, southwestern British Columbia. Canadian Journal of Earth Sciences, 17, pp.985-995.

Berry, M.J., and Forsyth, D.A. 1975. Structure of the Canadian Cordillera from seismic refraction and other data. Canadian Journal of Earth Sciences, 12, pp.182-208.

Bevier, M.L., Armstrong, R.L., and Souther, J.G. 1979. Miocene peralkaline volcanism in west - central British Columbia-its temporal and plate-tectonic setting. Geology, 7, pp.389-392.

Byrne, T. 1979. Late Paleocene demise of the Kula-Pacific spreading center. Geology, 7, pp.341-344.

Carpenter, B.S., and Reimer, G.M. 1974. Calibrated glass standards for fission track use. National Bureau of Standards, Special Publication 260-49, 17p.

Carslaw, H.S., and Jaeger, J.C. 1959. Conduction of heat in solids. 2nd edition. Oxford University Press, London. 510p.

Carter, N.C. 1974. Geology and geochronology of porphyry deposits in west-central British Columbia. Ph.D.thesis, University of British Columbia, 236p.

Coney, P.J. 1978. Mesozoic-Cenozoic Cordilleran plate tectonics. In Cenozoic tectonics and regional geophysics of the western Cordillera, ed. By Smith, R.B., and Eaton, G.P. Geological Society of America, Memoir 152, pp.33-50.

Coney, P.J., Jones, D.L., and Monger, J.W.H. 1980. Cordilleran suspect terranes. Nature, 288, pp.329-333.

Cox, R.L. 1962. Age and correlation of the Sooke Formation with a section on its palynology. M.Sc.thesis, University of British Columbia, 64p.

Culbert, R.R. 1971. A study of tectonic processes and certain geochemical abnormalities in the Coast Mountains of British Columbia. Ph.D.thesis, University of British Columbia.

Douglas, R.J.W., Gabrielse, H., Wheeler, J.O., Stott, D.F., and Belyea, H.R. 1970. Geology of western Canada. In Geology and economic minerals of Canada. Geological Survey of Canada, Economic Geology Report No.1, pp.365-488.

Ewing, T. 1980. Paleogene tectonic evolution of the Pacific Northwest. Journal of Geology, 88, pp.619-638.

Farquharson, R.B., and Stipp, J.J. 1969. Potassium-argon ages of dolerite plugs in the south Cariboo region, British Columbia. Canadian Journal of Earth Sciences, 6, pp.1468-1470.

Fleischer, R.L., Price, P.B., and Walker, R.M. 1975. Nuclear tracks in solids - principles and applications. University of California Press, Berkeley, 605p.

Frizzell, V.A., Jr. 1979. Petrology and stratigraphy of Paleogene nonmarine sandstones, Cascade Range, Washington. United States Geological Survey, Open-file Report 79-1149, 151p.

Gleadow, A.J.W., and Lovering, J.F. 1975. Fission track dating methods. University of Melbourne, Department of Geology, Publication no.3, 94p.

Gleadow, A.J.W., and Lovering, J.F. 1978a. Fission track geochronology of King Island, Bass Strait, Australia: Relationship to continental rifting. Earth and Planetary Science Letters, 37, pp.429-437.

Gleadow, A.J.W., and Lovering, J.F. 1978b. Thermal history of granitic rocks from western Victoria: A fission track dating study. Journal of the Geological Society of

Australia, 25, pp.323-340.

Gleadow, A.J.W., Hurford, A.J., and Quaife, R.D. 1976. Fission track dating of zircon: Improved etching techniques. Earth and Planetary Science Letters, 33, pp.273-276.

Haack, U. 1977. The closure temperture for fission track retention in minerals. American Journal of Science, 277, pp.459-464.

Harrison, T.M., Armstrong, R.L., Naeser, C.W., and Harakal, J.E. 1979. Geochronology and thermal history of the Coast Plutonic Complex, near Prince Rupert, British Columbia. Canadian Journal of Earth Sciences, 16, pp.400-410.

Harrison, T.M., and McDougall, I. 1980. Investigations of an intrusive contact, northwest Nelson, New Zealand-I. Thermal, chronological, and isotopic constraints. Geochimica et Cosmochimica Acta, 44, pp.1985-2004.

Holland, S.S. 1964. Landforms of British Columbia. British Columbia Department of Mines and Petroleum Resources, Bulletin 48, 138p.

Hollister, L.S. 1979. Metamorphism and crustal displacements: New insights. Episodes, 1979, no.3, pp.3-8.

Hopkins, W.S. 1968. Subsurface Miocene rocks, British Columbia-Washington, a palynological investigation. Geological Society of America Bulletin, 50, pp.763-768.

Hurford, A.J., and Gleadow, A.J.W. 1977. Calibration of fission track dating parameters. Nuclear Track Detection, 1, pp.41-48.

Hutchison, W.W. 1970. Metamorphic framework and plutonic styles in the Prince Rupert region of the central Coast Mountains. Canadian Journal of Earth Sciences, 7, pp.376-405.

Hyndman, R.D. 1976. Heat flow measurements in the inlets of southwestern British Columbia. Journal of Geophysical Research, 81, pp.337-349.

Johnson, N.M., McGee, V.E., and Naeser, C.W. 1979. A practical method of estimating standard error of age in the fission track dating method. Nuclear Tracks, 3, pp.93-99.

Johnson, S.Y. 1981. Sedimentation and tectonics of the Chuckanut Formation on Bellingham Bay, Washington.

Geological Association of Canada Cordilleran Section, Programme and Abstracts, p.25.

Keen, C.A. and Hyndman, R.D. 1979. Geophysical review of the continental margins of eastern and western Canada. Canadian Journal of Earth Sciences, 16, pp.712-747.

Lewis, T.J. and Hyndman, R.D. 1981. Heat flow in Jervis Inlet, southwestern British Columbia. EOS, v.62, no.6, p.59.

Mathews, W.H. 1968. Geomorphology, southwestern British Columbia. In Guidebook for geological field trips in southwestern British Columbia, Mathews, W.H., ed. Department of Geology,University of British Columbia, Report no.6, pp.18-25.

Mathews, W.H. 1972b. Geothermal data from the Granduc area, northern Coast Mountains of British Columbia. Canadian Journal of Earth Sciences, 9, pp.1333-1337.

Mathews, W.H., and Rouse, G.E. 1963. Late Tertiary volcanic rocks and plant-bearing deposits in British Columbia. Geological Society of America Bulletin, 74, pp.55-60.

Mathews, W.H., Berman, R.G., and Harakal, J.E. 1981. Mid-Tertiary volcanic rocks of the Cascade Mountains, southwestern British Columbia, ages and correlations. Canadian Journal of Earth Sciences, 18, pp.662-664.

Molnar, P., and Tapponier, P. 1977. Relation of the tectonics of eastern China to the India-Eurasia collision: Application of slip-line field theory to large-scale continental tectonics. Geology, 5, pp.212-216.

Monger, J.W.H. 1977. Upper Paleozoic rocks of the western Canadian Cordillera and their bearing on Cordilleran evolution. Canadian Journal of Earth Sciences, 14, pp.1832-1859.

Monger, J.W.H., Souther, J.G., and Gabrielse, H. 1972. Evolution of the Canadian Cordillera: A plate tectonic model. American Journal of Science, 272, pp.577-602.

Monger, J.W.H., and Price, R.A. 1979. Geodynamic evolution of Canadian Cordillera - progress and problems. Canadian Journal of Earth Sciences, 16, pp.770-791.

Muller, J.E., Northcote, K.E., and Carlisle, D. 1974. Geology and mineral deposits of Alert-Cape Scott map-area, Vancouver Island, British Columbia. Geological Survey of Canada Paper 74-8, 77p.

Naeser, C.W. 1976. Fission track dating. United States Geological Survey, Open-file Report 76-190.

Naeser, C.W. 1979. Fission track dating and geologic annealing of fission tracks. In Lectures in isotope geology, ed. By Jager, E., and Hunziker, J.C. Springer-Verlag, pp.154-169.

Naeser, C.W., and Faul, H. 1969. Fission track annealing in apatite and sphene. Journal of Geophysical Research, 74, pp.705-710.

Naeser, C.W., and Forbes, R.B. 1976. Variation of fission track ages with depth in two deep drill holes (abstract). EOS, 57, p.363.

Naeser, C.W., Gleadow, A.J.W., and Wagner, G.A. 1979. Standardization of fission track data reports. Nuclear Tracks, 3, pp.133-136.

Nelson, J.A. 1979. The western margin of the Coast Plutonic Complex on Hardwicke and West Thurlow Islands, British Columbia. Canadian Journal of Earth Sciences, 16, pp.1166-1175.

Parrish, R.R. 1980. Fission track estimation of paleo-heat flow, Coast Mountains of British Columbia, Canada. EOS, 61, p.1131.

Richards, T., and White, W.H. 1970. K-Ar ages of plutonic rocks between Hope, British Columbia, and the 49th parallel. Canadian Journal of Earth Sciences, 7, pp. 1203-1207.

Richards, T., and McTaggart, K.C. 1976. Granitic rocks of the southern Coast Plutonic Complex and northern Cascades of British Columbia. Geological Society of America Bulletin, 87, pp.935-953.

Riddihough, R.P. 1977. A model for recent plate interactions off Canada's west coast. Canadian Journal of Earth Sciences, 14, pp. 384-396.

Roddick, J.A., and Hutchison, W.W. 1974. Setting of the Coast Plutonic Complex, British Columbia. Pacific Geology, 8, pp.91-108.

Rouse, G.E., Mathews, W.H., and Blunden, R.H. 1975. The Lions Gate member: A new Late Cretaceous sedimentary subdivision in the Vancouver area of British Columbia. Canadian Journal of Earth Sciences, 12, pp.464-471.

Rouse, G.E., and Mathews, W.H. 1979. Tertiary geology and palynology of the Quesnel area, British Columbia.

Bulletin of Canadian Petroleum Geology, 27, pp.418-445.

Schaer, J.P., Reimer, G.M., and Wagner, G.A. 1975. Actual and ancient uplift rate in the Gotthard region, Swiss Alps: A comparison between precise leveling and fission track apatite age. Tectonophysics, 29, pp.293-300.

Shouldice, D.A. 1971. Geology of the western Canadian continental shelf. Canadian Petroleum Geology Bulletin, 19, pp.405-436.

Souther, J.G. 1977. Volcanism and tectonic environments in the Canadian Cordillera - A second look. In Baragar, W.R.A., and others, eds., Volcanic regimes in Canada. Geological Association of Canada Special Paper 16, pp. 3-24.

Stacey, R.A. 1974. Plate tectonics, volcanism, and lithosphere in British Columbia. Nature, 250, pp.133-134.

Steiger, R.H., and Jager, E. 1977. Subcommission on geochronolgy: Convention on the use of decay constants in geo- and cosmochronology. Earth and Planetary Science Letters, 36, pp.359-362.

Steven, T.A., Mehnert, H.H., and Obradovich, J.D. 1967. Age of volcanic activity in the San Juan Mountains, Colorado. United States Geological Survey, Professional Paper 575-D, pp. 47-55.

Sutherland Brown, A. 1968. Geology of the Queen Charlotte Islands, British Columbia. British Columbia Department of Mines and Petroleum Resources, Bulletin 54, 226p.

Tipper, H.W. 1963. Geology, Taseko Lakes, British Columbia. Geological Survey of Canada, Map 29-1963.

Tipper, H.W. 1969. Anahim Lake. Geological Survey of Canada Map 1202A.

Tipper, H.W. 1978. Taseko Lakes (92O) map-area. Geological Survey of Canada, open file map.

United States Geological Survey. 1974. Utilization of the Geological Survey TRIGA reactor facility. United States Geological Survey, informal report.

Wagner, G.A., and Reimer, G.M. 1972. Fission track tectonics: The tectonic interpretation of fission track apatite ages. Earth and Planetary Science Letters, 14, pp.263-268.

Wagner, G.A., Reimer, G.M., and Jager, E. 1977. The cooling

ages derived by apatite fission track, mica Rb-Sr, and K-Ar dating: The uplift and cooling history of the Central Alps. Memoir of the Institute of Geology and Mineralogy, University of Padova, Padova, Italy, XXX, 27p.

Wagner, G.A., Miller, D.A., and Jager, E. 1979. Fission track ages on apatite of Bergell rocks from Central Alps and Bergell boulders in Oligocene sediments. Earth and Planetary Science Letters, 45, pp.355-360.

Walcott, R.I. 1978. Present tectonics and Late Cenozoic evolution of New Zealand. Geophysical Journal of the Royal Astronomical Society, 52, pp.137-164.

Wanless, R.K., Stevens, R.D., Lachance, G.R., and Delabio, R.N. 1964-1979. Age determinations and geologic studies. Geological Survey of Canada, Papers 64-17, 65-17, 66-17, 67-2A, 69-2A, 71-2, 73-2, 74-2, 77-2, and 79-2.

Woodsworth, G.J. 1977. Pemberton (92J) map-area. Geological Survey of Canada, Open file map 482.

Woodsworth, G.J. 1979. Geology of Whitesail Lake map area, British Columbia. In Current research, Part A, Geological Survey of Canada, Paper 79-1A, pp.25-29.

Woodsworth, G.J., and Tipper, H.W. 1980. Stratigraphic framework of the Coast Plutonic Complex, western British Columbia. Geological Association of Canada Cordilleran Section, Programme and Abstracts, pp.32-34.

Yorath, C.J., and Chase, R.L. 1981. Tectonic history of allochthonous terranes: Northern Canadian Pacific continental margin. Geological Association of Canada Cordilleran Section, Programme and Abstracts, pp. 42-43.

Young, I. 1981. Structure of the western margin of the Queen Charlotte basin, British Columbia. M.Sc.thesis, University of British Columbia, 380 p.

Zimmermann, R.A. 1977. The interpretation of apatite fission track ages with an application to the study of uplift since the Cretaceous in eastern North America. Unpublished Ph.D. Thesis, University of Pennsylvania, 146 p.

Zimmermann, R.A., and Gaines, A.M. 1978. A new approach to the study of fission track fading. United States Geological Survey, Open File Report 78-701, pp.467-468.

CHAPTER 2.

CENOZOIC TECTONICS AND THERMAL EVOLUTION OF THE COAST MOUNTAINS OF BRITISH COLUMBIA II: HEAT FLOW MODELS, THERMAL EVOLUTION, AND THE CAUSES OF UPLIFT

Abstract

The thermal and tectonic evolution of the crust in the Coast Mountains of British Columbia has been examined using a quantitative fission track-derived history of isotherm migration and topographic evolution (Chapter 1). A heat flow program was written to incorporate variable uplift rate, erosion lagging behind uplift, changing sub-crustal geothermal flux, fluctuating surface temperature and exponentially decreasing heat production with depth. Estimated uplift rate, surface temperature, heat production, and present heat flow, when used as input for the thermal model, allow determination of the sub-crustal geothermal flux variations and a refinement of Cenozoic uplift and denudation history.

Early Cenozoic orogenesis in the central and northern Coast Mountains (52°-55°N) resulted in substantial crustal thickening and rapid Eocene uplift, and was followed by the development of a transform plate margin. The moderate (0.1-0.2 km/Ma) middle Cenozoic uplift rates in this region were the result of gradual isostatic uplift in consequence of erosion of thickened crust. This process eventually led to elimination of the crustal root. Late Miocene acceleration of uplift was probably the result of the sub-crustal passage of the Anahim 'hot spot' which thinned the lithosphere and caused changes in sub-crustal and surface heat flux.

The southern Coast Mountains (49° to 52°N) were characterized by very low middle Cenozoic uplift rates (<0.1 km/Ma) and sporadic Miocene arc volcanism. Latest Miocene-Recent uplift in the south, by contrast, was rapid (>0.4 km/Ma) and resulted in 2 to 3 km of uplift over a broad area. The lack of seismicity and crustal thickening strongly suggests that the mechanism for this uplift is thermal expansion in the upper mantle. During the Miocene, most of the southern Coast Mountains was in a fore-arc, low-heat-flow environment. As a result of downgoing slab steepening and plate motion reorganization in the latest Miocene or early Pliocene, the volcanic belt migrated westwards; upwelling of asthenosphere above the subduction zone warmed the mantle, resulting in lithospheric thinning and a plateau-like uplift. Steepened subduction also led to thickening of the lithosphere west of the Pliocene to Recent magmatic front and consequent subsidence in the Strait of Georgia. Warming of a proposed cut-off Late Miocene shallow dipping slab induced phase changes and thermal expansion and resulted in moderate (1 km) uplift of the southern Interior of British Columbia.

Introduction

Heat transfer models have been developed to simulate the thermal evolution of mountain belts which experience uplift and erosion and the consequent cooling of rocks. Such models can be constructed to satisfy isotopic dates which record the time when the blocking temperature isotherms of the various geochronologic systems moved through the rocks (Harrison and Clarke 1979). In some cases, the models can be inverted to determine geologic and geophysical parameters which may be poorly known.

Three parameters necessary to the formulation of accurate and realistic models are 1) uplift and erosion rates (function of space and time), 2) sub-crustal (reduced) geothermal flux (function of space and time), and 3) the thermal effect of intrusions (function of size, shape, and temperature contrast). In areas that are experiencing uplift without intrusive activity, the intrusive perturbations can be ignored. In addition, if lateral variations in thermal conductivity, reduced heat flow and uplift rate are small, a one-dimensional model will suffice to simulate heat transfer.

In this paper a numerical model is presented which simulates heat flow in a column of the earth's crust, with exponentially declining heat production downwards, which is experiencing time-dependent uplift, temporal variations in the sub-crustal geothermal flux, changing surface temperatures, and non-equality between erosion and uplift

giving rise to an elevated land surface. The model is then applied to various parts of the Coast Mountains of British Columbia to simulate post-intrusive syn- to late-orogenic (Cretaceous-early Tertiary) rapid cooling and uplift followed by post-orogenic slow uplift and most recently, late Neogene rapid uplift giving rise to the present Coast Mountains.

Estimates of paleo-uplift rates have been derived from geological data and fission track geochronometry (Chapter 1). Under special circumstances the fission track data can also provide values of paleo-geothermal gradients. Other boundary conditions and material properties are available from various published and unpublished sources.

Tectonic and geothermal inferences derived from both fission track dating and thermal modeling are useful in evaluating geophysical processes in tectonically active regions, especially with regard to the mechanisms of large-scale uplift.

Geology of the Coast Mountains

The Coast Mountains of British Columbia (see Roddick and Hutchison 1974, Monger et al 1972, Chapter 1) are largely coincident with the Coast Plutonic Complex, a belt of granitic plutonic rocks of Jurassic to Eocene age superimposed on a varied framework of stratigraphic rocks.

Though some of the crystalline rocks owe their origin to crustal shortening, the bulk of plutonic rock is the

result of episodic intrusion of plutons that formed the roots of a west-facing magmatic arc of late Mesozoic to early Cenozoic age (Monger et al 1972). Plutonism and metamorphism culminated during the Eocene in the northern Coast Mountains, after which orogenic activity nearly ceased altogether. During the middle Cenozoic, the area north of 51^{0}-52^{0}N was probably bounded offshore by the Queen Charlotte transform fault, whereas the region to the south had continuous, relatively slow subduction and sporadic magmatic activity through the remainder of the Cenozoic, in much the same fashion as observed today (Berman and Armstrong 1980, Souther 1977). Except for a few localities, all of the crystalline rocks in the Coast Mountains are of pre-Oligocene age. Basaltic volcanism in the Interior Plateau (Figure 1) coincided temporally with the late Neogene rapid uplift of the Coast Mountains, which produced the present mountains (Mathews 1968). Characterising the thermal evolution and understanding the causes of this late Neogene event are the main goals of this paper.

Thermal Modeling of Mountain Belts

Applications of thermal models to geologic problems began with the study of thermal effects of intrusions. Jaeger (1964), Lovering (1935), and others have presented both theory and examples of this type. This paper concerns itself with geological situations where igneous intrusion is not important, and consequently the flow of heat is

controlled predominatly by conduction upwards and influenced by uplift and erosion.

Situations where uplift is assumed constant can be described by the analytical solution of Carslaw and Jaeger (1959, p.388). Clark and Jager (1969) presented an analytical solution to the one-dimensional uplift problem where heat production was assumed uniform and the initial temperature distribution had a simple mathematical form. This model was used in conjunction with isotopic dating, metamorphic pressure and temperature estimates, and present heat flow values to place constraints on the uplift history in the Swiss Alps. Later Clark (1979) refined this model to incorporate an exponential distribution of radioactive heat sources in the crust, but retained a constant rate of uplift. Woodhouse and Birch (1980) presented a similiar model and applied it to the apparent linear relation between surface heat production and surface heat flow (Lachenbruch 1968).

Numerical methods suffer from decreased accuracy of the solution but have the advantage that they can accomodate a wide range of space- and time- dependent parameters that are more realistic.

Harrison and Clarke (1979) used a two-dimensional model that incorporated the effects of both igneous intrusion and uplift, and they utilized a variety of isotopic dating techniques to test their model. They did, however, retain a fixed subcrustal geothermal flux as well as constant surface

temperature and uniformly distributed heat production. Lee et al (1980) have recently developed a finite difference scheme to model, in two dimensions, the additional effects of topography and lateral inhomogeneities in material properties.

The Model

Many previously published models incorporate one or more inflexible parameters (ie. constant uplift rate) which cause some divergence from realistic situations. Because uplift rate (Chapter 1), average surface temperature (Rouse and Mathews 1979), and sub-crustal geothermal flux (Parrish 1980) are all functions of time, and reasonably well known, for the Coast Mountains of British Columbia, a one-dimensional finite difference model was developed that allowed temporal variations of these parameters.

The model numerically solves the differential equation,

$$\frac{\delta^2 V}{\delta Z^2} - \frac{W}{\alpha}\frac{\delta V}{\delta Z} - \frac{1}{\alpha}\frac{\delta V}{\delta t} = -\frac{Ao}{\kappa}\exp(-(Z-Wt)/D)$$

where V is temperature, Z is depth below the average land surface, W is uplift rate with respect to sea level, α is diffusivity, t is time, Ao is the initial heat production of surface rocks, κ is the conductivity, D is the scale height of the exponential distribution of heat production, and δ represents the partial derivative. The model incorporates an exponentially downwards decreasing distribution of heat

production (Lachenbruch 1970) given by

$$A(Z,t) = Ao \exp(-(Z-Wt)/D)$$

and an initial temperature distribution described by

$$V(Z,0) = a + (Q^*Z/\kappa) + (D^2Ao/\kappa)(1-\exp(-Z/D))$$

where a is the initial surface temperature and Q* is the reduced heat flow at depth. Lateral heterogeneities in material properties and in geothermal and uplift parameters are assumed to have a negligible effect on vertical heat flow. In the models presented in this paper κ and α are assumed constant throughout the finite difference grid; more complex models with spatial variation in these two material properties would require data not presently available. Other parameters are allowed to vary with time (W,a,Q*) or space (Ao), according to data available for each locality modeled.

The method of Crank-Nicolson is used with the implicit form of the finite difference equation as outlined by Carnahan et al (1969, p.440-451). A system of M-1 equations is developed for each time step where M is the number of depth grid points. The depth grid has a fixed size and surface boundary condition,

a(t) = surface temperature

a lower boundary condition,

Q*(t) = reduced heat flow

and uplift variation,

W(t) = uplift rate, with respect to sea level.

The system of equations resulting from each time step forms a tridiagonal coefficient matrix which is readily solved by Gaussian elimination.

In practice Q* and W are specified as step functions with incremental changes whereas a, the surface temperature, was chosen as a linear function of time. The depth of the finite difference grid was chosen as 40 km, approximately the thickness of normal continental crust. With usual values of the scale height, D, this assures that heat production at the base of the grid is <2% that of the surface, a condition consistent with the very low to negligible heat production thought to exist in the lowermost crust or uppermost mantle.

The present elevated landscape of the Coast Mountains is evidence that erosion has lagged behind uplift in the recent geologic past. This has caused an increase in the average altitude and a decrease in the average surface temperature according to the value of the atmospheric lapse rate. In the model, elevation of the land surface as a consequence of lagging erosion is simulated by a decrease in the surface temperature and by a decrease in the rate at which material passes through the top of the finite difference grid, which represents the land surface. When the land surface rises from lagging erosion, the denudation rate at the land surface (average altitude) is the uplift rate, W (with respect to sea level), mutiplied by the ratio of

denudation to uplift. This ratio of denudation to uplift can be varied to simulate realistic conditions. The late Neogene onset of lagging erosion is given by the parameter TNONEQ (in Ma before present).

The model has the capability of incorporating almost all realistic situations with the requirement that lateral heat transfer<<vertical heat transfer. Incremental step functions for Q* and W cause unrealistic short term second order discontinuities in geothermal parameters but reasonably approximate the uplift history. The changes in Q* at the base of the grid can only correspond to situations where convection dominates heat transfer beneath the base of the crust. This appears a reasonable approximation, considering the tectonic environment for the Coast Mountains region.

The numerical solution has been tested for accuracy against the analytical solution of Woodhouse and Birch (1980) for uniform uplift. After 50 Ma of thermal evolution, temperatures and heat flow values agree within approximately 5% and 3%, respectively. Both temperature and heat flow are lower for the finite difference solution because a small part (1-2% for a 40 km depth grid) of the heat production given by the exponential distribution is at depths greater than the base of the grid and is thus excluded by the condition of a specified thermal gradient at the base of the grid. The size of the finite difference grid varies from 40 km by 80 Ma to 40 km x 50 Ma; time and depth increments

of 1% were chosen for both models. Fewer mesh steps cause increasing deviations from the analytic solution, and no significant improvement was obtained by decreasing the mesh size. The FORTRAN program 'COASTMTN' is listed in Appendix 1.

Discussion of Parameters

Surface temperature variation

Paleoclimatic and geochronologic work by Rouse and Mathews (1979) in the Quesnel area in central British Columbia has established mean temperature variations throughout the Cenozoic which indicate a grossly linear decrease with time. This general pattern can be documented where Cenozoic deposits exist but can only be assumed for areas such as the Coast Mountains where such deposits are absent. In the models presented, mean annual paleotemperatures decrease from about 25°C 50 Ma ago to about 5-10°C at present. This decrease results in middle and late Cenozoic paleotemperature estimates similar to those of Rouse and Mathews (1979), although the retention of a linear decrease requires early Cenozoic and late Mesozoic paleotemperatures to be somewhat higher (up to 32°C) than would be expected. The overall effect of this higher surface temperature, however, will be very small. Though Cenozoic fluctuations in paleotemperature are well documented (Rouse and Mathews 1979), the overall pattern of a linear decrease

is a good approximation and is likely applicable for the entire region of the present Coast Mountains.

Heat production, Ao

The exponential downward decrease of heat production chosen for this model is based on both heat flow-heat production observations (Lachenbruch 1968, Roy et al, 1968) and a theoretical analysis of such a relation in areas of differential erosion (Lachenbruch 1970). Average surface heat production measurements for the Coast Mountains are provided by Lewis (1976 and unpublished data) and Lewis and Souther (1978), and cover most of the areas discussed in this study. Prior to Cenozoic erosion, surface heat production values, at least for the models, are required to have been greater (up to 5.6 kW/km^3) than at present. The mean and standard deviation of presently available heat production data for the Coast Mountains from 50° to 55°N (about 150 measurements) is 0.8 ± 0.5 kW/km^3 and range from 0.1 to 3.4 kW/km^3 (Lewis 1976 and unpublished data, Lewis and Souther 1978). The mean heat production of plutonic rocks in the Intermontane Zone and Omineca Crystalline Belt of British Columbia to the east is 2.6 kW/km^3 but values range from 1.0 to 8.0 kW/km^3 with 70% falling between 2.0 and 5.5 kW/km^3 (Lewis 1976). In many areas of the Coast Mountains where the depth of erosion is not particularly great, heat production is generally less than 1.5 kW/km^3. The models have been designed so that the final surface heat

production is approximately the average value for the Coast Mountains (0.8-0.9 kW/km^3). This requires initial Ao values to be between 1.5 and 5.6 kW/km^3, depending on the amount of uplift modeled.

Scale height, D

The absence of sufficient heat flow measurements in the Coast Mountains precludes estimating the scale height, D, from the linear heat flow - heat production relation (Lachenbruch 1968). Consequently, this value has been assumed to be 10 km, like that for the Sierra Nevada of California (Roy et al 1968). It is unlikely that this value would greatly vary from place to place within any one geologic province.

Conductivity, κ, and diffusivity, α

Values of conductivity have not been systematically measured for this study. Rather, since the rock composition in the Coast Mountains is rather uniform quartz-diorite or granodiorite (Roddick and Hutchison 1974), and since both fission track dates (Chapter 1) and modeling have been done for areas composed chiefly of these intermediate granitic rocks, a single average value has been applied to all models. A large number of conductivity measurements would be required to justify a more detailed approach. Values of 2.5 kW/km^oC (5.98×10^{-3} cal/sec-cm-^oC) and 32.0 km^2/Ma (0.0101 cm^2/sec) have been chosen for conductivity and diffusivity,

respectively. These estimates are identical to those chosen for the Sierra Nevada model of Lachenbruch (1968); the conductivity (2.5 kW/km°C) is close to average values for measured rocks from the Coast Plutonic Complex of British Columbia (2.7±0.3 kW/km°C; Lewis 1976, Lewis and Souther 1978, Harrison et al 1979) and for quartz diorite-granodiorite in general (3.1 kW/km°C; Clark 1966). The diffusivity, α, equals $\kappa/\rho c$ where ρ is 2.7 g/cm^3 and c, the heat capacity, is 0.22 cal/g°C (2.9 x 10^{-13} W Ma/kg°C).

Lapse rate

An atmospheric lapse rate of -7°C/km has been chosen. This value falls between the dry (no condensation) and saturated adiabatic rates of -10°C/km and -5.5°C/km, respectively (Strahler 1973) and is probably appropriate to this fairly humid region.

Erosion-uplift balance

Averaged over most of the Cenozoic, erosion and uplift have been essentially balanced. Until the late Neogene when vigorous uplift in the Coast Mountains began (Douglas et al 1970), relief and altitude were generally low. Only in the last several million years has rapid uplift caused a marked increase in the average altitude resulting from lagging denudation. The onset of lagging erosion as a result of accelerated uplift, termed TNONEQ in the model, is estimated to be from 5 to 10 Ma years ago. Uplift rates derived from

fission track data (Chapter 1) when combined with values of present average altitude of different areas of the Coast Mountains, dictate the ratio of erosion/uplift, according to the relation,

W x TNONEQ x (1-erosion/uplift) = average altitude.

The range of this ratio is 0.53 to 0.86 which results in average altitudes of 0.6 to 1.8 km for the specific areas discussed in this paper. The values of mean altitude were calculated by averaging altitudes of about 30 equally spaced points within a 15 km radius of each modeled locale. The model was designed to have the "model" average altitude identical to the actual value for each area (see Table V). The resulting surface temperature is lowered, in addition to the secular decrease, by an amount equal to the average altitude multiplied by the lapse rate (-7°C/km).

Reduced heat flow, Q*

Values of reduced heat flow Q*, corresponding to the heat flux entering the base of the finite difference grid, vary in models from 25 to 60 kW/km^2. These values fall between the extremes of very low heat flow in the arc-trench gap above active subduction zones (<20 kW/km^2) to high values in areas of thinned lithosphere and active volcanic and tectonic activity (>50 kW/km^2) such as the Basin and Range province of western United States (see Blackwell

1978). Q* for the models is generally assigned a high value of about 50 kW/km^2 in the syn-orogenic to immediately post-orogenic period to simulate both the higher than normal flux from the mantle as well as the dissipation of stored orogenic thermal energy caused by deformation, intrusion or both. In general, Q* and uplift rates were adjusted to obtain a good fit to fission track dates, reliable apparent uplift rates, and paleo-geothermal gradients (Parrish 1980, Chapter 1), as well as present heat flow (Hyndman 1976).

Uplift rate, W

Approximate values of uplift rate derived from fission track dating for various areas of the Coast Mountains are from Chapter 1. As discussed in Chapter 3, apparent uplift rates are equal to actual uplift rates only when several conditions are met. The most crucial condition is that the isotherms must remain at fixed distance with respect to the contemporary surface despite uplift; otherwise, misleading apparent uplift rates can be produced. Sustained (10-20 Ma), relatively low (less than 0.3 km/Ma) apparent uplift rates from apatite fission track data are accurate indicators of true uplift rate since erosion and uplift will likely be in balance during this time period, whereas higher values of zircon-derived apparent rates are not. The zircon data often overestimate the true uplift rate and reflect downward relaxation of isotherms following orogenic activity.

Late Neogene rapid uplift both elevated the land

surface and increased the downward movement of isotherms leading to higher apparent uplift rates. Derived apparent uplift rates in such a case will probably underestimate the rate of uplift with respect to sea level, since denudation will lag for the initial period. Apatite rates will, however, be within 25% of the value of surface denudation after only a brief (3 to 5 Ma) period (Chapter 3), and apatite fission track data can thus be used to provide reasonable estimates of middle and late Cenozoic uplift rates for use in thermal models.

When elevation of the land surface due to lagging erosion is simulated, the model adjusts the value of surface denudation to be less than W, the uplift rate with respect to sea level. The difference in rate between W and surface denudation is the rate at which the land surface is elevated. In addition, when elevation of the land surface occurs, the surface temperature is decreased as discussed under erosion-uplift balance.

Application to the Coast Mountains

Objectives of modeling

The objective of thermal modeling is a self-consistent quantitative thermal-uplift model that fits uplift history, fission track and other isotopic dates, paleogeothermal gradient measurements, and other geologic and geomorphic observations. The method is applied to five areas of the

Coast Mountains where fission track, geologic data, and heat flow estimates are available. These areas are, from north to south, Kemano, northern King Island - Ocean Falls, Mount Waddington, central Bute Inlet, and Mount Raleigh (Figure 1).

Presentation of the models

The parameters of the models are listed in Table V, along with their SI units. The computational parameters tmax, t, Zmax, and Z are the maximum time, time step size, the maximum depth, and depth step size, respectively. The sequential values of reduced heat flow (Q*1, Q*2, Q*3) and uplift rate (W1, W2, W3, W4) are changed at times tQ*1,tQ*2 and tW1,tW2, and tW3, respectively (in Ma before present). In the interest of clarity, uplift rates are shown as positive numbers.

The models and the relevant fission track and K-Ar isotopic data for each area are presented in the format of Figure 15a. The uplift path of rocks presently at the average altitude at each locality is shown by the depth vs. time curve. Abrupt changes in uplift rate are clearly evident. When combined in the model, the variations of W and Q* produce surface heat flow variations shown in the top part of Figure 15a. The value of paleo-heat flow (Q) at about 6 km depth is shown in Figure 15a by short bars. The 6 km deep Q values are shown for comparison with the estimate of paleo-heat flow derived from fission track

Table V. Parameters of Thermal Models

Parameter	Kemano	N.King Island-Oc.Falls	Mt.Waddington	Central Bute Inlet	Mt. Raleigh	Units
model:	A (B,C,D)*	A (B,C,D)*				
initial Ao	3.0	2.5	3.8	1.5	5.6	kW/km³
α	32.0	32.0	32.0	32.0	32.0	km²/Ma
κ	2.5	2.5	2.5	2.5	2.5	kW/km°C
D	10.0	10.0	10.0	10.0	10.0	km
a	24.0	24.0	25.0	31.0	32.0	°C
da/dt	-0.28	-0.28	-0.28	-0.28	-0.28	°C/Ma
tmax	50.0	50.0	55.0	75.0	80.0	Ma
dt	0.5	0.5	0.55	0.75	0.8	Ma
Zmax	40.0	40.0	40.0	40.0	40.0	km
dz	0.4	0.4	0.4	0.4	0.4	km
Q*1	50.0	35.0	50.0	30.0	50.0	kW/km²
tQ*1	45.0	45.0	45.0	--	60.0	Ma bp
Q*2	35.0	25.0	35.0	30.0	35.0	kW/km²
tQ*2	15.0	20.0	20.0	--	20.0	Ma bp
Q*3	50.0	60.0	50.0	30.0	50.0	kW/km²
W1	1.2	0.20	0.9	0.065	1.0	km/Ma
tW1-2	45.0	30.0	45.0	--	70.0	Ma bp
W2	0.18	0.14	0.2	0.065	0.2	km/Ma
tW2-3	35.0	10.0	35.0	--	50.0	Ma bp
W3	0.08	0.62	0.11	0.065	0.06	km/Ma
tW3-4	10.0	6.0	5.0	5.0	7.0	Ma bp
W4	0.24	0.30	0.75	0.47	0.6	km/Ma
lapse rate	-7.0	-7.0	-7.0	-7.0	-7.0	°C/km
erosion/uplift	0.58	0.86	0.53	0.53	0.6	-
TNONEQ	10.0	10.0	5.0	5.0	7.0	Ma bp
surf.alt.[1]	1.0	0.6	1.8	1.10	1.73	km
actual surf.alt.[2]	1.0	0.6	1.8	1.08	1.7	km
final Ao[1]	0.98	0.87	0.75	0.84	0.86	kW/km³

* Model B: same parameters as A except Q*1=Q*2=Q*3=40.0 kW/km²
* Model C: same parameters as A except uplift rates W1,W2,W3, and W4 are increased by 20%
* Model D: same parameters as A except uplift rates W1,W2,W3, and W4 are decreased by 20%

[1] output from the model; all other parameters are input

[2] measured from altitudes of 30 equally-spaced points in a 15 km radius of each locality

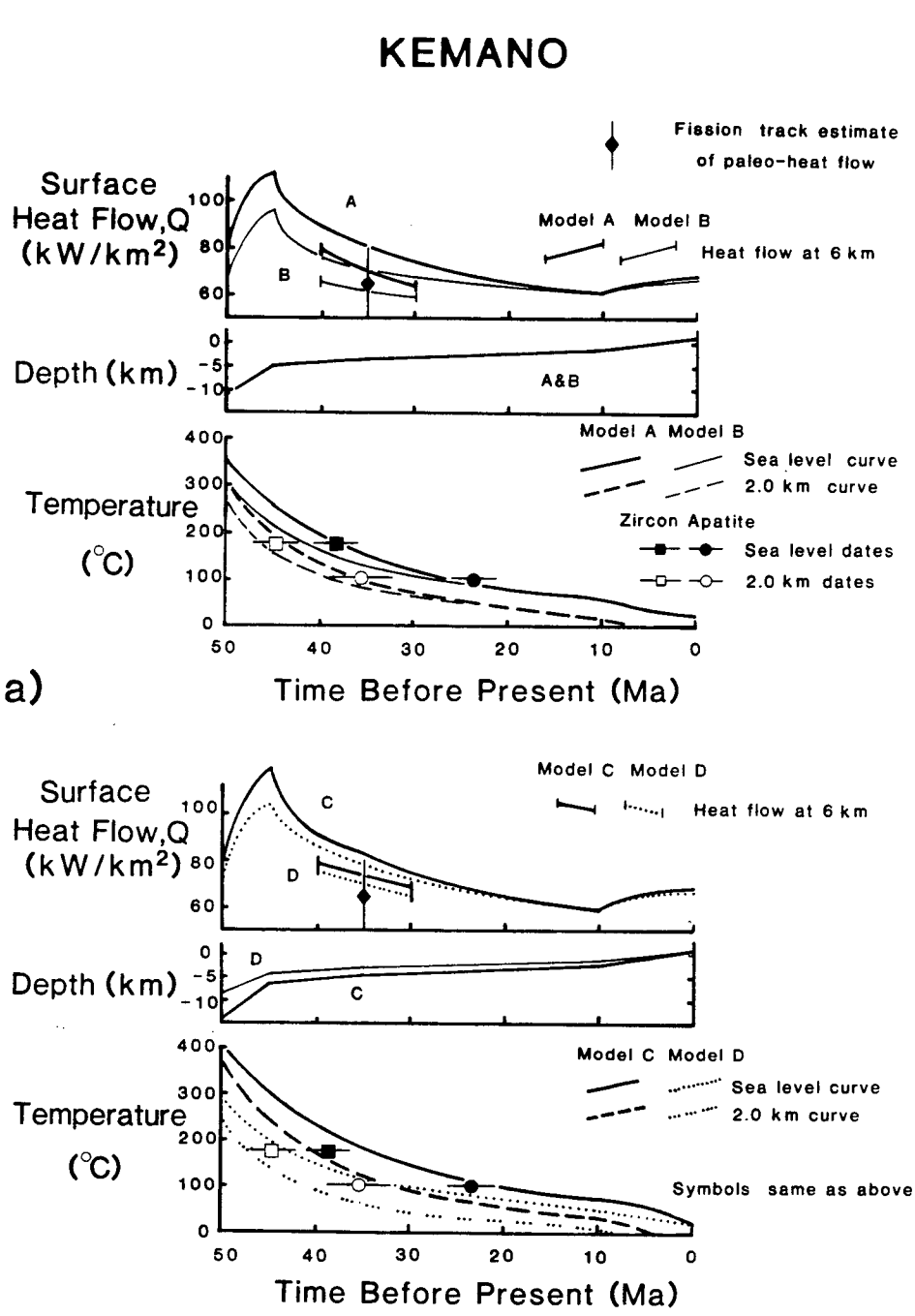

Figure 15a. Thermal evolution diagram for the Kemano area. Shown are surface heat flow (Q), depth, and temperature vs. time curves which are derived from models with parameters listed in Table V. Discontinuities in Q vs. time curve result from increments in uplift rate. Fission track dates and estimates of paleo-heat flow are from Chapter 1.

dating (Parrish 1980, Chapter 1), which corresponds to about that same depth.

In the temperature vs. time graph, two main curves are shown. The top curve represents the cooling curve of samples presently at sea level; the bottom curve represents the curve for rocks that are now at 2.0 km altitude. Since the cooling curve must pass through the fission track dates at the appropriate blocking temperature (105°C for apatite, 175°C for zircon), the fit of each of these two cooling curves to their respective fission track dates represents a consistent modeling of uplift rates, reduced heat flow, and fission track data. Other isotopic dates and their respective blocking temperatures can also be used, when available, to place further constraints on the models (see Harrison et al 1979). All fission track data are from Chapter 1 and other isotopic dates are from the Geological Survey of Canada (Woodsworth 1979, Baer 1973, Wanless et al 1979).

In order to assess the sensitivity of the model to variations in the parameters, three other models are shown on Figure 15a in addition to the best fit of model A.

Model B is identical to model A except that Q* is constant at 40 kW/km^2. Though the cooling curves of model B fall clearly off the centroid of the fission track dates from Kemano, they do fit the dates within error.

In the lower portion of Figure 15a, models C and D represent identical parameters as model A except that they

have uplift rates uniformly increased and decreased 20% from model A. It is apparent that although the heat flow data at 6 km depth is consistent with either model C or D, neither of the models can satisfy the fission track data. Presentation of each of models A, B, C, and D illustrates that uplift rate variations of at most ±15% can be tolerated and still remain consistent with fission track data. Changes in Ao will have a small effect on the resultant curves as long as those changes are not large and inconsistent with present values of Ao. Changes in κ and α will have considerable effect on the models, but since the variability of this parameter is limited in quartz diorite-granodiorite, such changes will not strongly affect conclusions drawn from the models.

Kemano

Dated rocks from Kemano are of foliated quartz diorite at Powell Peak, of Eocene or probably older age. The rocks are similiar to other rocks present within the central gneiss complex of the northern Coast Mountains (Roddick and Hutchison 1974). No K-Ar dates are available in the immedite vicinity of Kemano, although most dates in the gneiss complex farther northwest are Eocene. Fission track dates spread over the 2 km of altitude of Powell Peak range from 24 to 34 Ma for apatite and 36 to 44 Ma for zircon (Chapter 1). An estimate of paleogeothermal gradient 35 Ma ago is $26+4/-6^{\circ}C$ (Parrish 1980).

Model A of Figure 15a is the best thermal model within the constraints of the data, although it is not a unique solution. It incorporates variations in Q* from 35 to 50 kW/km^2 and uplift rate variations from 0.08 to 1.2 km/Ma.

Rapid uplift and high Q* in the Eocene following Eocene orogenic activity (Hollister 1979) gave way to low rates of uplift and Q* in the middle Cenozoic during a period of tectonic stability. Uplift rates and Q* are increased in the late Neogene at about 10 Ma, consistent with both fission track data, physiographic evolution (Chapter 1) and relatively high heat flow along the eastern part of the Coast Mountains (Hyndman 1976, Mathews 1972b, T. Lewis unpublished data). On the basis of this model, K-Ar biotite dates near Kemano would be expected to be about 45-50 Ma, assuming a blocking temperature of 280±40°C for biotite (Harrison and McDougall 1979). The present surface heat production of 0.98 kW/km^3 given by the model (see Table V) is virtually identical to the measured value of 1.0 kW/km^3 (T. Lewis unpublished data).

Northern King Island - Ocean falls

The geology of this region (Figure 1) has been described by Baer (1973). The rocks consist of plutons and subordinate metamorphic rocks which yield K-Ar biotite dates of 57-87 Ma. Preliminary Rb-Sr work on some of these plutonic rocks suggests they are mid-Cretaceous in age (R.L.Armstrong and R.R.Parrish unpublished data). Fission

track dates spread over 2 km of altitude vary from 8 to 24 Ma for apatite and 34 to 39 Ma for zircon. A fission track-derived value of paleogeothermal gradient 20 Ma ago is 17±2°C/km (Chapter 1) which represents a paleo-heat flow of about 43 kW/km^2, assuming κ=2.5 kW/km°C (5.98x10^{-3} cal/sec-cm-°C). This is significantly lower than the value derived for the Kemano area for 35 Ma ago.

Models A, B, C, and D of Figure 15b are similiar in format to those of Figure 2a. Model B is identical to the best fit model A except that Q* is a constant 40 kW/km^2. It is apparent that model B is consistent with neither the fission track derived value of paleo-heat flow nor all of the fission track data. Thus, it appears, as model A suggests, that Q* was significantly less than 40 kW/km^2 for most of the middle Cenozoic. Models C and D of Figure 15b, have uplift rates of ±20% of model A, but neither is consistent with fission track data. Their heat flow curves, however, are very similar and fall within the error limits of the fission track-derived paleo-heat flow determination. The final present surface heat production from model A is 0.87 kW/km^3, similar to present values of 0.9-1.0 kW/km^3 T.Lewis, unpublished data).

Model A, which fits all of the data very well, involves uplift rates that are very similar to those derived directly from fission track dating of apatite. These rates are moderate through the middle Cenozoic (0.14-0.2 km/Ma) but increase in the Late Miocene. Geomorphic arguments (Chapter

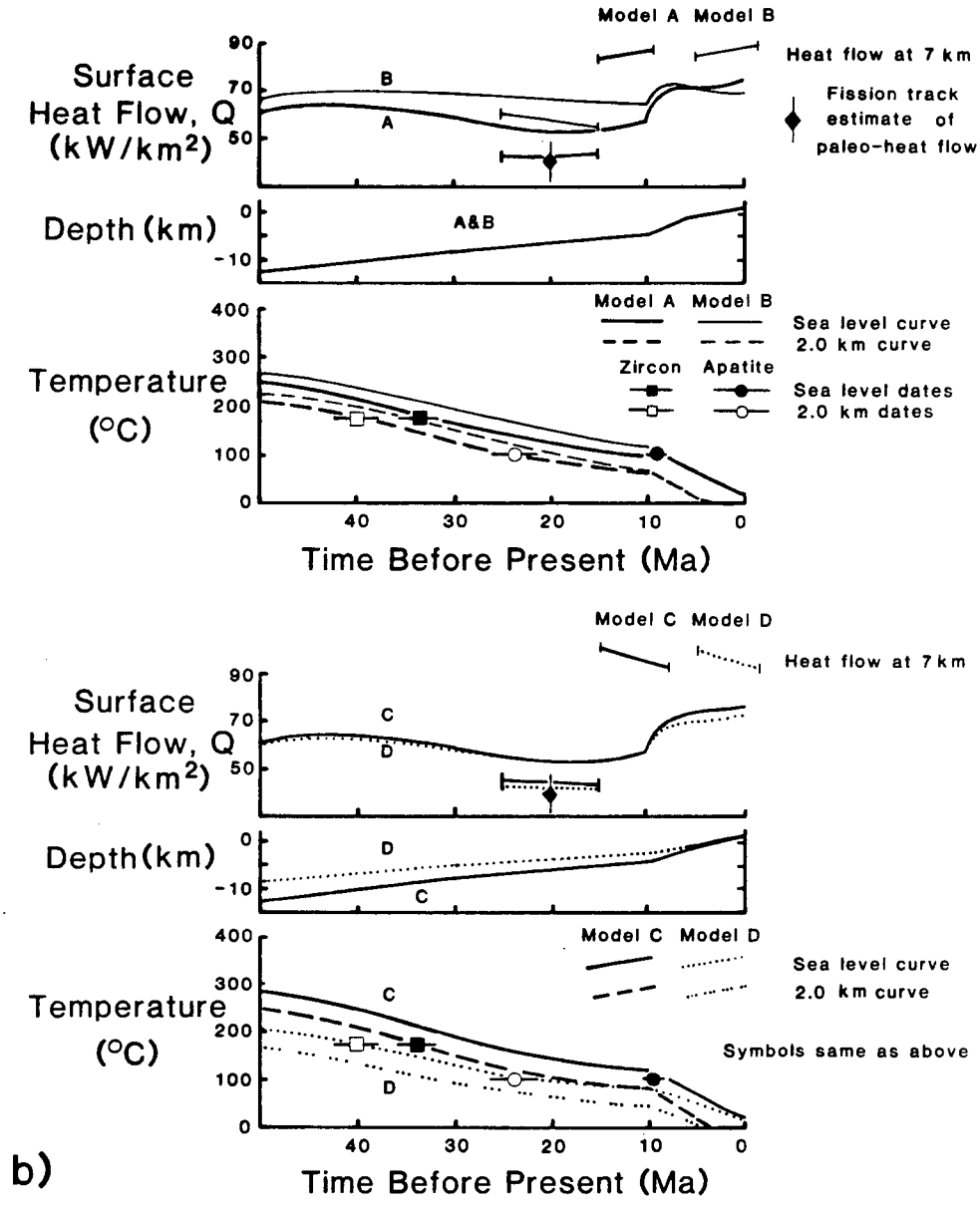

Figure 15b. Thermal evolution diagram for the King Island-Ocean Falls area.

1) suggest that the most rapid late Neogene uplift in this region was in the Late Miocene, followed by slower Pliocene to Recent rates. This slowing of rate has been incorporated in models for this region (see Table V).

Mount Waddington

Mount Waddington, with an altitude of 4 km, is the highest area in the Coast Mountains. It is composed of granitoid gneiss, migmatite, and more massive plutonic rock (G. Woodsworth, unpublished data) at least as old as Paleocene. K-Ar dates (calculated with constants listed in Table IV) range from 55 Ma for hornblende to 48 Ma for biotite. Little else is known about these rocks. Fission track dates from localities spread over 3 km in altitude range from 6 to 32 Ma for apatite, and 19 to 52 Ma for zircon (Chapter 1). Apatite dates clearly show altitude correlation but zircon dates do not. A reliable estimate of paleogeothermal gradient has been impossible to obtain, but present heat flow, uncorrected for uplift, is probably 70 to 90 kW/km^2 (shown in Figure 15c). This value of Q was derived by adding a 24% uplift correction, originally subtracted from heat flow measurements by Hyndman (1976), to the average Q value (about 63 kW/km^3) for the higher heat flow region of the Coast Mountains, of which Mount Waddington is part.

The best fit thermal model, shown in Figure 15c, has been constructed by early Cenozoic uplift rates which fit

the K-Ar and zircon fission track data. From 35 Ma to the present, apatite data are accurate enough to place good constraints on the uplift rates. The rates are rapid (0.9 km/Ma) in early Cenozoic time (55-45Ma) resulting in rapid cooling of the rocks. Middle Cenozoic slow uplift (0.11 km/Ma) is similiar to apparent uplift rates documented by fission track data (0.09 km/Ma). Late Cenozoic (post-5 Ma) rapid uplift (0.75 km/Ma) is required not only to fit apatite fission track data but also to explain the physiography of the region. Q* has been varied between 35 and 50 kW/km^2 to satisfy dates and the estimate, albeit imprecise, of present heat flow. The erosion/uplift ratio has been adjusted to result in an average altitude of 1.8 km.

The model suggests that rapid orogenic uplift during the Paleocene-Eocene was followed by very low middle Cenozoic rates implying low relief and altitude then. Late Neogene uplift appears to have been initiated very recently producing the present mountains.

Central Bute Inlet - Mount Raleigh

The last two areas modeled are from the Bute Inlet area of the southern Coast Mountains (Figure 1). It will be shown that their respective geochronology, thermal models, and tectonic histories are quite different and have implications for the orogenic history of this region.

K-Ar biotite dates from the dominantly plutonic Central

MT. WADDINGTON

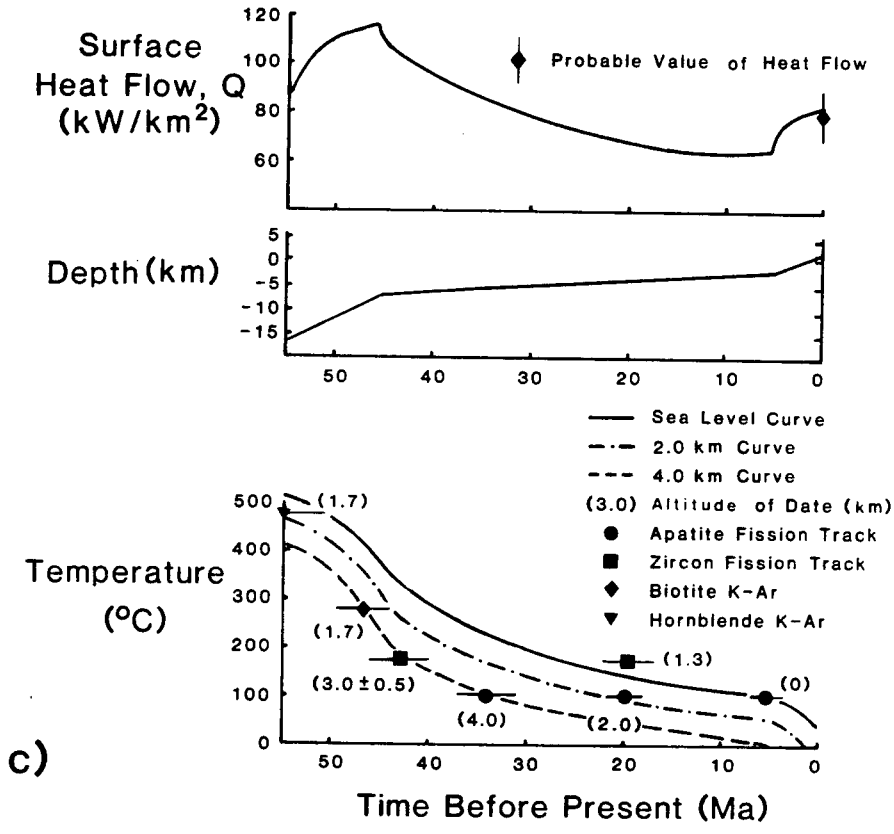

Figure 15c. Thermal evolution diagram for the Mount Waddington region. K-Ar dates are from Wanless et al (1979). The present heat flow is modified from Hyndman (1976).

Bute Inlet are 90-100 Ma (Roddick and Woodsworth 1977), and fission track dates range from 42 to 75 Ma for apatite and 73 to 100 Ma for zircon, depending on location and altitude. The present heat flow in Bute Inlet, uncorrected for uplift, is about 40 to 75 kW/km^2 (Hyndman 1976, Figure 15e). This low heat flow results from the heat sink effect of the descending oceanic plate during subduction, and since subduction has probably continued, apparently uninterrupted, since the late Cretaceous (Monger et al 1972), this low heat flow has likely persisted for some time. Apparent uplift rates derived from fission track data are less than 0.1 km/Ma since 75 Ma ago except for the Neogene, when rates increased to about 0.4 km/Ma (Chapter 1).

In the model (Figure 15e) the cooling curves for sea level and 2.5 km fit the apatite fission track data when Q* is a constant 30 kW/km^2. Uplift rates are approximately those derived from fission track dating. In addition, the predicted present heat flow is identical to values measured in Bute Inlet by Hyndman (1976), once the uplift correction is added. In this example, resultant surface heat production and surface altitude are 0.84 and 1.10 km, respectively, very close to actual values of about 1.0 kW/km^3 and 1.08 km. The rocks of this area have been uplifted only about 5 km since 75 Ma ago.

The Mount Raleigh area (Figure 1), about 30 km east of the previous example, is underlain by metamorphic and plutonic rocks of mostly Mesozoic age. Plutons of Late

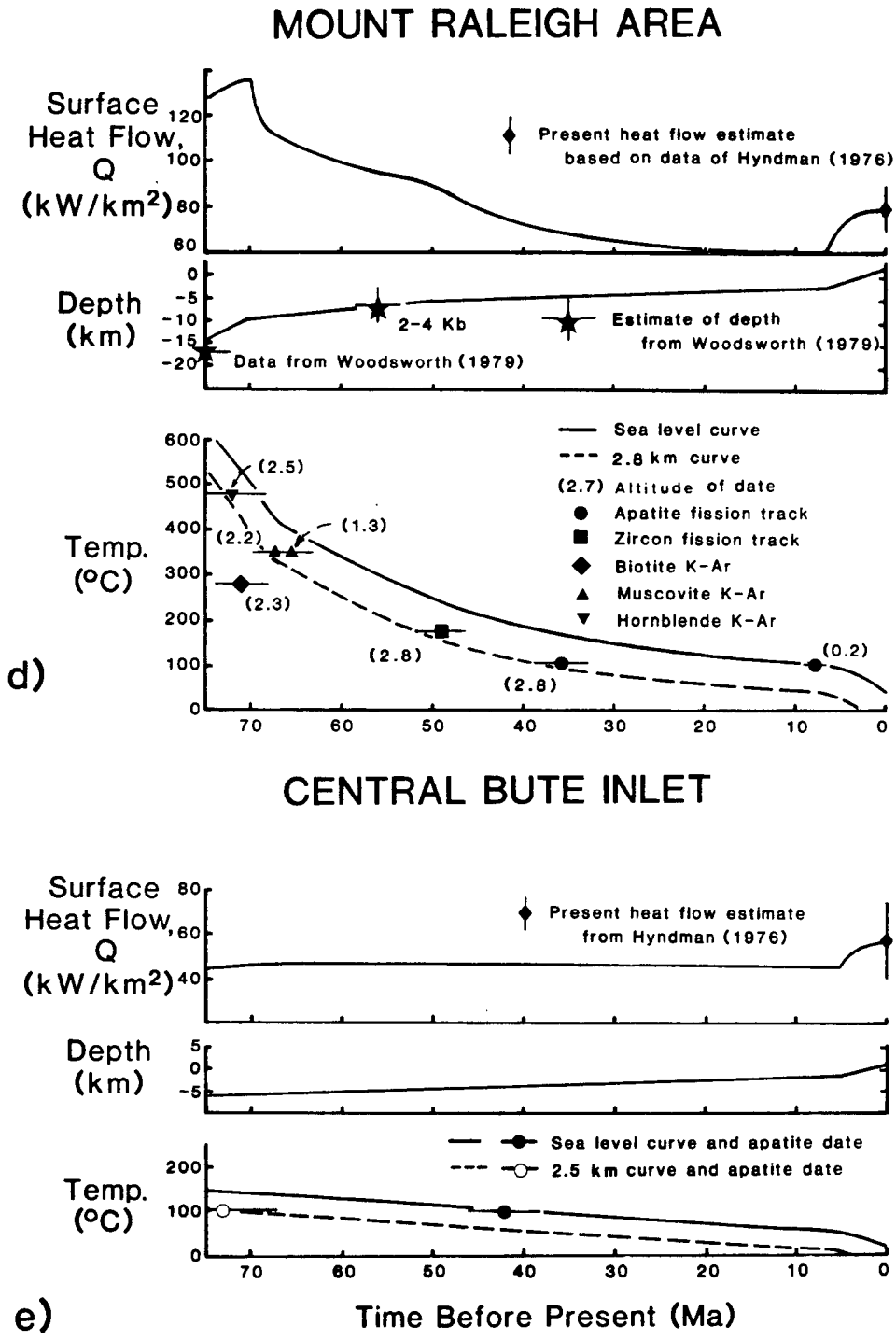

Figures 15d and 15e. Thermal evolution diagrams for the Mount Raleigh (d) and central Bute Inlet (e) areas.

Cretaceous-Paleocene age intrude rocks previously metamorphosed during the Late Cretaceous, about 70-90 Ma ago (Woodsworth 1979). A 55-60 Ma plutonic suite, the Bishop River Pluton, was emplaced at pressures of about 2-3 kb (200-300 MPa) following metamorphism to pressures of 5-6 kb (500-600 MPa) at least 80 Ma ago (Woodsworth 1979). K-Ar dates (calculated with constants listed in Table IV) on metamorphic rocks range from 71 Ma (hornblende) to 66-68 Ma (muscovite). A K-Ar biotite date on the Mount Gilbert pluton is 71 Ma. Neither heat production nor heat flow data are available but values of heat flow, uncorrected for uplift, of 70-90 kW/km^2 would be expected in the region (Hyndman 1976). The only zircon fission track date available is 49 Ma from 2.8 km altitude. Apatite dates from 2.8 and 0.2 km altitudes are 36 Ma and 7.8 Ma, respectively, implying an apparent uplift rate of about 0.1 km/Ma in the middle Cenozoic which increased to over 0.4 km/Ma in the late Neogene (Chapter 1).

As in the Mount Waddington model, the 75-50 Ma uplift rates were chosen to fit the K-Ar and fission track dates in addition to the metamorphic pressure estimates (Figure 15d). Rates of 1 km/Ma or more are required to fit this data. The lower rates in the middle Cenozoic (0.06-0.2 km/Ma) are close to those derived from fission track dating and fit the apatite dates closely. The values of Q* are consistent with estimates of present heat flow.

In contrast to Central Bute Inlet, the Mount Raleigh

area has experienced 15 km of uplift since 75 Ma. Because the two areas are only about 30 km apart, considerable differential uplift must have occurred in the Late Cretaceous and Paleocene. The culmination of deformation and plutonism in the two areas is clearly different and implies that orogenic activity and uplift have progressed from west to east across the Coast Plutonic Complex. This is consistent with patterns of K-Ar dates, geologic data, and age of plutons elsewhere (Roddick and Hutchison 1974).

Discussion of Models

The heat flow models integrate uplift rate, observed thermal history, heat production, heat flow and inferred parameters such as Q*. Cooling rate data for rocks is directly available through geochronometry, and when incorporated into models, estimates of uplift rates can be derived when fission track-derived uplift rate data are either not available or suspect (as for zircon dates). In several of the models (Mount Waddington, Mount Raleigh, Kemano), initial syn-orogenic to post-orogenic uplift rates of about 1 km/Ma are consistent with petrology and K-Ar geochronometry. This value (1 km/Ma) is close to that considered applicable for the Alps (Schaer et al 1975) and other active mountain belts.

The K-Ar and fission track data and the thermal models indicate that sequential plutonic emplacement, cooling, and subsequent rapid uplift progressed broadly from west to east

across the Coast Plutonic Complex. The Alaska border to the Kemano area was characterized by Eocene orogenic culmination.

The modeling of heat flow and uplift confirms the difference in middle Cenozoic uplift rates between northern (0.1-0.2 km/yr from 52° to 55°N) and southern (0-0.1 km/yr from 50° to 52°N) Coast Mountains (Chapter 1).

The values of apatite-derived apparent uplift rates are also found to be reasonable estimates for use in thermal models. As indicated in Chapter 3 the use of zircon date-altitude relations can overestimate rates of uplift and considerable caution must be used in their interpretation.

The reduced heat flow Q*, the most elusive of geothermal parameters, has been estimated utilizing a combined fission track-heat flow modeling approach. To remain consistent with fission track data Q* must lie between 25 and 60 kW/km^2 for all areas. In the Ocean Falls-King Island example (Figure 15b, Table V) Q* can be shown to have increased by a factor of 1.5 from 20 Ma ago to the present. Low surface heat flow 20 Ma ago, during a period of relative tectonic stability, increased in the Late Miocene due to the sub-crustal passage of a 'hot spot' related to the Anahim volcanic belt (Bevier et al 1979). Considerable lithospheric thinning may have resulted from this event.

Values of 25-60 kW/km^2 for Q* fall between the extremes of subduction related arc-trench gap low heat flow (about 20

kW/km^2) and extension-related high heat flow (60 kW/km^2) like the present Basin and Range (Roy et al 1968). The consistency between heat flow models, fission track dates for apatite and zircon and their derived apparent uplift rates, and estimates of paleogeothermal gradients is thus very satisfying.

Causes of Uplift

Three main uplift events in the Coast Mountains must be addressed. They are the syn-orogenic to late-orogenic uplift of Late Cretaceous-Eocene age, the subsequent middle Cenozoic low uplift rates and their spatial variations, and lastly, the late Neogene rapid uplift largely responsible for the present mountains.

Orogenic culmination and uplift

Orogenic plutonic activity in the Coast Mountains occurred from middle Cretaceous to Eocene time. The relevant geological data and tectonic interpretations are discussed by Monger et al (1972), Roddick and Hutchison (1974), Woodsworth (1979), Woodsworth and Tipper (1980), and Hollister (1979). In general the Coast Plutonic Complex represents an eroded volcanic arc above a subduction zone which consumed the Farallon plate. The culmination of events in the Eocene from Alaska south to the Kemano area involved large uplift, the development of a wide and unusually high-grade axial metamorphic belt, and voluminous Eocene

intrusive rocks, and resulted in synorogenic crustal thickening. Plutonic underplating may also have contributed to this episode. Present crustal thickness in the area is approximately 30 km (Berry and Forsyth 1975), and since surface rocks were metamorphosed during the Eocene to pressures of up to 6-9 kb (600-900 MPa, Hollister 1979), Eocene crustal thickness must have exceeded 50 km. Such a tectonically thickened crust would have responded isostatically by rapid uplift and as erosion proceded, cooling of rocks. Though the core of this Eocene orogenic belt has not been modeled in this study, areas near the periphery of the Eocene metamorphic core zone such as Kemano and farther south near Mount Waddington experienced Eocene uplift rates of about 1 km/Ma; their tectonic situation was likely related. Uplift rates in the core of the belt may have been several times this rate (perhaps >10 km/Ma, Hollister 1979), more comparable to rates presently experienced in the southern Alps of New Zealand (Wellman 1979). Plutonic underplating may also have contributed to this crustal thickening episode.

This Eocene event was little felt in the southern Coast Mountains which lacked Eocene plutonism and large-scale Eocene deformation and metamorphism. Eocene orogenic events in southern British Columbia were concentrated in the Intermontane Zone and Omineca Crystalline Belt (Ewing 1980).

Following the Eocene, nearly all of the British Columbia mainland was quiescent until the late Neogene

(Monger et al 1972).

Middle Cenozoic uplift

The axial region of the Coast Mountains from latitude 52°-55°N experienced uplift at rates of 0.1-0.2 km/Ma during the period from 30 to 10 Ma (Chapter 1). In contrast, fission track data and modeling indicate that rates in the south were no more than 0.1 km/Ma, and perhaps near zero. There is evidence that paleogeothermal gradients were low in the region near Ocean Falls (17°/km), which may have been representative of the northern (52° to 55°N) region as a whole. Thus, the more rapid uplift in the north was probably not related to the expansion of crust or mantle. The igneous activity of the Anahim Volcanic Belt largely postdates this middle Cenozoic period of uplift.

The coincidence of most rapid (0.1-0.2 km/Ma) Miocene uplift rates and maximum middle Cenozoic total uplift (Chapter 1) with the Eocene orogenic axial zone is thought to be significant.

A thickened Eocene crust in the northern area would have induced rapid uplift during orogenesis and diminishing uplift afterwards. There would likely have been a significant crustal root supporting a mountain system for some time after culmination of tectonic activity. Since the uplift rates in the region were probably quite steady (as in the Ocean Falls-King Island area), it is suggested that the middle Cenozoic uplift was simply related to the gradual

erosion of the mountains bouyed by such a crustal root. Erosion in this case induces additional uplift at a slowly decreasing rate in the absence of any thermal anomaly. Over a time of several tens of millions of years, such a root would essentially disappear. A mature mountain physiography has been documented in the Bella Coola region prior to the eruption of 10 Ma basalts (Chapter 1, Baer 1973), and this was probably the same kind of topography that persisted throughout the middle Cenozoic in the central and northern Coast Mountains (52° to 55°N).

In contrast, uplift rates in the southern Coast Mountains (50° to 52°N) during the middle Cenozoic were low and little relief is preserved on the erosion surface beneath basalts of the same Late Miocene age. Fission track dates place tight constraints on the total amount of middle Cenozoic uplift and erosion. It seems likely that the southern area was very stable, lacked a crustal root, and had little relief during most of the Cenozoic, except in areas near active volcanoes (Chapter 1).

Late Neogene uplift

Following the prolonged middle Cenozoic period of relative tectonic quiescence, late Neogene uplift, especially in the south, elevated the crust up to 3 km. Uplift rates in the south exceeded 0.5 km/Ma for at least the last 5 Ma (Chapter 1), and geologic evidence alone suggests total uplift of 2-3 km. The southern segment has

been above an active subduction zone for the entire Neogene and probably since 100 Ma ago.

The northern segment of the Coast Mountains from 52-55°N had an average altitude and local relief of about 1.0 km and 1.5 km, respectively, prior to the eruption of 10 Ma basalts (Chapter 1). Fission track data and heat flow models for the axial zone suggest additional late Neogene uplift of about 2-3 km. Since the average altitude is lower in the north than in the south, it is suggested that this additional uplift occured mainly in the Late Miocene rather than the Pliocene, as is the case in the south. The late Neogene uplift in the north, outside the axial region, is thus somewhat less than in the south. Since the northern Coast Mountains (north of 52°N) are adjacent to a transform fault plate boundary whereas the southern Coast Mountains are opposite a subduction zone, it appears that plate setting may have played an important role in the mechanism of uplift in the two regions.

Uplift in the north (52° to 55°N)

In part, the late Neogene uplift in the north is a continuation of the middle Cenozoic uplift pattern and as such requires no special explanation. An acceleration of the rate from 0.2 km/Ma to 0.4 km/Ma in the Bella Coola region (Chapter 1) may be related in part to the Anahim volcanic belt, or hot spot, which passed beneath the Coast Mountains from 14-8 Ma ago (Bevier et al 1979). This thermal anomaly,

which may have coincided with the Early Miocene triple junction between Vancouver Island and Queen Charlotte Islands (Yorath and Chase 1981), was likely a broad zone of asthenospheric upwelling that interacted with the overlying lithosphere. Yorath and Chase (1981) suggested that thermally-induced, crustal-pervasive faults initiated basin development and volcanism in both Queen Charlotte Islands and southern Queen Charlotte Basin. As the hotspot passed beneath the crystalline rocks of the Coast Mountains, the thickness of the granitic crust probably inhibited similiar faulting and the thinning of the lithosphere was probably accomplished entirely within the lithospheric mantle beneath the crust.

If the Early Miocene (20 Ma) lithospheric thickness was 100 km corresponding to an approximate surface heat flow of about 40 kW/km^2, then thinning of the lithosphere to 40 km by the Anahim hot spot would induce about 1 km of uplift by thermal expansion. This calculation assumes that the coefficient of thermal expansion is 30 x $10^{-6}/^{o}C$ (an average for forsterite in Skinner 1966), and the average rise in temperature over the 60 km of heated lithosphere was $500^{o}C$. If this were accomplished over a period of a few million years, the uplift rates would be approximately those observed. Moreover, an increase in sub-crustal heat flow about 15 Ma ago is required by fission track dates, past and present heat flow data, and thermal models (Table V and Figure 15b). Whether the transverse path of the Anahim hot

spot could induce a longitudinal NW-trending uplift in the northern Coast Mountains is an open question; if there was any remanent Eocene thermal structure the hot spot may have enhanced it. At any rate there is clear heat flow evidence that a thermal perturbation occurred in the Bella Coola area of the northern Coast Mountains at about the same time as somewhat increased regional uplift, and the two are probably related.

Uplift in the south (49° to 52°N)

The size of the mountains in western British Columbia in itself suggests analogy to the world's great mountain systems such as the Himalaya, European Alps, Alaska Range, and the Southern Alps of New Zealand. For several reasons, however, the origin of the uplift in the Coast Mountains cannot be the same as in these other systems.

Most great mountain systems owe their high elevation to crustal thickening (Walcott 1978, LeFort 1975). In the examples cited, the uplift is a direct response to large scale horizontal motions of crustal plates, and present plate boundaries lie within the mountain belts as deduced by seismicity and distribution of active faults.

In the Coast Mountains, the lack of seismicity (Milne et al 1978), absence of thickened crust (Berry and Forsyth 1975) and present structural integrity strongly suggest that the cause of the uplift must lie within the upper mantle and that the uplift is not the result of ongoing crustal

shortening.

The pattern of uplift is related to various geological and geophysical features. The 2-3 km late Neogene uplift in the southern (50° to 52°N) Coast Mountains (Chapter 1, Mathews 1968) is directly opposite the plate boundary offshore where subduction is occurring. However, the pattern of late Neogene uplift is less intense in southern Washington and Oregon adjacent to the main part of the Juan de Fuca plate. One interesting and probably important correlation is that the uplift began during a pronounced hiatus in arc volcanism in the Late Miocene and Pliocene. The youngest volcanic event within the Pemberton Volcanic Belt on the east side of the Coast Mountains is about 8 Ma (Berman and Armstrong 1980), and the oldest within the Garibaldi Volcanic Belt to the west is about 2 Ma (Bevier et al 1979). The westward migration of the magmatic front to produce the Garibaldi belt represents a marked change in the volcanic pattern.

Thermal and geophysical data indicate that the upper mantle opposite the subduction-related plate boundary is different from that farther north adjacent to the Queen Charlotte transform fault. Upper mantle Pn wave velocities are 7.8 km/sec in both the southern Coast Mountains and the southern Interior in contrast to more normal continental velocities of 8.1 km/sec farther north (Berry and Forsyth 1975, Cumming et al 1979). Heat flow data in Jervis and Bute Inlets and northeast of Vancouver indicate a sharp

transition from low fore-arc (<40 kW/km^2) to high arc and back-arc values (>60 kW/km^2) near the present volcanic front (Hyndman 1976, Jessop and Judge 1971). Heat flow data are unfortunately sparse in central and northern British Columbia. The heat flow data (>60 kW/km^2) and seismic velocities (7.8 km/sec) in southern British Columbia indicate an upper mantle with moderately low density and fairly high temperature, probably corresponding to hot, solid peridotite. In the southern Interior a distinct mantle low velocity layer (MLVL) is clearly present and lies beneath a thin mantle lid (Wickens 1977). A well-developed MLVL is not observed beneath the Coast Mountains (Wickens 1977). The lithospheric thickness in the southern Interior can be inferred to be about 50-80km, but it may be considerably more (>100 km) beneath both the northern Interior and Coast Mountains (Wickens 1977).

Crustal thickness (Figure 16), derived from seismic refraction and ray tracing, increases eastwards from 25 to 40 km beneath the southern Coast Mountains (Berry and Forsyth 1975, Wickens 1977) and across the southern Interior from about 33 km just east of the Coast Mountains to over 40 km near the Rocky Mountain Trench (Cumming et al 1979). The crustal thickness gradient in the Coast Mountains is clearly reflected in the gradient of Bouguer gravity, shown in Figure 16. The close correlation between crustal thickness, regional altitude, and Bouguer gravity and the lack of appreciable seismicity in the Coast Mountains

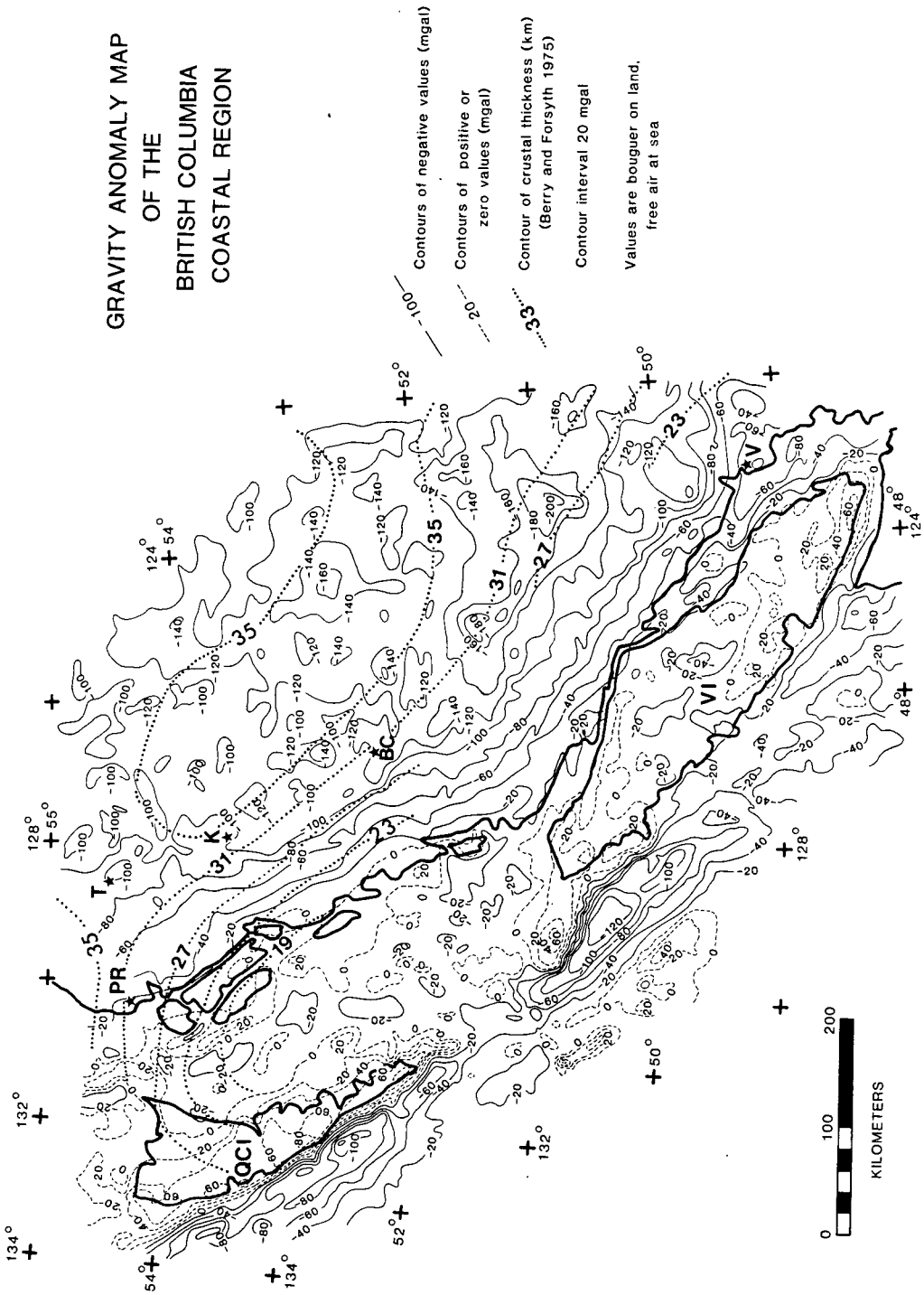

Figure 16. Gravity anomalies and crustal thickness in the Coast Mountains area. Gravity anomalies are bouguer on land and free air at sea, and are from the Earth Physics Branch (1980). Crustal thickness is from Berry and Forsyth (1975).

strongly suggests that the topography is isostatically compensated (Stacey 1973). If the crustal thickness values of Berry and Forsyth (1975) are correct, the mantle density must decrease southwards to explain the lower gravity and higher average altitude of the southern (50° to 52°N) Coast Mountains which have equally thick crust as the northern part (52° to 55°N).

Changes in the geometry and motion of oceanic plates as deduced from marine geophysical data can also be compared with the uplift history. Riddihough (1977) has suggested that important changes occurred about 4-5 Ma ago in the interaction between the American, Juan de Fuca, and Explorer plates. Prior to about 5 Ma, the Explorer plate was being subducted beneath the full extent of the southern Coast Mountains of British Columbia (Figure 17a). Subsequently, the Explorer-Juan de Fuca boundary, the Nootka fault zone, became more active and moved northwards to its position today off central Vancouver Island. The Pacific-Explorer-America triple junction has remained near the north end of Vancouver Island for at least 10 Ma and probably most of the Miocene. In addition to these geographic changes, the rates of convergence, as measured orthogonal to the continental margin, have not remained constant (Figure 17b). Riddihough (1977) notes a decrease in Explorer-America convergence from 4 cm/yr to 1.5 cm/yr from 3 to 5 Ma ago while Juan de Fuca-America rates declined from 4 to 3 cm/yr.

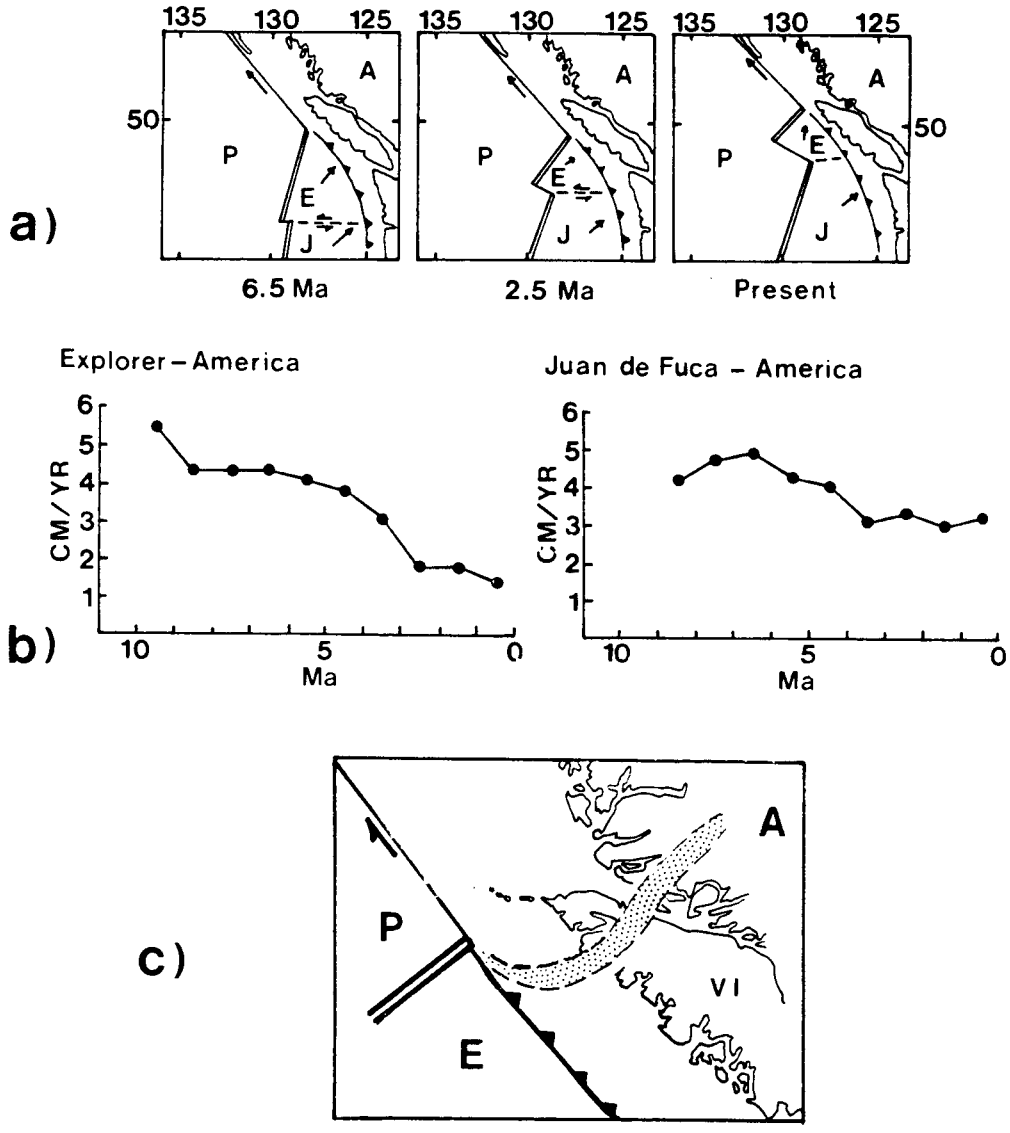

Figures 17a, 17b, and 17c. Reconstruction of past plate movements (a), orthogonal convergence rates (b), and the location of the northern edge of the subducted slab (c), modified from Riddihough (1977).

Reconstruction of this geometry indicates that prior to 5 Ma, rapid subduction of a single Explorer plate beneath southern British Columbia was occurring. The motion of this subducted plate slowed at 4 Ma and as the Nootka fault zone migrated northwards, the slow moving (<2cm/yr) Explorer plate was progressively replaced by a more rapidly moving (3-4cm/yr) Juan de Fuca plate. Thus, under the Coast Mountains north of Vancouver, the subducted slab was first a rapidly moving Explorer plate prior to 5 Ma, then a slowed Explorer plate, and finally a more rapidly moving Juan de Fuca plate. Figure 17c shows the trace of the northern edge of the plate since the Late Miocene. It seems reasonable that the observed discontinuity in volcanism may be an expression of these changes. The most recent period of volcanism, localized in the Garibaldi Volcanic Belt, is probably related to the renewed more rapid subduction of the Juan de Fuca plate, probably at a steeper angle as suggested by the westward jump in the locus of volcanism.

What plate tectonic and mantle processes could be responsible for the abrupt uplift documented by this study? Since the cause of uplift most likely resides in the mantle, a gross reduction in mantle density must be suspected. This could be thermal expansion caused by heating of the lithosphere, either internally by magma transfer or at its base by asthenospheric upwelling, or due to phase changes induced by heating. This change in mantle density must occur mainly beneath the Coast Mountains as opposed to the

Interior in order to explain the documented differential uplift.

The following sequence of events is suggested as an explanation. Since Pemberton volcanic belt volcanism was concentrated in the southeastern corner of the Coast Mountains region (Figure 1), and temporally overlapping basaltic volcanism occurred in the Interior Plateau (Bevier et al 1979), the Late Miocene subducted slab may have had a fairly shallow dip, perhaps less than 30°. The upper mantle and crustal region west of the Late Miocene Pemberton arc would have been in the low heat flow regime with surface heat flow less than 40 kW/km^2. In this western region, lithospheric thickness (including the America plate and the subducted slab) would have likely been 100-150 km (Figure 18).

During the reorganization of plate motion during the Late Miocene-Pliocene, as the Juan de Fuca plate replaced the Explorer plate, the subduction zone steepened to produce a westward shift in the locus of volcanism. The shallow-dipping, Late Miocene, subducted slab probably broke off and remained in place beneath the arc in a manner suggested by Thompson and Zoback (1979) for the Colorado Plateau region. Subduction then proceeded at a steeper angle as shown in Figure 18. The hiatus in volcanic activity in the Late Miocene and Pliocene probably resulted from both slowed Explorer convergence rates as well as initiation of the new zone of steeper subduction.

The material between the Pemberton and Garibaldi Volcanic Belts that was experiencing Late Miocene low heat flow (Figure 18) would have experienced relatively sudden heating resulting from steepened subduction and associated asthenospheric upwelling and magmatism. The warming of this lithospheric material above the slab would result in thermal expansion and uplift.

A >50% increase in surface heat flow from fore-arc low (<40 kW/km^2) to arc high (>60 kW/km^2) corresponds to an average temperature increase of about 500^0 for the fore-arc lithospheric thickness of about 100-150km. If the coefficient of thermal expansion for peridotite is assumed to be 30 x $10^{-6}/^0C$, then this temperature increase results in a density decrease of 1.5%. Mass balance implies 1.8 km of uplift by this process alone.

Additional uplift may have occurred by the conversion of eclogite to gabbro in the heated mantle region (Figure 18). Eclogitic material could have composed part of the lowermost crust or more likely the cut-off shallow slab. Assuming 5 km of eclogite converted to gabbro in this stagnant slab when the heat flux suddenly increased, an additional uplift of 0.5 km would have resulted (10% density decrease x 5 km thickness). Any partial melting would increase uplift even more. Convective upwelling of asthenospheric material above the region of subduction-related melting is essential to these models so that heat can be transported rapidly. The uplift of the

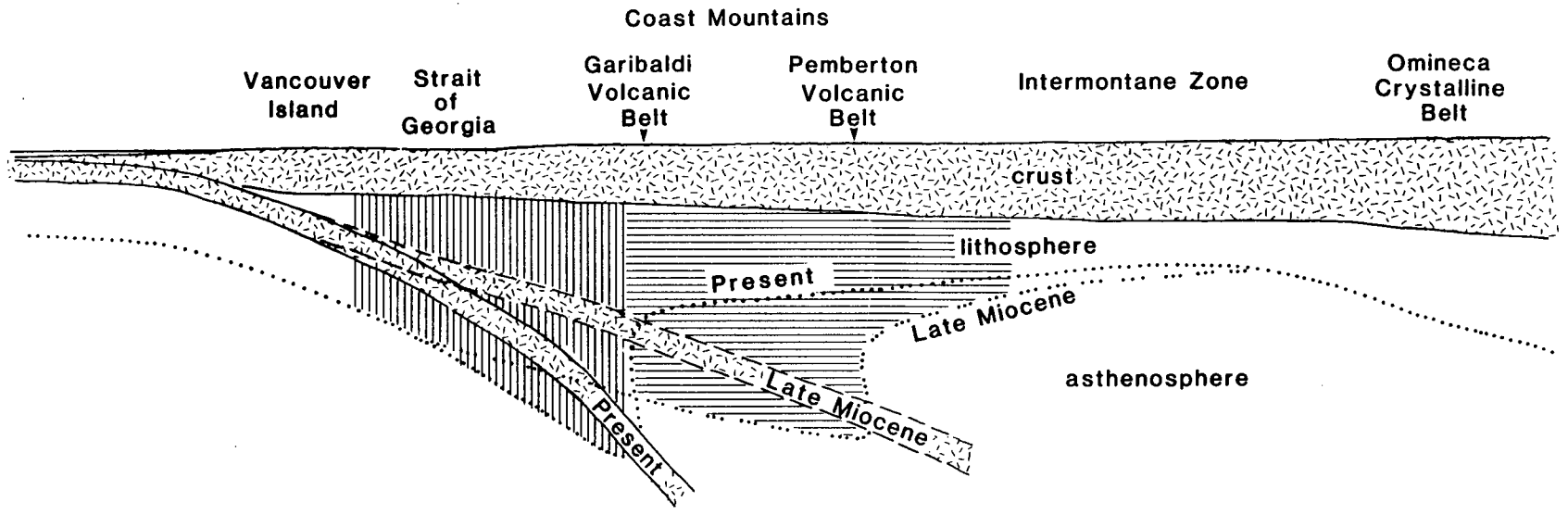

Figure 18. Schematic structural section across the southern Coast Mountains. Postulated lithosphere-asthenosphere boundaries are shown with the approximate position of the subducted plate in Late Miocene and Recent time; continental and oceanic crust, and the predominant volcanic belts are also outlined. The area of Miocene low heat flow that was heated as a consequence of steeper subduction is shown by horizontal lines. The adjacent area to the west where lithospheric thickening resulted from steeper subduction is shown by vertical lines.

southern Coast Mountains is thus related to heating of a formerly cool fore-arc upper mantle region by the upwelling of magma or hot asthenospheric material above a steepened subduction zone.

The region just west of this heated mantle region, shown in Figure 18, would have experienced lithospheric cooling and thickening as a direct result of steepened subduction in the Pliocene. This cooling and thickening would, by contrast, induce thermal contraction and subsidence. The lithospheric thickening, resulting from a density increase of 1-1.5% of former asthenospheric material, might be 20 to 30 km, and could induce 0.2 to 0.4 km of surface subsidence, approximately that observed in the Strait of Georgia.

The southern Interior was the locus of high back-arc heat flow and asthenospheric upwelling in both Miocene and Pliocene to Recent times; late Neogene uplift (about 0.5 to 1.0 km) in the southern Interior (Douglas et al 1970, Holland 1964) cannot be explained simply by the region's high heat flow. The generally elevated southern Interior (average altitude about 1.0-1.5 km) could be the result of the gradual warming, eclogite to gabbro conversion, and induced expansion of the flatter, cut-off, Miocene subducted slab that may have been present beneath much of the southern Interior. This explanation is similar to that of Thompson and Zoback (1979) for the uplift of the Colorado Plateau.

Summary

Heat flow models have been presented that simulate time-dependent uplift in a column of the earth's crust which is subjected to variable sub-crustal geothermal flux, changing surface temperature, erosion lagging behind uplift, and an exponentially downward declining distribution of heat production. An uplift history of the Coast Mountains, derived from fission track and geological data (Chapter 1) has been used with estimates of present and past heat flow (Hyndman 1976, Chapter 1) to derive models consistent with fission track and other isotopic data, heat flow measurements, and geological and physiographic data. These self-consistent models reinforce conclusions on uplift history drawn from Chapter 1.

The rapid uplift in the central and northern Coast Mountains (53° to 56°N) during the Eocene was felt around the periphery of the Eocene high-grade plutonic and metamorphic core zone with rates up to 1 km/Ma. This orogenic activity resulted in a substantially thickened crust which, during the middle Cenozoic, was gradually thinned by denudation-induced uplift. A Late Miocene episode of somewhat accelerated uplift was probably related to the passage of the Anahim hot spot beneath the area.

The southern Coast Mountains (50° to 52°N) experienced orogenic plutonic and metamorphic activity mainly during the Cretaceous and was tectonically stable throughout most of the Cenozoic, except for scattered volcanism. Late Neogene,

probably Pliocene to Recent uplift in the south, which resulted in 2 to 3 km of uplift of a broad area, was caused by Pliocene steepening and reorganization of subducted plate geometry and westward migration of the magmatic front. This migration caused abrupt heating of the formerly cool Miocene fore-arc mantle and consequent thermal expansion, leading to uplift. Steepened subduction also led to lithospheric thickening west of the magmatic front of the Garibaldi Volcanic Belt and subsidence of the Strait of Georgia. Warming of a proposed cut-off Miocene shallow-dipping slab under the southern Interior of British Columbia induced moderate uplift by thermal and possibly phase transiton expansion. The vertical movements documented in the Late Neogene were all thermally induced and were caused by changes in the plate tectonic regime.

Acknowledgements

During the course of this study, the author was supported by a Pre-doctoral fellowship at the University of British Columbia. Financial support was provided by a Natural Sciences and Engineering Research Council of Canada grant awarded to R.L. Armstrong, and through a Geological Society of America Grant-in-Aid. R.L. Armstrong was a constant source of support, advice, and ideas during the course of this study. The computing aspects were greatly improved through the advice of G.K.C. Clarke and E.H. Perkins, and W.H. Mathews, G.T. Nixon, T. Lewis, R.D. Hyndman, and G.K.C. Clarke provided ideas which improved both the manuscript and my understanding of geophysical and thermal processes. L. Gilmore assisted with drafting and cheerful field assistance, and K. Parrish aided with manuscript preparation and provided encouragement, for which the author is grateful.

References

Baer, A.J. 1973. Bella Coola-Laredo Sound map-areas, British Columbia. Geological Survey of Canada, Memoir 372, 122 p.

Berman, R.G., and Armstrong, R.L. 1980. The geology of the Coquihalla volcanic complex, southwestern British Columbia. Canadian Journal of Earth Sciences, 17, pp.985-995.

Berry, M.J., and Forsyth, D.A. 1975. Structure of the Canadian Cordillera from seismic refraction and other data. Canadian Journal of Earth Sciences, 12, pp.182-208.

Bevier, M.L., Armstrong, R.L., and Souther, J.G. 1979. Miocene peralkaline volcanism in west-central British Columbia-its temporal and plate-tectonic setting. Geology, 7, pp.389-392.

Blackwell, D.D. 1978. Heat flow and energy loss in the western United States. In Cenozoic tectonics and regional geophysics of the western Cordillera. Smith, R.B., and Eaton, G.P., eds. Geological Society of America, Memoir 152, pp.175-208.

Carnahan, B., Luther, H.A., and Wilkes, J.O. 1969. Applied numerical methods. John Wiley and Sons, Inc., New York.

Carslaw, H.S., and Jaeger, J.C. 1959. Conduction of heat in solids. 2nd edition. Oxford University Press, London. 510p.

Clark, S.P. 1966. Thermal conductivity. In Handbook of physical constants. Clark, S.P., ed. Geological Society of America, Memoir 97, pp.457-482.

Clark, S.P. 1979. Thermal models of the Central Alps. In Lectures in isotope geology. Jager, E., and Hunziker, J.C., eds. Springer-Verlag, New York, pp.225-230.

Clark, S.P., and Jager, E. 1969. Denudation rate in the Alps from geochronologic and heat flow data. American Journal of Science, 267, pp.1143-1160.

Cumming, W.B., Clowes, R.M., and Ellis, R.M.1979. Crustal structure from a seismic refraction profile across southern British Columbia. Canadian Journal of Earth Sciences, 16, 1024-1040.

Douglas, R.J.W., Gabrielse, H., Wheeler, J.O., Stott, D.F., and Belyea, H.R. 1970. Geology of western Canada. In

Geology and economic minerals of Canada. Geological Survey of Canada, Economic Geology Report No.1, pp.365-488.

Earth Physics Branch, 1980. Gravity anomaly map of the British Columbia coast area. Department of Energy, Mines, and Resources, Open File Map 80-13.

Ewing, T. 1980. Paleogene tectonic evolution of the Pacific Northwest. Journal of Geology, 88, pp.619-638.

Harrison, T.M., and Clarke, G.K.C.1979. A model of the thermal effects of igneous intrusion and uplift as applied to Quottoon pluton, British Columbia. Canadian Journal of Earth Sciences, 16, pp.411-420.

Harrison, T.M., Armstrong, R.L., Naeser, C.W., and Harakal, J.E. 1979. Geochronology and thermal history of the Coast Plutonic Complex, near Prince Rupert, British Columbia. Canadian Journal of Earth Sciences, 16, pp.400-410.

Harrison, T.M., and McDougall, I. 1980. Investigation of an intrusive contact, northwest Nelson, New Zealand-I. Thermal, chronologic, and isotopic constraints. Geochimica et Cosmochimica Acta, 44, pp.1985-2003.

Hollister, L.S. 1979. Metamorphism and crustal displacements: New insights. Episodes, 1979, no.3, pp.3-8.

Hyndman, R.D. 1976. Heat flow measurements in the inlets of southwestern British Columbia. Journal of Geophysical Research, 81, pp.337-349.

Jaeger, J.C. 1964. Thermal effects of intrusions. Reviews of Geophysics and Space Physics, 2, pp.443-466.

Jessop, A.M., and Judge, A.S. 1971. Five measurements of heat flow in southern Canada. Canadian Journal of Earth Sciences, 8, pp.711-716.

Lachenbruch, A.H. 1968. Preliminary geothermal model of the Sierra Nevada. Journal of Geophysical Research, 73, pp.6977-6989.

Lachenbruch, A.H. 1970. Crustal temperature and heat production: Implications of the linear heat-flow relation. Journal of Geophysical Research, 75, pp.3291-3300.

Lee, T.-C., Rudman, A.J., and Sjoreen, A.1980. Application of finite-difference analysis to terrestrial heat flow. Indiana Department of Natural Resources, Geological

Survey Occasional Paper 29, 53p.

Le Fort, P. 1975. Himalayas: The collided range. Present knowledge of the continental arc. American Journal of Science, 275-A, pp.1-44.

Lewis, T.J. 1976. Heat generation in the Coast Range complex and other areas of British Columbia. Canadian Journal of Earth Sciences, 13, pp.1634-1642.

Lewis, T.J., and Souther, J.G. 1978. Meager Mountain, British Columbia - a possible geothermal energy resource. Earth Physics Branch, Geothermal Series, no.9, 17p.

Lovering, T.S. 1935. Theory of heat conduction applied to geological problems. Geological Society of America Bulletin, 46, pp.69-94.

Mathews, W.H. 1968. Geomorphology, southwestern British Columbia. In Guidebook for geological field trips in southwestern British Columbia, Mathews, W.H., ed. Department of Geology, University of British Columbia, Report no.6, pp.18-25.

Mathews, W.H. 1972b. Geothermal data from the Granduc area, northern Coast Mountains of British Columbia. Canadian Journal of Earth Sciences, 9, pp.1333-1337.

Milne, W.G., Rogers, G.C., Riddihough, R.P., Hyndman, R.D., and McMechan, G.A. 1978. Seismicity of western Canada. Canadian Journal of Earth Sciences, 15, pp.1170-1193.

Monger, J.W.H., Souther, J.G., and Gabrielse, H. 1972. Evolution of the Canadian Cordillera: A plate tectonic model. American Journal of Science, 272, pp.577-602.

Monger, J.W.H., and Price, R.A. 1981. Evolution of Canadian Cordillera. Geological Association of Canada, Abstracts, 6, p.A-47.

Parrish, R.R. 1980. Fission track estimation of paleo-heat flow, Coast Mountains of British Columbia, Canada. EOS, 61, p.1131.

Riddihough, R.P. 1977. A model for the recent plate interactions off Canada's west coast. Canadian Journal of Earth Sciences, 14, pp. 384-396.

Roddick, J.A., and Hutchison, W.W. 1974. Setting of the Coast Plutonic Complex, British Columbia. Pacific Geology, 8, pp.91-108.

Roddick, J.A., and Woodsworth, G.J. 1977. Bute Inlet (92K)

map-area. Geological Survey of Canada, Open file map 480.

Rouse, G.E., and Mathews, W.H. 1979. Tertiary geology and palynology of the Quesnel area, British Columbia. Bulletin of Canadian Petroleum Geology, 27, pp.418-445.

Roy, R.F., Blackwell, D.D., and Birch, F. 1968. Heat generation of plutonic rocks and continental heat-flow provinces. Earth and Planetary Science Letters, 5, pp.1-12.

Schaer, J.P., Reimer, G.M., and Wagner, G.A. 1975. Actual and ancient uplift rate in the Gotthard region, Swiss Alps: A comparison between precise leveling and fission track apatite age. Tectonophysics, 29, pp.293-300.

Skinner, B.J. 1966. Thermal expansion. In Handbook of physical constants. Clark, S.P., ed. Geological Society of America Memoir 97, pp.75-96.

Souther, J.G. 1977. Volcanism and tectonic environments in the Canadian Cordillera - A second look. In Volcanic regimes in Canada. Baragar, W.R.A., and others, eds., Geological Association of Canada Special Paper 16, pp. 3-24.

Stacey, R.A. 1973. Gravity anomalies, crustal structure, and plate tectonics in the Canadian Cordillera. Canadian Journal of Earth Sciences, 10, pp.615-628.

Strahler, A.N. 1973. Introduction to physical geography, 3rd ed. John Wiley and Sons, Inc. New York.

Thompson, G.A., and Zoback, M.L. 1979 Regional geophysics of the Colorado Plateau. Tectonophysics, 61, pp.149-181.

Walcott, R.I. 1978. Present tectonics and Late Cenozoic evolution of New Zealand. Geophysical Journal of the Royal Astronomical Society, 52, pp.137-164.

Wanless, R.K., Stevens, R.D., Lachance, G.R., and Delabio, R.N. 1979. Age determinations and geologic studies. Geological Survey of Canada, Paper 79-2.

Wellman, H.W. 1979. An uplift map for the South Island of New Zealand, and a model for uplift of the Southern Alps. Royal Society of New Zealand, Bulletin 18, pp.13-20.

Wickens, A.J. 1977. The upper mantle of southern British Columbia. Canadian Journal of Earth Sciences, 14, pp.1100-1115.

Woodhouse, J.H., and Birch, F. 1980. Comment on 'Erosion, uplift, exponential heat source distribution, and transient heat flux' by T.-C.Lee. Journal of Geophysical Research, 85, pp.2691-2693.

Woodsworth, G.J. 1979. Metamorphism, deformation, and plutonism in the Mount Raleigh pendant, Coast Mountains, British Columbia. Geological Survey of Canada, Bulletin 295, 58p.

Woodsworth, G.J., and Tipper, H.W. 1980. Stratigraphic framework of the Coast Plutonic Complex, western British Columbia. Geological Association of Canada Cordilleran Section, Programme and Abstracts, pp.32-34.

Yorath, C.J., and Chase, R.L. 1981. Tectonic history of allochthonous terranes: Northern Canadian Pacific continental margin. Geological Association of Canada Cordilleran Section, Programme and Abstracts, pp. 42-43.

CHAPTER 3.

REFINEMENT OF APPARENT UPLIFT RATES

DETERMINED BY

FISSION TRACK DATING

Abstract

Fission track dating of apatite and zircon is widely used to infer cooling and uplift histories of rocks. Dating minerals from rocks collected at various altitudes usually reveals an increase in date with altitude which translates into an apparent uplift rate. This apparent rate will equal true uplift rate only if erosion equals uplift, isotherms remain fixed with respect to the surface, and when lateral heat flow is negligible compared to vertical heat flow. These conditions are rarely met; a heat flow model is used to derive corrections to fission track-derived apparent uplift rates so that they can be used with greater confidence in teconic interpretations.

Apatite-derived apparent rates will closely approximate true uplift rates when regional geothermal gradients are relatively high and when the dates record uplift following 3 to 5 Ma after the initiation or cessation of uplift. Apparent uplift rates derived from zircon dates must be used with caution since excessive or deficient rates can result from gradual isotherm relaxation or slow response to uplift initiation. Slightly excessive rates can also result from prolonged uplift accompanied by erosion of heat producing elements concentrated near the surface of the crust.

Introduction

Fission track dating of apatite has been used by numerous workers to infer paleo-uplift rates in mountains belts. The technique has been useful to infer uplift and cooling histories where little or no stratigraphic or geologic evidence has been available.

In the Alpine-Himalaya system, Wagner and Reimer (1972), Wagner *et al* (1977), Schaer *et al* (1975), and Zeitler (in preparation) documented an increase in fission track date with increasing altitude and inferred that the altitude-date slope represented the uplift rate of the rocks. This slope on the altitude-date graph will be referred to as the *apparent uplift rate* (Chapter 1). In an interesting application to the Bergell Massif, Wagner *et al* (1979) dated *in situ* plutonic rocks from different altitudes and clasts of Bergell intrusives in sediments of the adjacent Po Plain and documented not only inferred uplift rates, but also the original pre-erosion position of the transported clasts. Other workers including Gleadow and Brooks (1979) and Sharma *et al* (1980) have determined the cooling rates of rocks by dating different minerals (zircon, apatite) and inferred uplift rates by making an assumption of the paleo-geothermal gradient. Chapter 1 summarizes fission track dating of apatite and zircon collected at various altitudes from the Coast Mountains of British Columbia, Canada, and in conjunction with heat flow models, documents a Cenozoic uplift history.

Fission track dating of zircon and apatite has widespread application and importance to the study of relatively recent uplift and related tectonic processes, but the assumption of equating apparent uplift rates with actual rates is simplistic and valid only when several conditions are satisfied. These are that 1) erosion must equal uplift, 2) isotherms must have remained horizontal, uninfluenced by topography or heterogeneities in conductivity or geothermal flux, and 3) isotherms must remain fixed with respect to the surface regardless of the rate of uplift. Clearly, these assumptions will rarely be met. It is important to assess the effect of violations of these assumptions on the derived apparent uplift rates in order to confidently use them in tectonic interpretation.

Ways to Generate Apparent Uplift Rates

If a rock mass is suddenly uplifted and simultaneously denuded such that the surface remains at a constant altitude, then isotherms will be carried upwards with respect to the surface. This effect produces an initial increase in surface heat flow. Since the apparent uplift rate determined from fission track studies is in essence the rate that the critical track retention isotherm moves downward through the rock column, the apparent uplift rate will initially be less than the true uplift rate.

Eventually, with continued uplift, and with the condition that uplift equal erosion, isotherms can either

stabilize, continue slowly rising, or slowly fall, depending on the vertical distribution of heat producing elements (see Woodhouse and Birch 1980). In this situation, apparent uplift rates will equal, be slightly below, or slightly exceed the true uplift rate. Either way, they will be very close to the actual rate, once the initial transient lag has decayed away.

Upon the cessation of uplift or after the influx of heat has ceased in an area subject to either rapid uplift or higher than normal heat flow, isotherms will relax, sometimes rapidly. This thermal relaxation will produce positive apparent uplift rates, even when no uplift has occurred and will lead to misleading inferences of uplift.

Clearly one must distinguish between these possibilities when interpreting fission track data. The best way to evaluate this is through quantitative heat flow models.

A Heat Flow Model and its Application

A one-dimensional finite difference thermal model was developed to study the effects of variable uplift and erosion rates, changing sub-crustal geothermal flux and fluctuating surface temperature on a column of crust with an exponential downwards decreasing distribution of heat production. This model, described in Chapter 2, allows for a realistic approximation of heat flow and isotherm migration in areas of active uplift where lateral heat flow and

igneous intrusion are not important.

To test the effect of uplift on the movement of isotherms and the consequent setting of fission track clocks, eight models representing a wide variety of uplift rates have been run. The models incorporate an initial temperature distribution,

$$V(Z) = (Q^*Z/\kappa) + (D^2Ao/\kappa)(1-\exp(-Z/D)) + a$$

where V(Z) is the temperature at depth Z below the surface, Q* is the reduced heat flow, κ is the conductivity, D is scale height, Ao is the surface heat production, and a is the mean surface temperature. In the models that follow, κ=2.5 kW/km$^{\circ}$C (5.98x10^{-3} cal/sec-cm-$^{\circ}$C), D=10 km, a=0°C, and Q*=25 kW/km^2, and uplift is assumed to be matched by erosion.

Four of the models have Ao=1.0 kW/km^3 and uplift rates of 1.0, 0.6, 0.3, and 0.1 km/Ma, and are shown as the dotted curves A, B, C, and D of Figure 19a, respectively. Uplift is allowed to continue for 20 Ma, after which it ceases and isotherms are allowed to relax. Also shown in Figure 19a are the curves of "steady state" heat flow for each case. This is the value of heat flow, Q, that would eventually result if uplift was stopped at any time and isotherms allowed to fully relax. Increasing rates of uplift result in lower "steady state" equilibrium heat flow values since more of the heat producing elements are removed by erosion. Figure

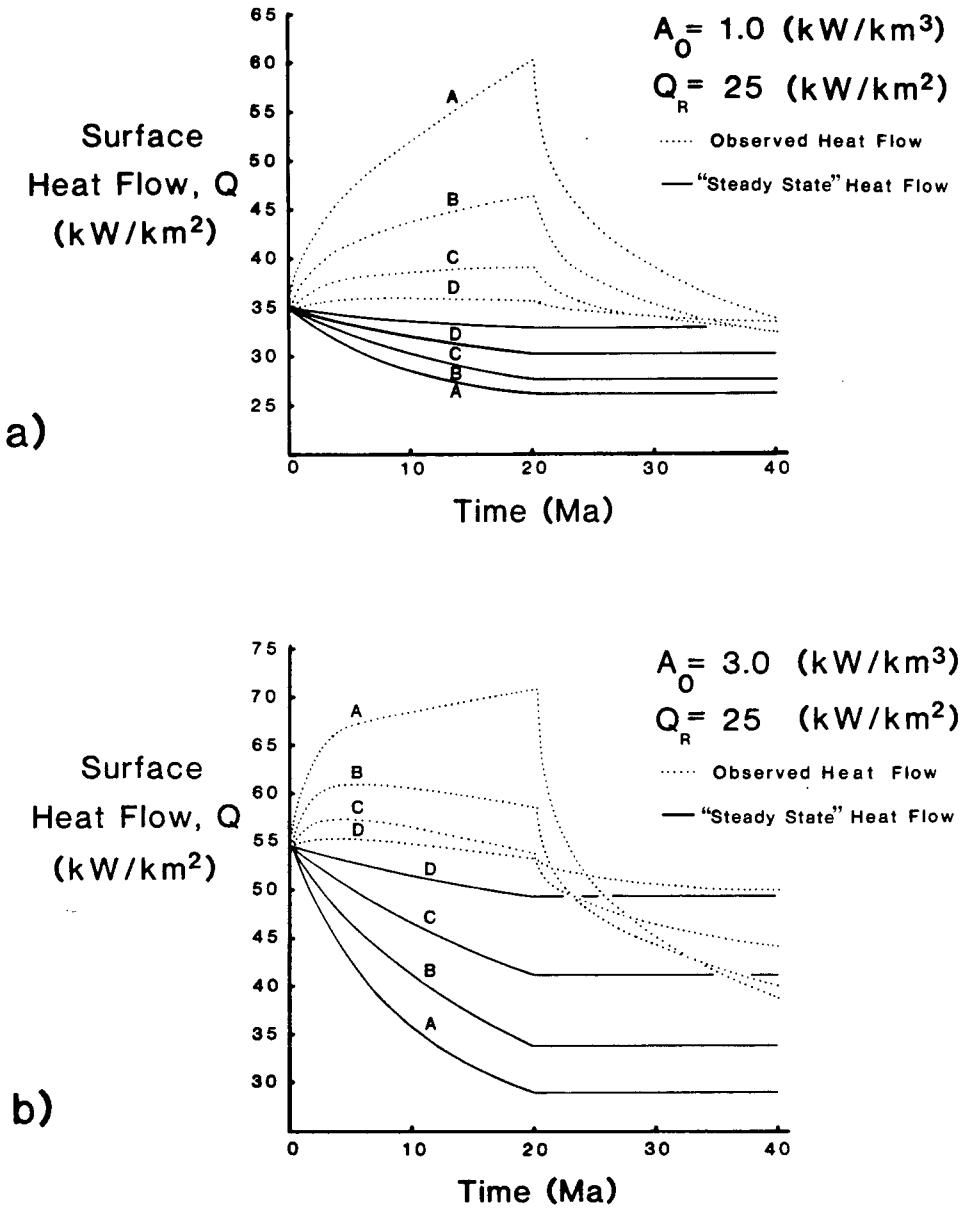

Figure 19. Surface heat flow vs. time curve for thermal models described in the text. Uplift rates are 1.0, 0.6, 0.3, and 0.1 km/Ma for models A, B, C, and D, respectively. The uplift rates are continued for 20 Ma but are zero from 20-40 Ma while thermal relaxation occurs. "Steady state" heat flow is that which would result if, at any time, uplift stopped and the isotherms were allowed to fully relax.

19b shows curves for the same four rates of uplift A, B, C, and D with the condition that Ao=3.0 kW/km^3. "Steady state" heat flow values in this case have decreased more than when Ao=1.0 kW/km^2, and tend with large uplift to approach the value of Q*. Figure 19 clearly shows the effect that uplift and erosion have on the surface heat flux.

Apparent vs. True Uplift Rates

Estimates of apparent uplift rate have been made for apatite and zircon by noteing the time that a rock at a specific depth passes below its respective track retention temperature during uplift-related cooling. The same is done for rocks at successively greater depths for each of the eight models. A depth-time curve for the two (105°C and 175°C) critical isotherms can thus be constructed. Subtraction of the slope of this curve from the given uplift rate (with respect to the surface) gives the apparent uplift rate. Curves of apparent uplift rate have been constructed for the four constant uplift rates and for the cases when Ao changes from 1.0 to 3.0 kW/km^3. These curves are shown in Figure 20. Note in Figure 20 that there can be a considerable difference between apparent uplift rate and true uplift rate.

Though tracks are increasingly retained over a range of temperature (Naeser and Faul 1969), the concept of an effective closure temperature is applicable here (Dodson 1973, Haack 1977) since all rocks will pass this closure

range in a similar fashion. In this calculation, closure temperatures of 105°C and 175°C were chosen for apatite (Zimmerman and Gaines 1978, Naeser and Forbes 1976) and zircon (Harrison et al 1979), respectively. The specific choice of closure temperature will not affect the conclusions of this paper.

Apparent Uplift Rates during Uplift

Because sudden inception of uplift causes upward movement of isotherms, the initial apparent rates will be far below the true rate. This is especially important in the first few million years of uplift (Figure 20), and the lag of apparent rates behind actual rates is longer for zircon than apatite since the isotherms move a greater distance upwards. The dashed lines show the time when the apparent rate is a fixed proportion (75%, 90%, 25%) of the actual or former uplift rate.

It is evident from Figure 20 that when geothermal gradients are initially higher, as when Ao=3.0 kW/km^3, the apparent rates approach true rates more rapidly since the 105°C and 175°C isotherms are initially nearer the surface and are displaced upwards by a smaller amount. Rocks passing upwards in this case move by isotherms more rapidly. This same effect would occur if Q* was higher.

When Ao=1.0 kW/km^3 and Q*=25 kW/km^2, the geothermal gradient is a rather low 14°C/km. Uplift proceeding in such a regime will result in apatite apparent uplift rates being

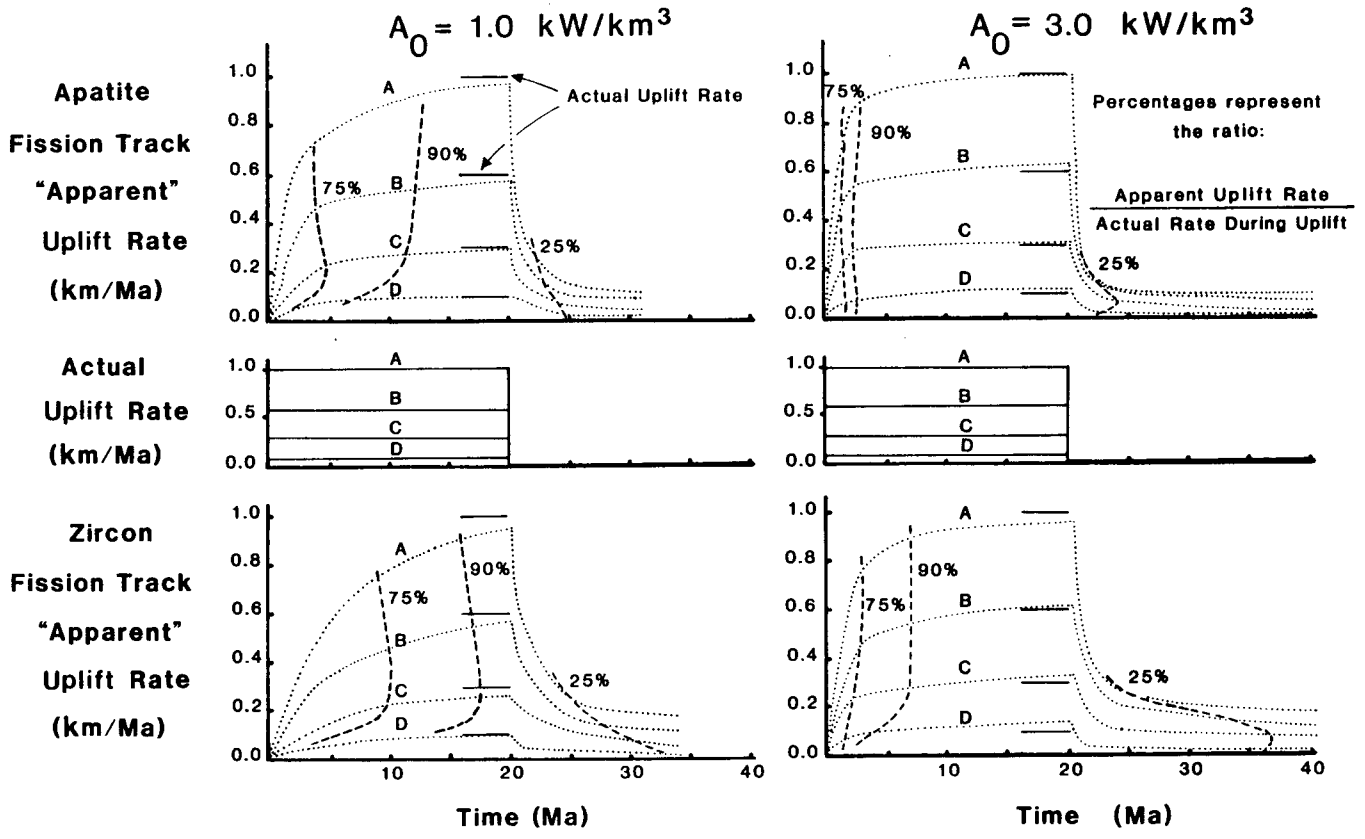

Figure 20. Apatite and zircon apparent uplift rate vs. time curves for models described in the text and shown in Figure 19. Rates of uplift for curves A, B, C, and D are shown by the middle diagram (actual uplift rate vs. time). The apparent uplift rate represents the rate at which the critical isotherms move downward through the rock column.

within 25% of the true value after a period of 3 to 5 Ma (Figure 20). Since most mountain systems are characterized by higher geothermal gradients, this 5 Ma lag period is a maximum; in most cases, it will be less and apparent rates will be very close to true rates within only a few million years. Consequently, in most cases of uplift, apparent apatite rates will closely approach true rates and may be used as such.

The corresponding lag after which apparent rates are 75% of true rates is greater for zircon, and may be up to 10 Ma after uplift commences (Figure 20). It is thus less responsive than apatite for uplift studies, where uplift rates are subject to rapid fluctuation.

The uplift rate and the denudation of heat producing elements are competing processes which determine the movement of isotherms and variations in heat flow. With all models, the first stage in thermal evolution after initiating uplift is a rise in isotherms and Q. If uplift rate is sufficiently high (>0.2 km/Ma for Ao=1.0 kW/km^3, >0.6 km/Ma for Ao=3.0 kW/km^3, >1.2 km/Ma for Ao=6.0 kW/km^3), heat flow will continue to increase, despite the removal of upwards-concentrated heat producing elements. This results in continued upward migration of isotherms with the consequence that apparent uplift rates will always be less than the true rate of uplift. If uplift rate is less than these estimates for a given Ao, isotherms and resultant heat flow will begin to decline, reflecting reduced heat

production in the upper crust. When isotherms decline, apparent uplift rates will exceed true rates of uplift. Even for long (and sometimes unrealistic) periods of uplift, the apparent rates for apatite and zircon will not exceed the true rate by more than about 20% so that this effect is not very important. After declining for a considerable time as a result of removal of heat producing elements, isotherms will begin to slowly rise again. This will cause apparent uplift rates to be slightly less than true rates. Clearly, however, once the initial 3 to 5 Ma period since inception of uplift has passed, apparent uplift rates for apatite will remain very close (±20%) to the true rate of uplift. This situation is more complex when uplift and erosion are not in balance, but will average out over long uplift periods.

Apparent Rates during Isotherm Relaxation

Misleading apparent uplift rates are produced when isotherms relax through either a cessation of uplift (Figure 20) or through the cooling of an intrusive body. For apatite, the fictitious apparent rates produced by downward-moving isotherms drop to less than 25% of the former rate within a few million years, but take several times longer for zircon. Zircon date-altitude trends, therefore, can be strongly affected by this thermal relaxation and the interpretation of uplift from such zircon data can be misleading. Clearly a combination of diminishing uplift and isotherm relaxation will produce an effect

between the extremes described here.

Inspection of Figure 20 reveals that if a relatively constant uplift continues for a significant (10-20 Ma) period of time, then the fission track-derived estimates of apatite apparent uplift rates preserved in the rocks will closely approximate the true uplift history. A similar observation for zircon is not possible since the position of the 175°C isotherm is shifted much more during uplift and thermal relaxation. The approach, described in Chapter 2, where fission track-derived uplift histories are evaluated and/or verified by thermal modeling provides the best method of arriving at an accurate uplift history. In several examples in Chapters 1 and 2, zircon apparent rates are significantly in excess of the most likely uplift rates consistent with thermal models and geologic data. Apatite apparent rates, on the other hand, are usually very good indicators of the actual rates of uplift.

Discussion

A combined approach of heat flow modeling and fission track dating of apatite and zircon can provide excellent documentation of the uplift history of rocks in mountain belts. Thermal modeling does show, however, that in areas of low geothermal gradient (produced by low Q*, low Ao, or both) the corrections that must be made to fission track-derived apparent uplift rates can be large, and modeling should be done to find the actual uplift rates that

will produce the observed fission track date-altitude trends.

The fission track-derived rates can be either more or less than the true uplift rate depending on whether the dates preserved were frozen in the rocks at the end or beginning of an uplift episode. A knowledge of the timing of uplift from geological data can help to choose between these alternatives.

If a knowledge of Ao, Q*, or average geothermal gradient is available for an area where fission track dating studies on samples from different altitudes is done, the curves of Figure 20 can be used as a general guideline in evaluating the possible error in calculated apparent rate.

Apatite can continue to be widely used in a manner similar to that of Wagner et al (1979), Schaer et al (1975) in Chapter 1, but the extension of the method to zircon should proceed with caution unless thermal modeling accompanies the analysis of zircon data. Geothermal inferences gained from such work (such as constraints on Q*) can provide useful insight on the causes of uplift.

Acknowledgements

This paper has benefited from discussions on heat flow with G.K.C.Clarke. W.H.Mathews and T.J.Lewis encouraged me to quantify the relationship between uplift, movement of isotherms, and fission track derived apparent uplift rates. Their comments, and those of R.L.Armstrong, are appreciated. This work was supported by the Natural Sciences and Engineering Research Council of Canada as a grant awarded to R.L.Armstrong.

References

Dodson, M. 1973. Closure temperature in cooling geochronologic and petrologic systems. Contributions to Mineralogy and Petrology, 40, pp.259-274.

Gleadow, A.J.W., and Brooks, C.K. 1979. Fission track dating, thermal histories and tectonics of igneous intrusions in east Greenland. Contributions to Mineralogy and Petrology, 71, pp.45-60.

Haack, U. 1977. The closing temperature for fission track retention in minerals. American Journal of Science, 277, pp.459-464.

Harrison, T.M., Armstrong, R.L., Naeser, C.W., and Harakal, J.E. 1979. Geochronology and thermal history of the coast plutonic complex, near Prince Rupert, British Columbia. Canadian Journal of Earth Sciences, 16, pp.400-410.

Naeser, C.W., and Faul, H. 1969. Fission track annealing in apatite and sphene. Journal of Geophysical Research, 74, pp.705-710.

Naeser, C.W., and Forbes, R.B. 1976. Variation of fission track ages with depth in two deep drill holes (abstract). EOS, 57, p.363.

Schaer, J.P., Reimer, G.M., and Wagner, G.A. 1975. Actual and ancient uplift rate in the Gotthard region, Swiss Alps: A comparison between precise leveling and fission track apatite age. Tectonophysics, 29, pp.293-300.

Sharma, K.K., Bal, K.D., Parshad, R., Lal, N., and Nagpaul, K.K. 1980. Paleo-uplift and cooling rates from various orogenic belts of India, as revealed by radiometric ages. Tectonophysics, 70, pp.135-158.

Wagner, G.A., and Reimer, G.M. 1972. Fission track tectonics: The tectonic interpretation of fission track apatite ages. Earth and Planetary Science Letters, 14, pp.263-268.

Wagner, G.A., Reimer, G.M., and Jager, E. 1977. The cooling ages derived by apatite fission track, mica Rb-Sr, and K-Ar dating: The uplift and cooling history of the Central Alps. Memoir of the Institute of Geology and Mineralogy, University of Padova, Padova, Italy, XXX, 27p.

Wagner, G.A., Miller, D.A., and Jager, E. 1979. Fission track ages on apatite of Bergell rocks from Central Alps and Bergell boulders in Oligocene sediments. Earth and

Planetary Science Letters, 45, pp.355-360.

Woodhouse, J.H., and Birch, F. 1980. Comment on 'Erosion, uplift, exponential heat source distribution, and transient heat flux' by T.-C.Lee. Journal of Geophysical Research, 85, pp.2691-2693.

Zimmermann, R.A., and Gaines, A.M. 1978. A new approach to the study of fission track fading. United States Geological Survey, Open file Report 78-701, pp.467-468.

APPENDIX 1.

COASTMTN, A FINITE DIFFERENCE COMPUTER PROGRAM FOR USE IN HEAT FLOW MODELING

```
C  FINITE DIFFERENCE SOLUTION TO THE 1-DIMENSIONAL HEAT FLOW
C  PROBLEM WITH VARIABLE UPLIFT, SURFACE TEMPERATURE, REDUCED
C  FLOW, AND EXPONENTIALLY DECREASING DISTRIBUTION OF HEAT
C  PRODUCTION
C
C  THE PROGRAM IS DESIGNED FOR THE CENOZOIC HISTORY OF THE
C  BRITISH COLUMBIA COAST MOUNTAINS.  THE SURFACE TEMPERATURE
C  CAN BE CHANGED TO SIMULATE CONDITIONS WHEN UPLIFT AND
C  EROSION ARE NOT IN BALANCE.
C
C  THE PROGRAM IS DESIGNED FOR A MAXIMUM GRID OF 200X200.  TO
C  BE REALISTIC, THE HEAT PRODUCTION AT THE BASE OF THE GRID
C  SHOULD BE LESS THAN 2% THAT OF THE SURFACE.
C
      INTEGER TT
      REAL LAM,K,LAPSE
      DIMENSION A(210),B(210),C(210),DD(210),V(210),QR(210)
      DIMENSION TSURF(210),U(210,210),W(210,5),P(210),PP(210)
      DIMENSION TOTUP(210),UPL(210),AQSURF(210)
      DIMENSION UU(210,210), SURFEL(210)
      DIMENSION A0BASE(210),A0SURF(210),AQT(210),AQB(210)
      WRITE (6,800)
      READ (5,900) A0,K,DIF,D,Q0
      WRITE (6,810)
      READ (5,910) TSURF0,DTSURF
      WRITE (6,820)
      READ (5,920) ZMAX,TMAX
      WRITE (6,830)
      READ (5,930) DZ,DT
C
C  SET LOWER BOUNDARY CONDITIONS-VARIABLE FLUX; 2 CHANGES IN
C  REDUCED HEAT FLUX ARE ALLOWED AT TIMES TQR1 AND TQR2; THE
C  THREE HEAT FLUX VALUES-OLDEST TO YOUNGEST-ARE QR1,QR2,AND
C  QR4.
C
      WRITE (6,840)
      READ (5,940) QR1,TQR1,QR2,TQR2,QR3
C
C  SET UPLIFT RATE CONDITIONS-3 CHANGES IN UPLIFT RATE ARE
C  PERMITTED AT TIMES TUPL1, TUPL2, TUPL3; THE 4 RATES ARE
C  UPL1,UPL2,UPL3, AND UPL4.
C
      WRITE (6,850)
      READ (5,950) TUPL1,TUPL2,TUPL3,UPL1,UPL2,UPL3,UPL4
C
C  SET CONDITIONS WHEN UPLIFT .NE. EROSION
C
      WRITE (6,1100)
      READ (5,1110) LAPSE
      WRITE (6,1120)
      READ (5,1130) AAA
      WRITE (6,1140)
      READ (5,1150) BBB
      WRITE (6,1160)
```

```
      READ (5,1170) TNONEQ
C
C  CALCULATE UPL VECTOR, WITH RESPECT TO SURFACE
C
      X1=TUPL1/DT+0.1
      X2=TUPL2/DT+0.1
      X3=TUPL3/DT+0.1
      X4=TMAX/DT+0.1
      J101 = IFIX(X1)
      J102=IFIX(X2)
      J103=IFIX(X3)
      J104=IFIX(X4)
      J101A=J101+1
      J102A=J102+1
      J103A=J103+1
      J104A=J104+1
      DO 20 JV=1,J101
      UPL(JV)=UPL1
   20 CONTINUE
      DO 25 JV=J101A,J102
      UPL(JV)=UPL2
   25 CONTINUE
      TN=(TNONEQ/DT)+1.0
      DO 30 JV=J102A,J103
      RJV=FLOAT(JV)
      UPL(JV)=UPL3
      IF (RJV.GT.TN) UPL(JV)=UPL3*BBB
   30 CONTINUE
      DO 35 JV=J103A,J104
      UPL(JV)=UPL4*BBB
   35 CONTINUE
C
C  CALCULATE QR VECTOR
C
      X5=TQR1/DT+0.1
      X6=TQR2/DT+0.1
      J105=IFIX(X5)
      J106=IFIX(X6)
      J105A=J105+1
      J106A=J106+1
      DO 40 JQ=1,J105
      QR(JQ)=QR1
   40 CONTINUE
      DO 45 JQ=J105A,J106
      QR(JQ)=QR2
   45 CONTINUE
      DO 50 JQ=J106A,J104A
      QR(JQ)=QR3
   50 CONTINUE
C
C  CALCULATE TSURF AND SURFEL VECTORS
C
      ALTINC=0.0
      ALPHA=0.0
```

```
      DO 60 JS=1,J104A
      TSURF(JS)=TSURF0+DTSURF*FLOAT(JS-1)*DT
      TN=(TNONEQ/DT)+1.0
      RJS=FLOAT(JS)
      IF (RJS.LT.TN) SURFEL(JS)=0.0
      IF (RJS.EQ.TN) SURFEL(JS)=0.0
      IF (RJS.GT.TN) ALPHA=DT*UPL(JS-1)*LAPSE*AAA
.*(1.0-BBB)/BBB+ALPHA
      IF (RJS.GT.TN) TSURF(JS)=TSURF(JS)+ALPHA
      IF (RJS.GT.TN) ALTINC=DT*(1.0-BBB)*UPL(JS-1)
.*AAA/BBB+ALTINC
      IF (RJS.GT.TN) SURFEL(JS)=ALTINC
   60 CONTINUE
      LAM=(DIF*DT)/(DZ*DZ)
C
C  SET INITIAL CONDITIONS
C
      X7=ZMAX/DZ+0.1
      J107=IFIX(X7)
      J107A=J107-1
      DO 300 JZ=1,J107
      Z=FLOAT(JZ)*DZ
      T0=TSURF0+Q0*Z/K
      T0=T0+(D*D*A0/K)*(1.0-EXP(-Z/D))
      U(1,JZ)=T0
  300 CONTINUE
      TOTUPL=0.0
C
C  PERFORM TIME INCREMENT
C
      DO 100 TT=2,J104A
      T=(FLOAT(TT)-1.0)*DT
      GAM=((UPL(TT-1)+UPL(TT))*DT)/(4.0*DZ)
C
C  CALCULATE TOTAL SURFACE DENUDATION VECTOR
C
      TOTUPL=DT*UPL(TT-1)+TOTUPL
      TOTUP(TT-1)=TOTUPL
C
C  CALCULATE HEAT PRODUCTION VALUES AT BASE AND SURFACE
C
      A0BASE(1)=A0*EXP(-ZMAX/D)
      A0BASE(TT)=A0*EXP(-(ZMAX-TOTUP(TT-1))/D)
      A0SURF(1)=A0
      A0SURF(TT)=A0*EXP(TOTUP(TT-1)/D)
C
C  PERFORM DEPTH INCREMENT
C
      LAST=IFIX(X7)-1
      DO 120 JZ=1,LAST
      Z=FLOAT(JZ)*DZ
      A(JZ)=LAM+GAM
      B(JZ)=-(2.0*LAM+2.0)
      IF (JZ.EQ.LAST) B(JZ)=-(LAM+2.0+GAM)
```

```
      C(JZ)=LAM-GAM
C
C    SET ASTAR (HEAT PRODUCTION TERM)
C
      ASTAR1=-(Z-TOTUP(TT-1))/D
      ASTAR=(2.0*DIF*DT*A0/K)*EXP(ASTAR1)
C
C   SET RIGHT HAND SIDE VECTOR DD
C
      IF (JZ.EQ.LAST) GO TO 350
      IF (JZ.EQ.1) GO TO 360
      DD(JZ)=-A(JZ)*U(TT-1,JZ-1)+(2.0*LAM-2.0)*U(TT-1,JZ)
      DD(JZ)=DD(JZ)-C(JZ)*U(TT-1,JZ+1)-ASTAR
      GO TO 120
C
  350 DD(LAST)=-A(JZ)*U(TT-1,LAST-1)+(LAM-2.0+GAM)*U(TT-1,LAST)
      DD(LAST)=DD(LAST)-C(JZ)*(QR(TT-1)+QR(TT))*DZ/K-ASTAR
      GO TO 120
C
  360 DD(1)=(2.0*LAM-2.0)*U(TT-1,1)-C(1)*U(TT-1,2)
      DD(1)=DD(1)-A(1)*(TSURF(TT)+TSURF(TT-1))-ASTAR
  120 CONTINUE
C
C   COMPUTE NEW TEMPERATURES U(TT,JZ) USING SUBROUTINE TRIDAG
C
      CALL TRIDAG (1,LAST,A,B,C,DD,V)
C
      DO 500 JZ=1,LAST
      U(TT,JZ)=V(JZ)
  500 CONTINUE
      U(TT,LAST+1)=U(TT,LAST)+DT*QR(TT-1)/K
C
C   SET HEAT FLOW MATRIX
C
      I=TT-1
      IJ=I+1
      W(I,1)=T
      W(I,2)=((U(I,1)-TSURF(IJ))/DZ)*K
      X8=ZMAX/(10.0*DZ)
      JR1=IFIX(X8)
      K10=JR1+1
      W(I,3)=(U(I,K10)-U(I,JR1))*K/DZ
      X10=ZMAX/(5.0*DZ)
      JR2=IFIX(X10)
      K11=JR2+1
      W(I,4)=(U(I,K11)-U(I,JR2))*K/DZ
      W(I,5)=TOTUP(I)
C
  100 CONTINUE
C
C   PRINT PARAMETERS
C
      WRITE (7,1001)
      WRITE (7,1003) A0,K,DIF,D,Q0,TSURF0
```

```
      WRITE (7,1005) DTSURF,ZMAX,TMAX,DZ,DT
      WRITE (7,1007) QR1,TQR1,QR2,TQR2,QR3
      WRITE (7,1009) UPL1,TUPL1,UPL2,TUPL2,UPL3,TUPL3,UPL4
      WRITE (7,1300) LAPSE
      WRITE (7,1310)
      WRITE (7,1320) AAA
      WRITE (7,1330)
      WRITE (7,1340) BBB
      WRITE (7,1350) TNONEQ
      WRITE (7,1050)
      WRITE (7,1015)
C
C  PRINT TIME HEADINGS
C
      DO 600 J6=1,21
      P(J6)=(TMAX/20.0)*FLOAT(J6)-TMAX/20.0
  600 CONTINUE
      WRITE (7,1011)(P(J6), J6=1,21)
      WRITE (7,1015)
C
C  PRINT SURFACE TEMPERATURES
C
      DO 610 J7=1,21
      ZDT=TMAX/DT+0.1
      J8=(IFIX(ZDT)/20)*J7-(IFIX(ZDT)/20)+1
      PP(J7)=TSURF(J8)
  610 CONTINUE
      WRITE (7,1013)(PP(J7), J7=1,21)
C
C  PRINT TEMPERATURE MATRIX
C
      DO 650 J2=1,50
      ZDZ=ZMAX/DZ+0.1
      J50=J2*IFIX(ZDZ)/50
      DO 660 JT=1,20
      J51=(IFIX(ZDT)/20)*JT+1
      UU(JT,J50)=U(J51,J50)
  660 CONTINUE
      WRITE (7,1014) U(1,J50),(UU(JT,J50),JT=1,20)
  650 CONTINUE
C
      WRITE (7,1015)
      WRITE (7,1015)
C
C  PRINT HEAT FLOW-TOTAL UPLIFT MATRIX
C
      X12=DZ/2.0
      X13=DZ*(2.0*FLOAT(JR1)+1.0)/2.0
      X14=DZ*(2.0*FLOAT(JR2)+1.0)/2.0
      X15=ZMAX/50.0
      WRITE (7,1020)
      WRITE (7,1021) X12
      WRITE (7,1022) X13
      WRITE (7,1023) X14
```

```
      WRITE (7,1024)
      WRITE (7,1015)
C
      DO 680 JB=1,20
      J9=(IFIX(ZDT)/20)*JB
      WRITE (7,1030) (W(J9,J10), J10=1,5)
  680 CONTINUE
      WRITE (7,1015)
      WRITE (7,1040) X15
      IZDT=IFIX(ZDT)
      IZDZ=IFIX(ZDZ)
      WRITE (7,1042) ZDT, IZDT
      WRITE (7,1043) ZDZ, IZDZ
      WRITE (7,1015)
      WRITE (7,1015)
      WRITE (7,1070)
      WRITE (7,1050)
      WRITE (7,1011)(P(J6),J6=1,21)
      WRITE (7,1015)
C
C  PRINT VALUES OF HEAT PRODUCTION AT SURFACE AND BASE
C
      DO 700 J20=1,21
      J21=J20*IFIX(ZDT)/20-IFIX(ZDT)/20+1
      AQT(J20)=A0SURF(J21)
      AQB(J20)=A0BASE(J21)
      AQSURF(J20)=SURFEL(J21)
  700 CONTINUE
      WRITE (7,1080)(AQT(J20),J20=1,21)
      WRITE (7,1080)(AQB(J20),J20=1,21)
      WRITE (7,1015)
C
      WRITE (7,1180)
      WRITE (7,1015)
C
C  PRINT SURFACE ALTITUDE VALUES
C
      WRITE (7,1190) (AQSURF(J20),J20=1,21)
C
C  FORMAT STATEMENTS
C
  800 FORMAT ('A0,K,DIF,D,Q0-DECIMAL SEPARATED BY COMMA')
  900 FORMAT (5F10.3)
  810 FORMAT ('SURFACE TEMP PARAMETERS, TSURF0,DTSURF(DEG/MA)')
  910 FORMAT (2F10.3)
  820 FORMAT ('GRID PARAMETERS: ZMAX,TMAX--REAL')
  920 FORMAT (2F10.0)
  830 FORMAT ('DEPTH STEP(DZ),TIME STEP(DT)--REAL')
  930 FORMAT (2F10.3)
  840 FORMAT ('QR1,TQR1,QR2,TQR2,QR3--REAL')
  940 FORMAT (5F10.3)
  850 FORMAT ('TUPL1,TUPL2,TUPL3,UPL1,UPL2,UPL3,UPL4--REAL')
  950 FORMAT (7F10.3)
 1001 FORMAT ('1')
```

```
 1003 FORMAT ('SURFACE HEAT PROD. A0= ',F5.2,12X,
     .'CONDUCTIVITY= ',F5.2,
     ./,  'DIFFUSIVITY= ',F5.2,22X,'SCALE HEIGHT= ',F6.1,/,
     .  'INITIAL Q(REDUCED)= ',F5.1,15X,'INITIAL TSURFACE= ',
     .F5.1,/)
 1005 FORMAT ('DTSURF(DEG/MA)= ',F5.2,19X,'ZMAX= ',F5.0,/,
     .  'TMAX(MA)= ',F5.1,25X,'DZ(KM)= ',F5.2,/,
     .  'DT(MA)= ',F5.2,//)
 1007 FORMAT ('REDUCED HEAT FLOW PARAMETERS: QR1= ',F5.1,/,
     .  'TQR1(MA)= ',F5.1,25X,'QR2= ',F5.1,/,
     .  'TQR2(MA)= ',F5.1,25X,'QR3= ',F5.1,//)
 1009 FORMAT ('UPLIFT PARAMETERS: UPL1= ',F5.3,/,
     .  'TUPL1(MA)= ',F5.1,24X,'UPL2= ',F5.3,/,
     .  'TUPL2(MA)= ',F5.1,24X,'UPL3= ',F5.3,/,
     .  'TUPL3(MA)= ',F5.1,24X,'UPL4= ',F5.3,///)
 1011 FORMAT (1X,50F5.1)
 1013 FORMAT (1X,50F5.1)
 1014 FORMAT (1X,50F5.0)
 1015 FORMAT (' ')
 1020 FORMAT ('COL.1=TIME(MA) ')
 1021 FORMAT ('COL.2=Q AT DEPTH= ',F5.2,'KM')
 1022 FORMAT ('COL.3=Q AT DEPTH= ',F5.2,'KM')
 1023 FORMAT ('COL.4=Q AT DEPTH= ',F5.2,'KM')
 1024 FORMAT ('COL.5=TOTAL DENUDATION AT SURFACE(AVE.ALT),(KM)')
 1030 FORMAT (1X,5F10.3)
 1040 FORMAT ('DEPTH PRINTING INTERVAL = ',F5.2,'KM')
 1042 FORMAT ('ZDT= ',F10.2,5X,'IFIX(ZDT)= ',I3)
 1043 FORMAT ('ZDZ= ',F10.2,5X,'IFIX(ZDZ)= ',I3)
 1050 FORMAT (50X,'TIME(MA)')
 1070 FORMAT ('HEAT PRODUCTION AT SURFACE AND BASE OF GRID',/)
 1080 FORMAT (1X,50F5.2)
 1100 FORMAT ('ATMOSPHERIC LAPSE RATE: -DEG/KM')
 1110 FORMAT (1F5.1)
 1120 FORMAT ('ERO.LT.UPL.,TYPE(-1.0);UPL.LT.ERO.(1.0),
     .(0.0)IF.EQ.')
 1130 FORMAT (1F5.0)
 1140 FORMAT ('ERO/UPL OR UPL/ERO, WHICHEVER APPLIES;FROM
     .0.0-1.0')
 1150 FORMAT (1F5.2)
 1160 FORMAT ('TIME OF ONSET OF NON-EQUILIBRIUM BETWEEN UPL AND
     .ERO')
 1170 FORMAT (1F5.0)
 1180 FORMAT ('ALTITUDE(KM) OF SURFACE ABOVE SEA LEVEL WHEN
     .UPL.NE.ERO')
 1190 FORMAT (2X,50F5.2)
 1300 FORMAT ('LAPSE RATE= ',F5.1)
 1310 FORMAT ('IF EROSION IS LESS THAN UPLIFT, AAA= -1.0')
 1320 FORMAT ('IF UPLIFT IS LESS THAN EROSION, AAA= 1.0',10X,
     .  'AAA= ',F5.1)
 1330 FORMAT ('IF EROSION IS EQUAL TO UPLIFT,  AAA= 0.0')
 1340 FORMAT ('RATIO OF EROSION/UPLIFT OR UPLIFT/EROSION=',F5.2)
 1350 FORMAT ('TIME OF ONSET WHEN EROSION .NEQ. UPLIFT= ',
     .F5.1,//)
C
```

```
C
      STOP
      END
C
C
C  SUBROUTINE FOR SOLVING A SYSTEM OF LINEAR SIMULTANEOUS
C  EQUATIONS HAVING A TRIDIAGONAL COEFFICIENT MATRIX.  THE
C  EQUATIONS ARE NUMBERED FROM 1 TO LAST, AND THEIR SUBDIAGONAL,
C  DIAGONAL, AND SUPER-DIAGONAL COEFFICIENTS ARE STORED IN THE
C  ARRAYS A, B, AND C.  THE COMPUTED SOLUTION VECTOR
C  U(TT,1)...U(TT,LAST) IS STORED IN THE ARRAY V.
C
C
      SUBROUTINE TRIDAG (IFIRST,LAST,A,B,C,DD,V)
      DIMENSION A(210),B(210),C(210),DD(210),V(210)
      DIMENSION BETA(210),GAMMA(210)
C
C  COMPUTE BETA AND GAMMA ARRAYS
C
      BETA(IFIRST)=B(1)
      GAMMA(IFIRST)=DD(1)/B(1)
      LL=IFIRST+1
      DO 400 L=LL,LAST
      BETA(L)=B(L)-(A(L)*C(L-1))/BETA(L-1)
      GAMMA(L)=(DD(L)-A(L)*GAMMA(L-1))/BETA(L)
  400 CONTINUE
C
C  COMPUTE FINAL SOLUTION VECTOR V
C
      V(LAST)=GAMMA(LAST)
      LK=LAST-IFIRST
      DO 410 K=1,LK
      JKL=LAST-K
      V(JKL)=GAMMA(JKL)-(C(JKL)*V(JKL+1))/BETA(JKL)
  410 CONTINUE
C
      RETURN
      END
```